2023

Coalition Formation and Beamsteering Optimization for Directional Software-Defined Radios

Sayanta Seth
University of Central Florida

COALITION FORMATION AND BEAMSTEERING OPTIMIZATION FOR DIRECTIONAL SOFTWARE-DEFINED RADIOS

by

SAYANTA SETH
M.S. University of Central Florida, 2018

A dissertation submitted in partial fulfilment of the requirements
for the degree of Doctor of Philosophy
in the Department of Electrical Engineering
in the College of Engineering and Computer Science
at the University of Central Florida

Fall Term
2023

Major Professor: Murat Yuksel

ABSTRACT

Dynamic Spectrum Access (DSA), also known as Dynamic Spectrum Management, is the method of utilizing a set of spectrum techniques in real time to provide the ability to share wireless channels between Primary (or licensed) users (PUs) and Secondary (or unlicensed) users (SUs). The system is so designed that under normal circumstances, the PUs always get priority, but DSA enables the SUs to use the licensed bands as long as they do not create any interference on the PUs. Hence, the goal of utilizing the spectrum more efficiently can be achieved. Though DSA has been researched extensively as a new concept, it is still under development and several challenges remain unsolved. DSA is recognized as a vital component in 5G-and-beyond network deployment scenarios. Although 5G networks can work in sub-6GHz bands, higher frequency bands (like 28 GHz and 60 GHz) are particularly of interest as they offer much larger bandwidth and regulatory agencies have been announcing licensing plans for these emerging bands. These higher frequency bands could enable extremely high-speed wireless communication by leveraging the gains of highly directional antennas. Smart devices used worldwide has already surpassed 22 billion and is only going to increase in the coming years. Channel allocation and high-speed communication will be the backbone to drive this enormous network of devices, and DSA and directional antenna communication mechanisms will be the key factors governing the future communication infrastructure.

In this dissertation, we show how omnidirectional DSA techniques can be applied towards directional cases, i.e., replacing the omnidirectional antennas with directional antennas working in the millimeter wave (mmWave) bands. MmWave enables ultra-high speed transmission and reception, but with some caveats; these antennas should be deployed in line-of-sight (LOS) and a lot of transmission and reception properties depend on how the antennas are aligned, their steering angle, beamwidth and field-of-view (FOV). It is a challenge to

take into consideration all of these factors and come up with a solution of ideal signal-to-interference-plus-noise-ratio (SINR) combination between a set of transmitters and receivers. This dissertation sets a guideline on how small cell mmWave transmitters and receivers can be deployed in a densely populated area by working in a coalition (such as by smartly allocating channels to coalitions with more users). Mobility and varying orientations of mmWave as part of dynamic coalitions present new challenges we undertake. Hence, an area where this research can be very apt is vehicular networks, leveraging the high-speed communication provided by mmWave networks. Since the nodes in this case, the vehicles, will be primarily in motion, our research can be applied especially, because we are investigating the antenna designs by considering their beamwidths, steering angles power budgeting.

To my mamma, Kanta.

ACKNOWLEDGMENTS

I am grateful to my advisor Dr. Murat Yuksel for guiding, supporting and believing in me over the years of my Ph.D studies. Without his experienced mentoring, my dream of earning a Ph.D would not have come true. I would like to express sincere appreciation of my committee members Dr. Nazanin Rahnavard, Dr. Azadeh Vosoughi, Dr. Wasfy Mikhael and Dr. Samiul Hasan for serving in my committee. Their constructive feedback and comments have helped me in improving my dissertation. I would like to thank Dr. Mainak Chatterjee who helped me get started in my PhD journey. I would also like to thank all my colleagues at the Networks and Wireless Systems Laboratory and all my friends who have always inspired me while working as a Ph.D. student. In addition, I would like to thank the Department of Electrical Engineering at the University of Central Florida for offering me with all these wonderful classes which enriched my knowledge along the course of my education. I would like to acknowledge the role of my parents (Kanta and Salil Kumar Seth) and my school and college teachers for motivating and supporting my desire of pursuing higher studies. Thank you Kanta Seth (Mamma) for believing in me and making me who I am today; thank you Debashri Roy (Debashri di) - you helped me kickstart my PhD career with my first ever research paper; thank you Moinak Chakraborty (Moinak) for being my best buddy throughout my PhD journey and thank you Sohini Sikdar (Shoi) for your friendship, immense emotional support and for just being there during the final phase of my PhD career.

TABLE OF CONTENTS

LIST OF FIGURES

LIST OF TABLES

CHAPTER 1: INTRODUCTION

Motivation

As of May 2022, the number of IoT devices have been projected to grow to 14.4 billion globally, an increase by 18% compared to 2021 [1]. It is predicted (Fig. 1.1) that compared to Q4 2021, the number of 5G IoT/connected devices will see a humongous 159% jump by the end of 2025. Hence, in near future, we can confidently say that we will see a dramatic increase in IoT, high-quality streaming and multi-user video-conferencing, Augmented Reality (AR) and Virtual Reality (VR) applications, and vehicular communications. Further, when the novel Coronavirus pandemic hit the globe, we saw a sharp spike in bandwidth consumption as workplaces and schools locked down and majority of the workflow shifted online. As the world is recovering from the novel Coronavirus pandemic, we have seen the trend of 'work-from-home' is still in place in many organizations [4]. Some companies like Airbnb and Aquent have permanently switched to total online operations, while Meta and Lyft offer flexible workplace option to their employees. If we take a look at the cellular data usage

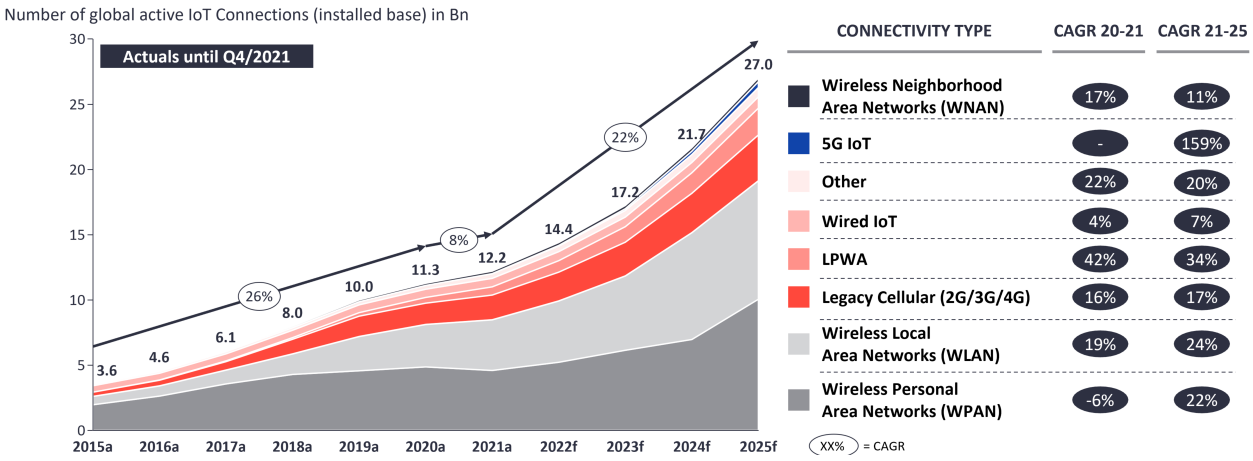

Figure 1.1: 5G IoT projections by IoT Analytics [1]

during the pandemic, some telcos have reportedly [5] used up to 60% more data on their networks than they did before the crisis. This gave a huge increase in high-speed wireless data consumption and, as a result, a major boost in revenues for the wireless carriers. It is also reported that video has been the main driving force behind the increase in wireless data consumption. All of this suggests that the conventional sub-6 GHz wireless Internet framework is and will continue to be heavily stressed for handling the exorbitant amounts of wireless traffic being generated world-wide.

A pre-pandemic article [6] suggests that wireless data traffic is projected to increase by 10,000 fold within the next fifteen years. This number will only explode given the current global scenario. While the extremely wide bandwidths accessible using millimeter-wave (mmWave) frequencies (30-300 GHz) were largely unexplored till recent times, this area of wireless communications has now started to gain more traction. Because mmWave waves have short wavelengths, the devices enable large antenna arrays to be packed in small physical dimensions. Compared to microwave, with the same antenna size, it is possible to pack more antenna elements, resulting in narrower and directional beams.

Underlying Architecture for 5G Deployment

As telcos are rolling out 5G services all over the globe, the first challenge regarding deployment is that of the deployment architecture. S. Sathyanarayan, in his online article [7], enumerates the challenges the mobile carriers are facing regarding the architecture to use for deployment of 5G services. 3GPP TR 21.915 [2] lists the details regrading the two deployment options defined for 5G:

1. In "Non-Stand Alone" (NSA) architecture (see Fig. 1.2), 5G Radio Access Network

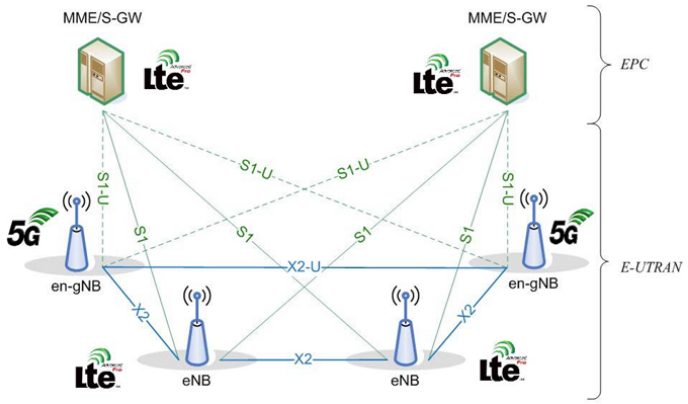

Figure 1.2: 5G NSA [2]

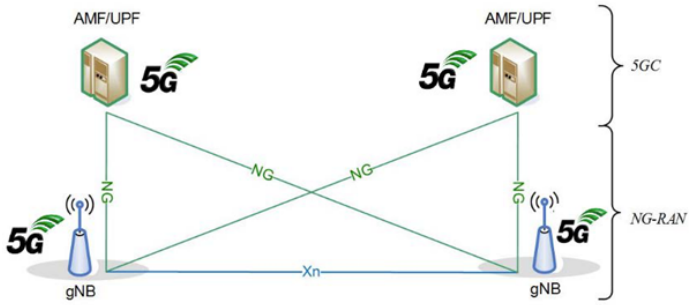

Figure 1.3: 5G SA [2]

(RAN) and its New Radio (NR) is used along with the existing Long Term Evolution (LTE) infrastructure Core Network. This helps make the NR technology available without network replacement. Although, in this configuration, only 4G services are supported, the capacities offered by 5G NR (e.g., lower latency) can be enjoyed. The NSA is also known as "E-ULTRA-NR Dual Connectivity (EN-DC)" or "Architecture Option 3".

2. In "Stand-Alone" Architecture (see Fig. 1.3), the NR is connected to the 5G Core network. Only in this configuration, the full set of 5G services is supported.

Challenges of mmWave in 5G: Attenuation and Directionality

Super-fast mmWave 5G networks are based on bands ranging from 24 to 70 GHz (FR2 bands), whereas, the low-to-mid bands range from 3.4 to 6 GHz (FR1 bands) [8]. At the higher carrier frequencies (e.g., FR2 bands), severe attenuation occurs due to oxygen absorption. Some special bands such as 35, 94, 140 and 180 GHz experience relatively small attenuation. Blockage by solid objects like animals and buildings also play a negative role in the antenna throughput. A very distinguishing and characteristic feature of mmWave radio signals is directional propagation [9]. Because the wavelengths of mmWave signals is small, large-scale directional antenna arrays are leveraged to synthesize highly directional beams that provide substantial array gains, helping maximize the overall system throughput. The authors further mention that due to the directional nature of both the signal and noise powers in mmWave networks, Angle of Arrival (AoA) and Angle of Departure (AoD) play a very significant role in determining the received signal strength. Due to the ability of directional antenna arrays to provide variable power gains, even a slight shift of AoA/AoD may lead to a large array gain variation. Hence, it is crucial to incorporate robust algorithms to carefully tweak/steer these directional beams for maximizing data rates. Being able to differentiate Line-of-Sight (LOS) vs. non-LOS channels and proper beam alignment are critical components of managing links in mmWave networks.

Researchers at Qualcomm [10] have demonstrated mobility in indoor and outdoor environments for mmWave networks. When mobility of user equipment (UE) is considered in a mmWave network, traditional concepts of cellular boundaries need to be re-imagined. In many cases, a nearby base station (BS) might be blocked and a faraway BS might provide the best signal quality due to availability of LOS to it. Also, as mentioned before, attenuation through foliage not only causes problems, but it becomes a dynamic issue based on seasonal variation.

A UE driving on a route in winter months may not be affected as badly when compared to driving in summer months, because the trees lose their leaves in winter and get them back in summer. Also, it has been shown that in office buildings using dry walls (like in the US) there is only a few dB of attenuation, unlike severe attenuation occurring in countries using concrete walls in office buildings. This will affect the placement of BS and UEs inside similarly designed office spaces and, most importantly, the mobility of UEs within the office spaces.

Terahertz (THz) bands exhibit behaviors similar to mmWave bands. Song et al. in [11] have mentioned the major challenges that need to be overcome for successful THz implementation, such as several critical hardware limitations, power- and spectrum-Efficient waveform design, and LOS challenges. As it has been already mentioned, we will definitely see a lot more IoT devices in the near future. Commercial scale router manufacturing company Cisco says that 5G offers wide-area coverage for low-powered and low-bandwidth IoT devices for real-time IoT use cases. These applications require very high data rates and extremely low latency [12]. Self-driving vehicles (including robots and autonomous vehicles), for example, will lead to wide acceptance of both private and public 5G. In big cities, such large-scale deployments will increase the density of 5G capable nodes. *Coalitions of such nodes then becomes a necessity for smooth operations. As the node density increases, it becomes impractical to manage them from a central entity* like a BS.

Further, when infrastructure fails, nodes can still communicate if they are arranged in a coalitional structure. In emergency situations, the public safety spectrum is used. Public safety channels are available in the VHF band, 220 MHz band, UHF, T-Band, 700 MHz narrowband, 700 MHz broadband, 800 MHz band, 4.9 GHz, and 5.9 GHz bands according to FCC [13], and they are typically accessed by omni-directional radios. However, during severe cases (like hurricanes) when the infrastructure fails, public safety communication

infrastructure is jeopardized. Hurricane Michael wrecked havoc in Florida Panhandle area in 2018 causing total communication system breakdown [14]. Hence, we need to implement solutions that do not rely on infrastructure. In such scenarios, a *tactical bubble* [15] is created (in an ad-hoc manner) off of the 5G infrastructure meant for civilian usage. This bubble helps in maintaining data privacy of the tactical network traffic, while using the BSs for civilian networks. If we use 5G backbone for such communications, then needless to say, coalition structures are essential to maintain reasonable throughput in the infrastructure-less ad-hoc communication systems.

Contributions and Thesis Organization

Our work is targeted towards eliminating the shortcomings of mmWave/THz communications, that employ directional antennas, by using coalition structures. We start off by presenting our literature survey of various types of wireless communication devices, antennas like omni-directional and directional antennas, channel models for 5G and THz communications and challenges and opportunities of software-defined radios (SDRs) in general. In Chapter 3, we introduce and establish the need for coalition structures by diving deep into the concepts of cognitive radio networks (CRN). We propose an intelligent coalition formation algorithm without overlapping transmission power radii among the cognitive radio nodes, ensuring communication interference is avoided. We then devise a coalition formation algorithm under adversarial attacks. We consider two types of attack strategies - smart and naive. We also present a stability criterion for the convergence of the coalition formation algorithm, so that the users maintain coalitions according to their payoffs. We then extend our CRN studies and validation by implementing a network of cognitive radio nodes and adversaries on the world's largest wireless test bed Colosseum. We call this novel framework 'Cognisseum'

as we have implemented a first-of-its-kind CRN on Colosseum. In this real-world emulation setup, we show how legitimate radios can improve their payoffs by switching coalitions after being attacked by an adversary.

In Chapter 4, we propose our coalition formation mechanisms for directional SDR nodes, perfect for 5G mmWave and THz applications, using both centralized and decentralized frameworks. In this chapter, we provide a step-by-step formal method to categorize directional antenna nodes based on their field-of-views (FoVs) and an illustration of the method on networks of nodes of varying sizes. We formulate directional link capacities when transmissions are randomly scheduled. We show calculation of coalitional sum rate or throughput using the scheduling methods and channel allocation schemes. Finally, we provide heuristics for forming coalition sets that may or may not place all network nodes to a coalition based on the strictness of all-covering property of our coalition sets, and explore possibilities of merging coalitions to improve the network sum rate.

In Chapter 5, we point our attention to a very significant aspect of sum-rate maximization within an individual coalition by employing beamsteering tactics. Here, we show, within a coalition, how to extract links and form the nodes into groups, for which three different types of transmission becomes possible: uplink, downlink, and ad-hoc. Next, we formulate directional uplink, downlink and ad-hoc link capacities when transmissions are randomly scheduled. We calculate average network throughput by optimizing beamsteering angles of all nodes for uplink, downlink, or ad-hoc transmission, jointly or separately, keeping in mind the constraints presented by varying the FoV of the directional nodes. We employ exhaustive methods to optimize beamsteering angles and compare our results to two of the most well-known evolutionary algorithms, Genetic Algorithm (GA) [16] and Recursive Random Search (RRS) [17].

Finally, the conclusion is drawn at the end of this dissertation.

CHAPTER 2: LITERATURE SURVEY

In this chapter, we survey the literature covering the existing work related to the individual chapters of this thesis. In essence, this work touches to cooperation among cognitive radios, spectrum access in sub-6 GHz and mmWave/THz bands, and beamsteering methods for directional radios. We survey these topics in the subsections below.

Cognitive Radios (CR)

In CRNs, it is crucial for an SU to predict with high accuracy when the PU arrives so that it can vacate its band without much impact on the PU. Hence, most of the literature focused on improving this prediction and reducing the interference on the PUs. Since SUs are competing for the unused spectral resources, the contention among them attracted significant attention from researchers. Effective sensing of the spectrum and learning and predicting the spectrum usage patterns of the PUs attracted a lot of attention. Centralized and distributed spectrum sensing models were proposed [18–21]. These techniques employed a novel power allocation scheme that uses dynamic sub-channel method based on a Nash Bargaining game among SUs. In a similar vein, Saad *et al.* [22, 23] introduced the idea of cooperative spectrum sensing among SUs for single-PU scenarios, where the SUs increase their sensing accuracy by participating in a coalitional game. The authors explored the trade-off between the probability of detecting the PU and the probability of false alarm on the SU network topology and dynamics. These efforts focused on reducing the interference on PUs via various mechanisms of spectrum sensing and SU coordination. Different strategies of PU-SU interaction are well investigated. Many studies considered game-theoretic approaches to capture the strategies of the SUs in presence of the PUs. The studies outlined application

of game theory to the SU strategy design and showed how non-cooperative [24–26] and cooperative [27, 28] games can be used as tools to model the PU-SU interaction of cognitive radios.

Spectrum (usage) prediction is another area where a lot of research has been conducted. The two widely used spectrum prediction techniques are local and cooperative spectrum prediction. In the local spectrum prediction, the SU uses a Hidden Markov model to predict the status of the current channel in which it functions. Based on its prediction, it may switch to another channel when needed. The cooperative technique is where the selfish SUs might have to form a coalition to increase their individual payoffs. Cooperative spectrum sensing in CRNs with single PU has been studied in [22]. Further, significant work [29] have been conducted on centralized collaborative sensing, where, given the mobile ad hoc nature of the cognitive radio users, a distributed game-theoretic framework has been proposed which reduces the average probability of the false detection of the PU significantly compared to the non-cooperative sensing.

We, in Chapter 3, contribute to this literature in terms of SU strategies in CRNs. Our work formulates the activities of SUs in the presence of multiple adversaries. We propose a novel framework where SUs cooperatively form coalitions in a dynamic manner to increase the payoffs of the coalition as a whole. Initial experimentation using the Colosseum platform have been covered extensively in [30] and [31]. These papers show us how to utilize the wireless channel emulator for a variety of scenarios. In other words, they are more of tutorial in nature. To the authors' best of knowledge, proper utilization and experimentation using this platform on a CRN has not yet been performed. In this paper, we aim to show how real-world version of cognitive radios can be implemented on Colosseum and perform extensive experiments on this Cognisseum system.

Super-6 GHz Spectrum: Directional Radios, 5G, mmWave, and THz Systems

The problem of increasing aggregate throughput of a wireless network is an old one. Interesting works have been performed in the field of Dynamic Spectrum Sharing using sub-6 GHz 5G spectrum like [32], where the authors have proposed a unique and novel wireless peering concept for cellular operators in the United States. However, directionality of (5G mmWave/THz) transmissions brings in new challenges in attaining high throughput. Prior work explored sub-channel allocation and scheduling methods for directional antennas in mmWave spectrum. Studies included algorithms to efficiently allocate sub-channels to improve resource utilization and network capacity of a Device-to-Device (D2D) network [33], methods to allocate sub-channels to D2D links in a densely populated environment [34] with superior results compared to conventional D2D approaches [35], and QoS-aware scheduling algorithms for concurrent transmission using game-theoretic methods [36].

Traditional problems such as interference management has also been going under a revisit within the context of directional wireless. Among others, approaches included Non-Orthogonal Multiple Access (NOMA) to control beamwidth of a hybrid mmWave communication system for overcoming the limitation of narrow beams in mmWave systems by tuning main lobe power losses [37], and use of scheduling based on a coalitional game to attain self-interference (SI) cancellation technology for full-duplex mmWave communications [38]. None of the work in currently available literature have tried to tune mmWave directional radio throughput by optimizing the steering angles of the antenna beamwidths in a coalitional setting. Also, to the best of our knowledge, no prior work has been done to look into the issues of fast and efficient coalition formation in very high node density cases. Our work deals with both improving directional coalition SINR keeping in mind the further improvement brought upon by carefully tuning and optimizing the beamsteering angles of each directional antenna within

a coalition.

One of the main problems of the 5G wireless networks is the saturation of the currently assigned wireless bandwidth. This, along with the explosion of the growth in mobile traffic demand, the contradiction between the spectrum shortage and capacity requirements has become prominent. [39] and [40] have done extensive work showing how radio frequency (RF) circuits have paved the way for electronic products in the mmWave bands. In [41], the authors have reasoned why the 3-300 GHz spectrum band should be given tremendous importance for mobile broadband applications. They have demonstrated the feasibility of the implementation of a mmWave mobile broadband (MMB) system that can serve as potentially next generation mobile communication system. The authors have tested the setup to achieve gigabit-per-second (Gbps) data speeds for a distance of up to 1 Km in urban mobile development. This research involves mobile broadband system air interface design using beamforming processing technique for directional signal transmission and reception. Researchers in [42] have looked in to the matter of the problems of short range and non-line-of-sight (NLOS) coverage issues for the directional antennas using mmWave bands. Historically, mmWave bands have suffered from these issues and hence have always been ruled out for mainstream communication solutions. The authors have diligently looked into the development of advanced algorithms from recent channel measurement campaigns [43], [44], [45] and come up with a design that clarifies misconception regarding propagation loss at higher frequencies (e.g., 30 GHz) by matching he experimental results with the theoretical Friis equation, involving actual patch antennas at 3 GHz and array antennas at 30 GHz of the same physical aperture.

For improving network capacity, directional wireless communication has offered new features to utilize. In particular, mmWave beams are amenable to beamsteering, opening new ways to improve the aggregate network throughput, or sum rate [46]. Going beyond channel resource

allocation [47], the impact of scheduling in the optimality of beamsteering angles needs to be considered to fully take advantage of what is available in directional wireless. Beamsteering optimization of directional antennas are shown to help significantly in mobile fronthaul [48] and cognitive radios [49]. Recent studies have investigated the role of beamsteering in improving throughput, as demonstrated in research such as [50, 51]. Notably, these investigations have omitted the consideration of scheduling's impact on optimizing beamsteering angles for directional antennas. Previous endeavors have focused on optimizing beamsteering angles [48] and/or transmit powers [52] for scenarios like mobile fronthauls, primarily addressing uplink or downlink transmissions. The exploration of joint optimization involving beamsteering angles and physical layer coding schemes has also been undertaken [53]. Pertinent to our work are studies such as [49, 54], wherein the authors explored how adaptive beamsteering angles and transmit power control in cognitive radio setups influence the attainable channel rate between a pair of cognitive transmitter and receiver. In our research, we focus on an ad-hoc network featuring multiple transmitters and receivers, where nodes are scheduled randomly for transmission. Here, our emphasis lies in optimizing the beamsteering angles of directional antennas, while keeping transmit powers fixed, with the overarching objective of maximizing the network capacity.

Most relevant literature to ours are the recent works on increasing wireless network throughout using mmWave bands and the models for coalitional communication among radios using legacy sub-6 GHz bands. When coalitions are considered as part of the throughput optimization of directional wireless communication, the problem gets more complicated with inter-play of transmit power, beamsteering angles, scheduling, and channel allocation [33], as well as intra- and inter-coalition interference. Putting constraints on the transmit power has proved to be fruitful in reducing the problem's complexity. Applying a transmit power limit on each individual node and dividing the problem into two stages enabled convex optimization

solutions [55] in a scenario where scheduling is assumed optimal. When random scheduling is assumed for a single coalition, it was shown that beamsteering optimization can be done fast and comprehensively [56]. These studies did not consider all-covering coalition formation and can yield unfair solutions. We consider a regulated scheduling method based on the structure of directional topology and develop novel and efficient heuristics for forming a set of coalitions that maximize the throughput while making sure all coverable nodes are placed in a coalition.

There have been exciting studies on mmWave beamforming, but mostly for a single transmitter or receiver. Using ray tracing simulations [57] studies mmWave beamforming techniques in a multi-user indoor environment at 70 GHz frequency band, focusing on beamsteering strategies for an access point that is accommodating multiple users. Raghavan et. al. in [58] have studied the performance of a class of directional beamsteering co-phasing schemes which leverages currently existing beamsteering solutions for point-to-point transmissions. Although these studies have considered multiple users, they do not consider the effect of nodes' transmission scheduling.

CHAPTER 3: COALITION FORMATION AMONG OMNI-DIRECTIONAL RADIOS

Introduction

A network of unlicensed users that dynamically detect unused licensed spectrum for their own use without interfering licensed users is called a cognitive radio network (CRN). CRNs promise to deliver an intelligent solution to the issues in conventional wireless technology related to their limited and under-utilized spectrum [59]. Despite these promises that CRNs bring on paper, there is a need to conduct extensive studies, simulation and real-world experiments to validate their effectiveness in solving the spectrum under-utilization challenge. There exists two types of users [60] in a CRN: Primary Users (PUs), who are licensed owners of the specific frequency spectrum in question, and Secondary users (SUs), who opportunistically exploit the unoccupied licensed spectrum. In the United States, according to Federal Communications Commission (FCC) [61, 62], most of the radio spectrum is used inefficiently, which results in over-utilization of many of its bands [63]. For example, in most places around the globe, cellular bands have become very congested due to high demand from civilian applications. Whereas, other bands exclusively utilized by military equipment and paging devices are under-utilized most of the time in most places. CRNs attempt to alleviate the problem of spectrum under-utilization by letting the SUs utilize the bands allocated to PUs in a way such that the PU communications are not compromised. The SUs temporarily using the PU channels must immediately vacate the channel whenever required by the legal channel owner [63].

Consideration of adversaries on CRNs changes the dynamics significantly. An attacker trying

to degrade the performance of a CRN can block the channels being used by SUs. Recent work [64] studied the performance of CRNs when there is a single attacker eavesdropping the transmission among SUs. However, to our knowledge, the case of multiple SUs being attacked by multiple adversaries has not been considered.

In this chapter, we follow the general concept of CRN by allowing SUs to opportunistically use the shared spectrum with the PUs. However, there is a plethora of researches on such opportunistic channel allocation between the primary and secondary users, e.g., [65, 66]. Different from those studies, our chapter is focused on maximizing the channel utilization for the channels allocated to the SUs in the presence of multiple adversaries trying to block the SUs. We focus on a CRN design where each SU transmits based on its power budget. We consider an SU transmitter and SU receiver to be a single entity, henceforth referred to as an 'SU pair'. For simplicity, we assume that there is a fixed number of PUs which are always present and are constantly accessing their own channels. We further assume that the channels being used by the PUs are known. The remaining channels get allocated to the *SU coalitions*. When the SU pairs work together to maximize their overall payoffs, we determine that they have formed a coalition. Also, the adversaries considered in the system, are capable of only attacking the SU pairs, and not the PUs, following the FCC mandated rules [67]. We consider the problem of tuning transmission power of such SU pairs under the presence of multiple adversaries. We use this transmission power criterion to decide the coalition formation of the SU pairs. *Overall, we consider a game-theoretic framework to study the multi-SU-pair multi-adversary scenario in CRNs. We design an algorithm for SU pairs to form coalitions to maximize their payoffs/utilities, i.e., throughput among them. Further, we study, using simulations, the stability of the coalitions formed and record the total value of all coalitions in terms of the total throughput (i.e., sum rate) in the presence of adversarial attack.*

Figure 3.1: Colosseum [3]: High-performance USRP devices arranged in stacks known as 'quads'.

Beyond the simulation-based study of the concept, we focus on developing a CRN framework in the presence of adversaries on Colosseum (refer to Fig. 3.1), which is the world's largest wireless emulator with 256 software-defined radios (SDRs) to emulate up to 65,536 100 MHz-RF channels [3]. The SUs are implemented on real USRP devices that can be accessed via Colosseum. To the best of our knowledge, this is the first study to present coalitional cognitive radios on Colosseum, which we name *Cognisseum*. In Cognisseum, we focus on already-formed coalitions consisting of SU pairs, each being initialized with a number i.i.d of channels. After running emulation for some time, we introduce adversarial presence and record the before and after attack throughputs. This hardware-based emulation will serve as a benchmark in the field of dynamic spectrum access (DSA) by cognitive radios facing adversaries.

The main contributions of this chapter are as follows:

1. We propose an intelligent coalition formation algorithm without overlapping transmission power radii, ensuring communication interference is avoided.

2. We devise an adversarial coalition formation algorithm, keeping in mind the smart and

naive attack strategies of the proposed framework.

3. We present a stability criterion for the convergence of the coalition formation algorithm, so that the SUs maintain coalitions according to their payoffs.

4. We perform hardware emulation on Colosseum, a large-scale wireless emulator. Using real USRP devices, we show how wireless channels of various pathloss values affect the sum rate of the coalition sets.

5. On Colosseum, we emulate an adversarial network and show how legitimate radios can improve their payoff by switching coalitions after being attacked by an adversary.

Key insights from this study include:

1. In simulation, we show how the average utilities of the SU pairs vary: After attack, the average utilities vary from around 66% to 75% with adversary count increasing by 14.2%. We also demonstrate that coalition utility increases by 28.5% with increasing channels, for constant number of SU pairs and adversaries.

2. We observe, for the same number of SU pairs and channels, the average coalitional utilities decrease with increasing adversary count.

3. We observe that smart attack strategy unleashes 14.66% more damage on the proposed framework when compared to the naive one.

4. In emulation, we show how we can utilize Colosseum as a wireless test-bed for our setup.

5. We observe significant improvement in overall coalition throughput (sum rate) after the affected pair switches coalition.

Cognisseum: System Model and Assumptions

We consider a 2-dimensional geographical plane for CRN nodes. The system is pre-occupied by $\mathcal{T}$ PUs and multiple SUs.

PU Modeling: We model the $\mathcal{T}$ PUs to frequently access some specific sub-channels, while leaving the remaining sub-channels empty during a particular time period in the day. The authors in [68] have given an example of the Disney TV channel as a PU that is active for 75% of the time during the day, which shows frequent and almost continuous PU activity on its own licensed spectrum. In this research, we assume that the frequent on-off activity and the channel utilization of the PUs is known by the SU pairs with a probability $\mathbb{P}$. Since each SU pair is made up of a single transceiver, devoid of interference, we simply multiply $\mathbb{P}$ with the link rate R for each practicable link. For example, if $\mathbb{P} = 0.5$, then the SU pairs can successfully predict PU activity in the system 50% of the time. During that time of the day, the SUs can use those remaining sub-channels for their communication, which enables us to run our SU-based experiments during that time.

SU Modeling: The CRN system also consists of multiple legitimate SU radios are then categorized into equal number of transmitters and receivers and formed into pairs, each called an 'SU pair'. Each of the transmitter and the receiver of the SU pairs is assumed to have a *virtual proximity area* directly proportional to their power radii. Referring to Fig. 3.2a, we can see that the overall power radii of a transmitter SU and a receiver SU, comprising of the pair. From this, we build up the notion of an SU pair, which has a single transceiver, imposing the requirement of having pairs of individual SUs when forming a coalition. When two SUs are exchanging data they have to dedicate their transceivers to only one wireless link, at any point in time. Overall, this requires the number of SUs that are actively transmitting/receiving data to be in multiples of 2. We represent such legitimate

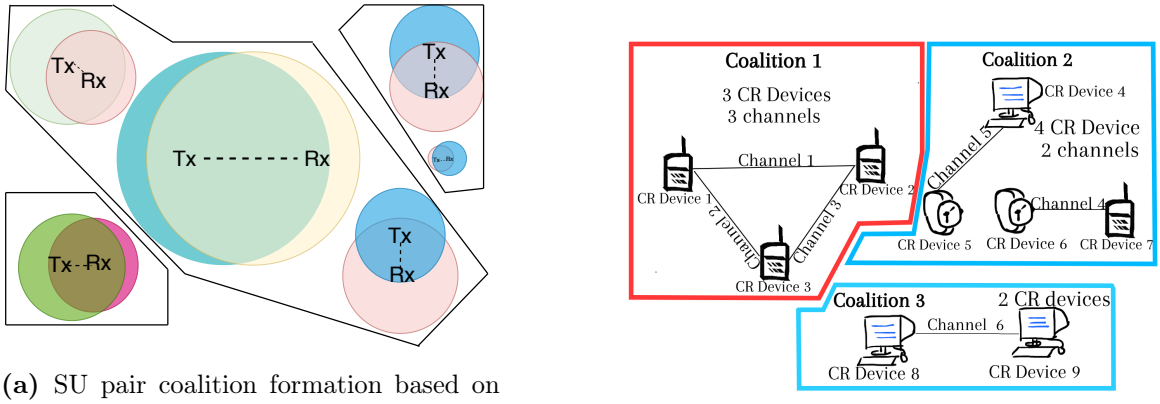

(a) SU pair coalition formation based on power radii

(b) Coalition formation among SU pairs

Figure 3.2: Coalition formation concepts in Cognisseum

SU pairs as $\mathcal{N} = \{N_1, N_2, ...N_\eta\}$ which are initialized with varying power budget, denoted by the set $\mathcal{P} = \{P_{N_1}, P_{N_2}...P_{N_\eta}\}$ respectively.

SU Coalition Modeling

We assume that SUs form coalitions to better utilize the available bandwidth in the presence of attackers trying to bring down their effective bandwidth. In Fig. 3.2a, we show how SU pairs form coalitions. The SUs participate in spectrum sensing and access jointly, in a cooperative manner [69]. Fig. 3.2b shows a typical scenario of such cooperative behavior, where SUs (devices) are shown to form three different coalitions. The red coalition has three CRN devices in it. As per the system model, this is not possible because even in a singleton, there must be at least two SUs, as we have considered an SU pair to be a single entity. The rest of the coalitions in blue are feasible because both of them have SUs in multiples of two.

When the SU pairs become part of different coalitions, all of them still can access their Common Control Channel (CCC), which is the communication medium for SU pairs to

use for decision making about joining or leaving a coalition in the event of an attack. For example, SU pairs of a coalition might want to be part of a bigger coalition when they feel vulnerability to adversarial attacks. An adversarial attack could signify that the attacked coalition might be left without any channel to communicate. If the attacked coalition joins another coalition, then it is likely that its SU pairs can transmit using the existing channel(s), which becomes an incentive to join a bigger coalition.

Channel Allocation Scheme

We assume that a total of W Hz is the available bandwidth to the coalitions of SU pairs. This does not include the bandwidth the PUs are frequently using as we assume that the channels PUs are using are known with a probability P. The total bandwidth W is further divided into $\mathcal{C} = |\mathcal{N}|/2$ independent and identically distributed (i.i.d.) sub-channels, where $|\mathcal{N}|/2$ refers to the total number of SU pairs formed. Hence, each SU pair gets one sub-channel initially.

The total number of available sub-channels is allocated to the individual SU pairs in a random fashion. So, for SU pairs, the number of channels allocated to coalitions is directly proportional to the number of SU pairs present in a particular coalition. For example, if there are 10 SU pairs formed into 5 coalitions with each coalition consisting of 2 SU pairs. Since there will be 10 sub-channels, then each coalition will get 2 sub-channels. But under real-world circumstances, the channel allocation might not be as expected, and in some cases, coalitions can end up receiving a very small number of channels compared to the number of SU pairs present in them. However, if the number of channels is greater than or equal to the number of SU pairs, then we can expect a good channel allocation number for most of the coalitions. If the number of channels is fewer than the number of SU pairs, they will have to

rely on techniques like Time Division Multiple Access to utilize the fewer channels in turn, in consecutive timestamps.

Cognisseum: Game-Theoretic Framework

We propose a coalition formation game for both SU pairs and adversaries in the CRN. The SU pairs work in a joint manner to communicate their channel vacancy information with their peers, so that they can improve their own channel capacities as a coalition.

Game Setup

The players and their goals: From before, let $\mathcal{N} = 1, 2, 3, ..., N$ be the set of SUs. The players are $|\mathcal{N}|/2$ SU pairs. Let the players be incorporated into a set $\mathcal{P}$. If there exists a subset S of $\mathcal{P}$, then the subset S is known as 'a coalition'. The goal of the SU pairs is to maximize their channel usage while that of the adversaries is to block as many channels as possible. If channels are blocked, then the SU pairs talking on those channels will also be affected. We design a cooperative hedonic game where the players (SU pairs) may want to join or leave a coalition, or even stay alone.

The payoff: A function $v(.)$ is used to assign a value to each subset of players, or in other words, to each coalition. If all the members inside the subset S of $\mathcal{P}$ act in unison towards achieving the same goal, then $v(S)$ is the payoff to all members of the coalition. In other words, the value/payoff of the coalition is $v(S)$.

Power radius: The power radius of each SU pair (a randomly generated positive real number in our case; a constant in reality, unique to a transmitter) means the geographical

area that can be covered by each SU pair with its omni-directional antenna range. The transmitter SU of the SU pair is at the center of the said area and the receiver SU can reside anywhere within that area. Here, the blue dots signify the legitimate SU pairs. The lines joining them represent that they can potentially form coalitions, based on their power-radii. The yellow dots represent the malicious users or adversaries. [1]

Coalition as a Cooperative Game: At the beginning of the game, no coalition exists, hence $v(\phi) = 0$. Based on their common interests, as the members/players start forming coalitions, we have $v(S) > 0, \forall S \subseteq \mathcal{N}$. A detailed discussion in [70] presents the ideas of cooperative game theory. In the characteristic form, an outcome of a game can be as follows: (i) A coalition structure, essentially a partition of $\mathcal{P}$ players into smaller coalitions, and (ii) a payoff vector to distribute the payoff value of each coalition among its members. A non-empty collection of non-empty non-overlapping subsets can be referred to as a coalition structure (CS), $CS = S_1, S_2, S_3, ..., S_k$ where $S_i \subseteq \mathcal{P}$ represents coalition i and k is the total number of coalitions, which satisfies the followings:

$$\bigcup_{i=1}^{k} S_i = \mathcal{P}; \quad S_i \cap S_j = \phi \text{ if } i \neq j \tag{3.1}$$

Stability Criteria of Coalitions

Two types of stability criteria are considered for our proposed coalitional game: (a) inner and (b) outer. When an SU pair has no incentive to leave its current coalition to become a singleton, then the players (SU pairs) within that coalition have achieved *inner stability*.

[1] Upon multiple iterations of our experiments, we have come across multiple such cases, where just eyeballing the positions of the SU pairs seems that they are far away from each other, yet they haven't taken part in the same coalition. But, in reality, the system-generated random power radius of a particular SU pair might be large enough to render our assumption useless.

Similarly, when an SU pair has no incentive to join another coalition, or in other words, no coalition in a CS has any incentive to merge with another coalition, we refer to it as *outer stability*. For example, if we consider a CS with two coalitions S_1 and S_2, then the inner stability conditions will be:

$$v(S_1) > v(i), \forall i \in S_1 \quad \text{and} \quad v(S_2) > v(i), \forall i \in S_2 R \tag{3.2}$$

and the outer stability conditions will be:

$$v(S_2) > v(S_1 \cup S_2) \quad \text{and} \quad v(S_1) > v(S_1 \cup S_2) \tag{3.3}$$

For the rest of the paper, we will express the value function $v(.)$ of joining a coalition as the *payoff function*, quantifying the data rate achieved by joining that coalition.

Payoff Function

Gaussian fading is considered for our proposed framework, for broader applicability. Hence, the wireless transmission parameters are modelled based on Gaussian complex channel. The achievable data rate R in a Gaussian complex channel of bandwidth W is given by the Shannon's information capacity formula [71]:

$$R = W \log_2 \left(1 + \frac{P_t G_t G_r \lambda^2}{d^2 \ 4\pi N_0 W}\right) \tag{3.4}$$

where P_t is the transmit power, G_r and G_t are the receive and transmit antenna gains, λ is the wavelength, and d is the distance between the transmitter and receiver within an SU pair. The SU pair's transmitter-receiver channel follows the Friis' transmission equation, and $N_0 W$ is the cumulative noise of that channel. Based on the achievable data rate expression

in (3.4), we can write the payoff or the sum-rate of a singleton i consisting of an SU pair is:

$$R_i = \mu_i W \log_2 \left(1 + \frac{P_t^i G_t^i G_r^i \chi}{d_{ii}^2 \mu_i}\right) \tag{3.5}$$

where $\chi = \dfrac{\lambda^2}{4\pi N_0 W}$, d_{ii} is the distance between the transmitter and the receiver of the SU pair i, P_t^i is the transmit power of the transmitter of the singleton pair i, G_t^i and G_r^i are the transmit and receive gains for the singleton pair i, and μ_i is the portion of the total bandwidth W allocated to the singleton i. If we represent the channel component as $h_{ii} = \dfrac{P_t^i G_t^i G_r^i}{d_{ii}^2}$, the sum rate can be re-written as: $R_i = \mu_i W \log_2 \left(1 + h_{ii}\chi/\mu_i\right)$. Extending this concept for a whole coalition S_c (where we index the SU pairs within coalition S_c with k), we have:

$$R_{S_c} = \mu_{S_c} W \sum_{k \in S_c} \log_2 \left(1 + \frac{h_{kk}\chi/\mu_k}{N_0 W \mu_{S_c} + \sum\limits_{j \in S_c, j \neq k} h_{jk}\chi/\mu_{S_c}}\right) \tag{3.6}$$

where $\sum\limits_{j \in S_c, j \neq k} h_{jk}\chi/\mu_{S_c}$ is the interference received by the receiver of SU pair k from transmitters of all other SU pairs in coalition S_c, $\mu_{S_c} = \sum_{k \in S_c} \mu_k$ is the portion of the bandwidth W being allocated to coalition S_c, h_{kk} represents the channel component for the SU pair k, and h_{jk} represents the channel component between the transmitter of SU pair k and receiver of SU pair k. After the coalition formation algorithm has converged, the set of coalitions will be $CoA = S_1, S_2, S_3, ..., S_C, ..., S_\zeta$, where ζ is the total number of formed coalitions. When ζ is less than or equal to the number of sub-channels ($\mathcal{C}$), then all coalitions will get at least one channel. Whereas, if $\zeta > \mathcal{C}$ then, there will be at least one coalition which will not get any channel. Therefore, the second case may not converge. Further, ζ or the size of the set CoA should lie between 1 and $|\mathcal{P}|$, i.e., $1 \leq \zeta \leq |\mathcal{P}|$. Naturally, the second case of $\zeta > |\mathcal{P}|$ is unrealistic.

Algorithm 1 Algorithm for SU pair coalition formation

Inputs: Total number of PUs (T), total number of SU pairs ($|\mathcal{P}|$), total number of channels (C), probability of SU pairs picking up a channel (P).
Output: List of Coalitions of (CoA)

/*Phase 1: Finding the potential SU pairs for coalition formation or Initialization*/
/*Phase 2: Coalition Formation*/
Use pseudo-random number generator to pick SU pairs i and j.
while *SU pair i and SU pair j do not change their coalitions* **do**
  Check and compare their payoffs with each other;
  if *(SU pair i's payoff is less than the combined payoff of SU pair i and SU pair j) AND (SU pair j's payoff is less than the combined payoff of of SU pair j and SU pair i)* **then**
    max_pay = combined payoff of SU pair i and SU pair j **else**
      max_pay = payoff of individual SU pair i
    end
end
Formation of intermediate coalition list CoA based on max_pay.
/*Phase 3: Check stability criteria*/
$Maxpay$ = MAX(payoff of coalition k with all of its member SU pairs, payoff of coalition k with all of its member SU pairs along with one member SU pair from coalition j, payoff of singleton coalition k).
if $Maxpay$ = *payoff of coalition k with all of its member SU pairs* **then**
  Continue
else if $Maxpay$ = *payoff of coalition k with all of its member SU pairs along with one member SU pair from coalition j* **then**
  Remove the SU pair from coalition j and merge it with coalition k
else
  Remove the SU pair coalition j and maintain it as singleton.
end
Return the final stable coalition list (CoA)

Coalition Formation Algorithm

In Algorithm 1, we present the methodology for SU pair coalition formation. The coalition is formed based on the product of the probability of each SU pair picking up a channel and the incentive or value function associated with each coalition. The probability of each SU pair picking up a channel is a system-defined parameter depending on the configuration of the specific CRN. The initialization phase of the algorithm includes initializing the PUs and the SU pairs on the plane, randomly initializing the power radii of each SU pair, calculating

the Euclidean distance between the given SU pair and other SU pairs, and based on these, forming the potential coalition list. This information is broadcasted over CCC. In most of the cases, the incentive for an SU pair to join the biggest coalition is the highest as there are already more SU pairs in a bigger coalition and more channels are assigned. Then, again, it is imperative that all the SU pairs will judge their own incentive and decide to join the biggest coalition, resulting in a grand coalition.

Ideally, the communication between an SU pair of a coalition should not prevent another SU pair of the coalition from successful communication. This is the reason we decided to introduce the factor of power radius, so that the SU pairs only form an alliance with other pairs who are far enough from each other. This factor results in non-overlapping power radii, which in turn, creates the basis of a healthy communication mechanism. The point to be noted here is that the total combined power radius of an SU pair cannot overlap that of another SU pair. If the combined power radii of two or more SU pairs overlap with each other, then there will be probable communication loss. One could argue that if multiple channels are allocated to a coalition, then in spite of overlapping power radii, different SU pairs could choose different channels and the communication could be carried out successfully. But, we do not always have abundant channels and the proposed algorithm also helps in overcoming the problem of shortage of available channels.

Once initial coalition is formed by checking the max_pay value, we then try to evaluate the stability of a coalition k as follows:

1. Find the maximum payoff max_pay of coalition k with all of its members.
2. If max_pay of coalition k is the greatest, then the coalition is already stable.
3. If max_pay of coalition k is the greatest if one SU pair member comes in from coalition

j, then the new member is incorporated into k, which then becomes stable.

4. If the max_pay value of the member SU pair of coalition j, alone is greater than that of coalition k itself, then we remove that member from coalition j and put it as a singleton.

These calculations are repeated for all the combinations of coalitions and their members, and the final combination with the maximum max_pay value is chosen as the stable coalition(s).

Algorithm 2 Algorithm for modelling adversarial attack

Inputs: SU pair coalition list (CoA)
Output: SU pair coalition list after adversarial attack (CoA)

/*Phase 1: Initiating the adversaries in the same way as the SU pairs*/
/*Phase 2: Attack strategy*/
if *Smart Strategy:* **then**
  1. Communicate the potential target list to other adversaries through adversaries' dedicated CCC.
  2. Attack a SU pair from the potential target list.
  3. Broadcast the attacked target to other adversaries through CCC such that the other adversaries may remove the already attacked SU pairs from their attack list.
else
  4. Attack a SU pair from the potential target list without updating the other adversaries.
end
Return the updated coalition list (CoA)

Adversarial Attack Model

The adversaries in our case are individual SUs, which are capable of transmitting Additive White Gaussian Noise (AWGN) and in turn disrupting the transmission of one SU pair at a time. The adversaries become successful if they are able to block or jam any SU pair's communication, or in other words, forcing the legitimate SU pairs to adopt a different strategy to keep going on with their transmission. Following the concept of Euclidean geometry, we have calculated the distance between an adversary and any one of the SU

pairs. If the power radius of the said adversary overlays (partially or fully) that of the said SU pair, then it is safe to assume that the adversary should be able to block channel used by the SU pair. In Algorithm 2, we show how the adversaries can effectively hamper the stable communication between SU pairs. We propose two types of attack strategies, where adversaries can act either smartly or naïvely rendering to different destructive effect on the proposed framework.

Preliminary Experiments through Simulation

We conduct preliminary experiments through simulation to orchestrate the emulation experimental framework. The simulation for the multi-channel, multi-SU-pair and multi-adversary game has been performed under geographical boundary conditions. Since the objective of this paper is to investigate the coalition formation among multiple SU pairs, we set the values of the parameters which reflect the properties of an SU pair as a whole, such as channel gain and interference between two SU pairs. Hence we keep the trivial properties like distance and the antenna gain between the transmitter and receiver of individual SU pairs to unity. There are 50 SU pairs along with 10 PUs in the system. Each of the PUs use their own designated channel. SU pair knowledge of PU activity is according to the Q values. We have used the following parameters for our simulation runs: Bandwidth $W = 10$ MHz; node deployment area = 100 m^2; transmit power for each node is randomly initialized to a value in (0,1) Watts; and $N_0 = -110$ dBm/Hz. The communication range of each node is set proportional to its transmit power, based on actual IEEE 802.11g WiFi standard [72]. We assume a unity channel gain, i.e., $h_{ij} = 1$ for all transmitters $i = 1..100$ and receivers $j = 1..100$. We study how the average utilities of the coalitions vary when we introduce more adversaries into the system keeping the number of SU pairs and channels constant. For each experiment, we run 10 times and then average them out.

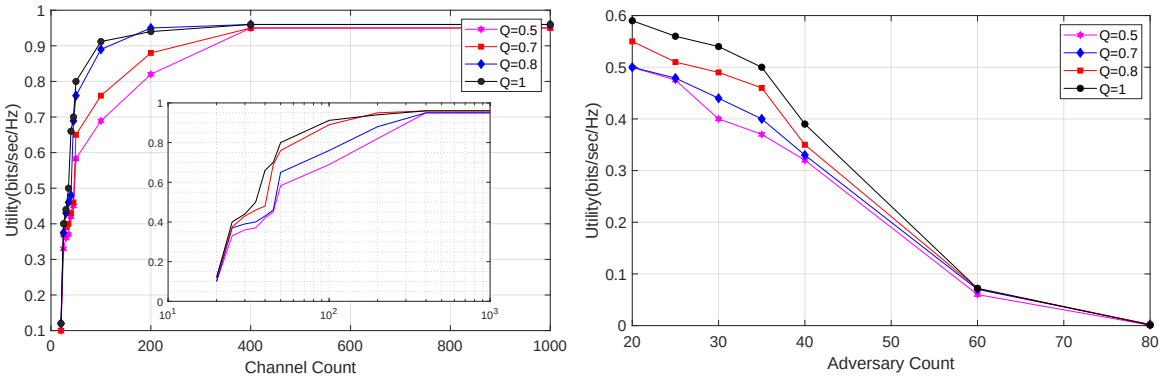

(a) Impact on utility with increasing channel count (35 adv.)

(b) Impact on utility with increasing adversary count (35 channels)

Figure 3.3: Cognisseum Simulation Results: Channel and adversary variations

Procedure

We write the simulation setup in Python 3.10 and run it on a general purpose computer system. Since the main component of our simulation consists of SUs, we take extra care in modeling their game according to the Cognisseum framework, as detailed earlier in this section. We implement the coalition formation algorithm in Algorithm 1 and reinforce the stability criteria of the coalitions. Finally, we introduce the adversarial component into our simulation and implement both the naïve and smart attack strategies by the adversaries. In this process, we vary the Q value and the number of adversaries and channels.

In the following sections, we discuss in detail the insights that we gain after running our simulations.

Impact of increasing channel count on utility

In Fig. 3.3a, we show the general increase in utility (in bps/Hz) in each of the coalitions after adversarial attack with respect to the channel count. Here, for various Q values, we have demonstrated the general trend in the increase of the coalitional utility with increasing channel counts. The total number of adversaries is kept constant at 35. For the case when SU pairs have perfect knowledge of PU activity, i.e., $Q = 1$, we see that the utility increases with increasing channel count, but for extremely high channel counts (over 200), the utility saturates and tends to 1 bps/Hz. When Q is increased from 0.5 to 1, we observe an overall increase in the utility across the range. This behavior is expected because if the SU pairs can predict the PU activities with a higher confidence, their coalitional sum-rate will improve. This set of simulations show that the aggregate utility of the CRN increases with increasing channel count and then it saturates when the channel counts become large. As we increase the number of channels, we observe that the total utility of the 25 coalitions increases by 160%, on average. This happens because, when under attack, the SU pairs have more leeway

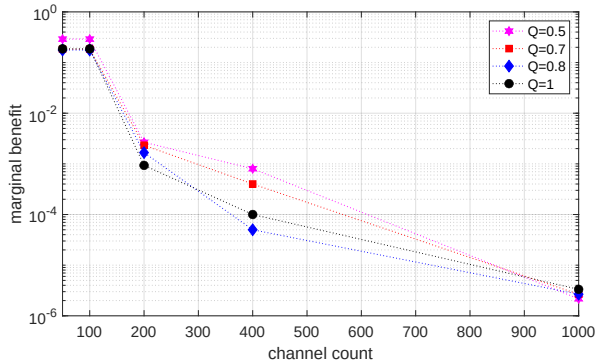

(a) Marginal benefit per additional channel (w.r.t Fig. 3.3a)

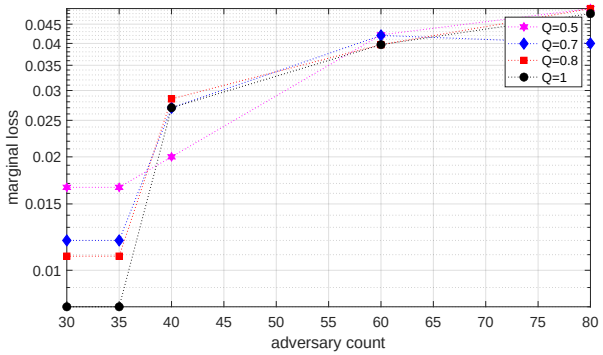

(b) Marginal loss per additional adv. (w.r.t Fig. 3.3b)

Figure 3.4: Marginal utility: Additional benefit or loss w.r.t channel and adversary counts, respectively

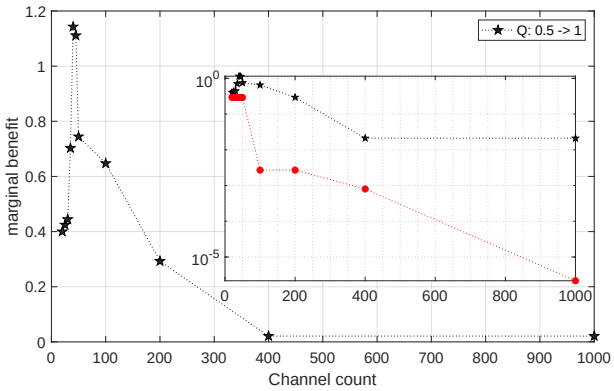

(a) Marginal benefit per additional channel (w.r.t Fig. 3.3a)

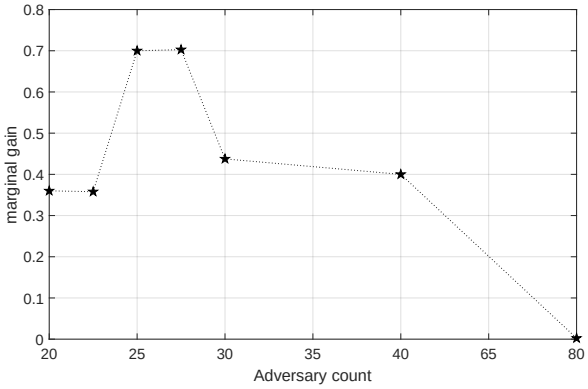

(b) Marginal loss per additional adv. (w.r.t Fig. 3.3b)

Figure 3.5: Advantage of knowing PU activity: Marginal benefits and losses w.r.t. channel and adversary counts

to switch to other channels and continue with their communication.

Impact of increasing adversary count on utility

In Fig. 3.3b, we show the general decrease in utility (in bps/Hz) in each of the SU coalitions after adversarial attack, with respect to the adversary count. Here, for various Q values, we have demonstrated the general trend in the decrease of the coalitional utility with increasing adversary count. The total number of channels is constant at 35. When Q is increased from 0.5 to 1, we observe an overall increase in the utility across the range, due to reasons explained before. This set of simulations show that the aggregate utility of the CRN decreases with increasing adversary count. We infer that the total utility for 25 coalitions decreases with increasing number of adversaries from 20 to 80. As we increase the number of adversaries, we calculate the total utility of the 25 coalitions decreases by about 200%. It is evident that when the number of adversaries deployed becomes large enough, they can render the entire system of CRN useless.

Marginal utility calculation

Now, we focus on the aspect of marginal utility calculation. In Fig. 3.4a, we show the marginal benefit in utility per additional channel. In order to calculate this, we consider the percentage improvement in utility per additional channel. For example, when the number of channels is increased from 20 to 50 (in Fig. 3.3a), we calculate the percentage increase in the utility. Then, we divide this percentage increase by the increase in channel count, i.e., $50 - 20 = 30$, in this case. This gives us marginal utility per additional channel. For every Q value, we plot these marginal benefits per additional channel as shown in the figure. We notice that for channel count increment till 50, for every Q value, the marginal benefit is the biggest, so much so to make other benefits negligible. This has been captured in this figure with by switching the y-axis to logarithmic scale. From this figure we conclude that only when the channel count is initially increased from 20 to 50, we see the highest marginal benefit compared to the rest of increment sets.

In Fig. 3.4b, we show the marginal loss in utility per additional adversary. In order to calculate this, we consider the percentage deterioration in utility for a set amount of increment in adversary count. For example, when the number of adversaries is increased from 20 to 30 (in Fig. 3.3b), we calculate the corresponding percentage decrement in utility. Then, we divide this percentage decrement amount by the increment in adversary count, i.e., $30 - 20 = 10$, in this case. This gives us additional loss in terms of utility that we suffer per additional adversary. For every Q value, we plot these marginal losses for adversary increments as shown in this figure (y-axis in logarithmic scale). We notice that for every Q value, we see progressively worse marginal benefit or higher marginal loss when adversaries are added.

A key issue is the amount of advantage possible with more knowledge of PU activity. In

Fig. 3.5a, we show the marginal benefit in utility with higher Q value, shown with the black scatter plot. In order to calculate this, we consider the percentage improvement in utility from $Q = 0.5$ to $Q = 1$. For example, when the Q value is increased from 0.5 to 1 for 100 channels (in Fig. 3.3a), we calculate percentage increase in utility. Then, we divide this percentage increase in utility by the increase in Q values, i.e., $1 - 0.5 = 0.5$. This gives us the marginal benefit in terms of utility that we get with higher Q value. For every channel count we plot these marginal benefits for Q value increment. We notice that for channel count range from 20 to 1,000, the marginal benefit increases and then drops down. The highest marginal benefit is observed for 40 channels. Comparing this to Fig. 3.4a, for the case $Q = 0.5$, we see the marginal benefits while increasing channel count from 20 to 50 is much less than that seen while increasing the Q values. Not only that, the marginal benefit for $Q = 0.5$ across the range of channel increments (denoted by the dotted red line in the inner plot, with y-axis in logarithmic scale) is lower than that offered by increasing the Q values (denoted by the dotted black line in the inner plot). This enables us to conclude that investing in techniques to improve the SU pair knowledge probability about PU activity in the CRN offers more fruitful outcomes in terms of improving the utility of the coalitions, as compared to investing in increasing the channel count.

In Fig. 3.5b, we show the marginal benefit in utility with higher Q value as adversary count varies. In order to calculate this, we consider the percentage increase in utility as Q increases frpm 0.5 to 1. For example, when the Q value is increased from 0.5 to 1 for 30 adversaries (in Fig. 3.3b), we calculate the percentage increase in utility. Then, we divide this percentage increase by the overall increase in Q, i.e., $1 - 0.5 = 0.5$. This gives us additional benefit in terms of utility that we get per increase in Q. For every adversary count we plot these marginal benefit of knowing more about the PU activity. We notice that for adversary count range from 20 to 80, increasing Q from 0.5 to 1, the marginal benefit increases and then

drops down. The highest marginal benefit is observed when there are about 30 adversaries in the system.

Observation 1 *With increasing number of channels, the Cognisseum framework enables better channel utility (see Fig. 3.3a). Also, with decreasing knowledge of PU activities among the SU pairs while increasing channel count, coalitional utility takes a hit (see Fig. 3.4a).*

Observation 2 *With increasing number of adversaries, the Cognisseum framework suffers worse channel utility (see Fig. 3.3b). But, with increasing knowledge of PU activities among the SU pairs while increasing adversary count, coalitional utility actually improves (see Fig. 3.5b).*

Observation 3 *The marginal benefit of increasing the knowledge of the SU pairs about PU activities in the CRN proves to be more when compared to that of just increasing the channel count (see Fig. 3.5a).*

Observation 4 *The marginal loss incurred by increasing the adversary count deteriorates the overall R of the CRN (see Fig. 3.4b).*

Smart vs. naïve attack strategies by the adversaries

The adversaries can choose to be smart or naïve. If they act smart, they should be communicating among themselves through their dedicated CCC and broadcast their SU communication blocking information to others. The potential targets for an adversary are decided by its power radius. Any of the SU pairs falling under that power radius could be chosen by the adversary to block. Now, based on the random geographical position in which

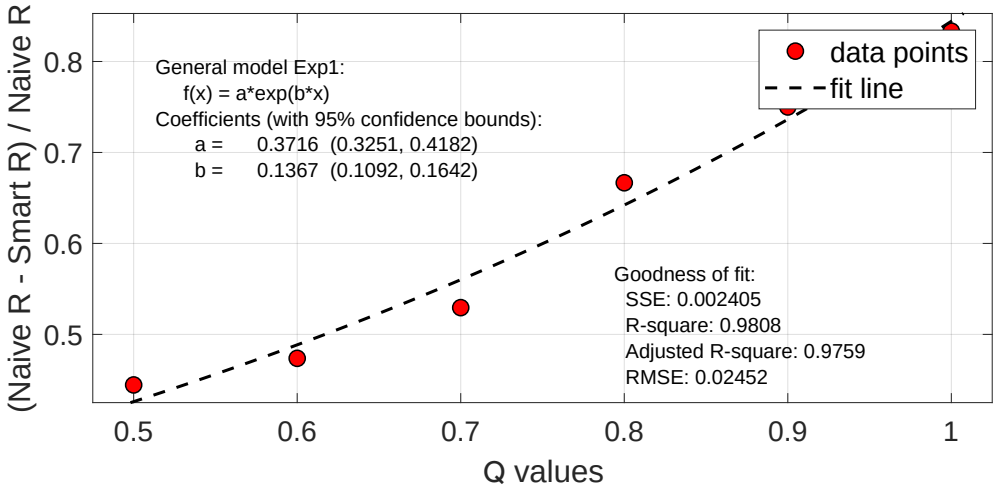

Figure 3.6: Cognisseum Simulation Results: Smart vs. naïve normalization for various Q values

all the SU pairs and adversaries are deployed, it could so happen that another adversary might have the same SU pair in its potential blocking list as the previous one. If both of them end up blocking the same one, then they will be wasting their resources and their payoffs as the whole adversarial group will drop. Hence, a smart adversary should always choose an SU pair and communicate its choice to other adversaries (over dedicated CCC), so that they can concentrate on blocking others. In this way, the adversaries as a coalition will be able to wreck a bigger havoc.

On the other hand, adversaries working naïvely without communication will not be able to do as much damage as compared to them working smartly. In Fig. 3.6, we have compared the normalized utilities of all the 25 formed coalitions with respect to the naïve approach (by taking the utility difference of the two approaches and dividing that with the utility of the naïve approach). In this figure, for various P values, we have plotted the coalitional utility normalized with respect to the naïve attackers. With increasing P values, the normalized utility increases following an exponential curve, denoted by the dotted fit

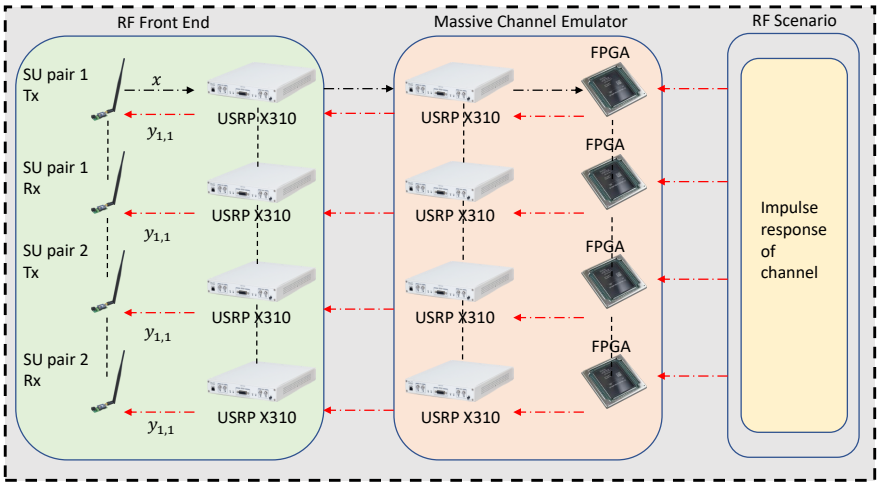

Figure 3.7: Colosseum Architecture

line in the graph. The goodness of fit for this curve is 0.9808. Hence, we conclude that with increasing knowledge of PU activities, smart attack strategy by the adversaries is able to deal exponentially more damage on the CRN.

Cognisseum: Hardware Emulations on Colosseum

In this section, we discuss how we setup our CRN experiments on the emulation platform Colosseum. We implement the multi-SU-pair multi-attacker CRN concept on Colosseum [3], a large-scale wireless emulator.

Colosseum Wireless Emulator

The Colosseum emulator was originally developed to support DARPA's Collaborative Spectrum Challenge [73] and is now a part of the NSF Platform for Advanced Wireless Research (PAWR) [74] program. A detailed description of the Colosseum architecture has been given

in [75]. Here, we will discuss some of the important features for the ease of understanding the rest of the discussion.

From a birds-eye view, Colosseum consists of 128 Standard Radio Nodes (SRNs), a Massive Channel Emulator (MCHEM), a Radio Frequency (RF) server, and a management infrastructure. Users can control the SRNs remotely to conduct experiments. Each SRN is a combination of 48-core Intel Xeon server, an NVIDIA Tesla GPU and Ettus USRP X310, operating between 10 MHz and 6 GHz. In Fig. 3.7, we have shown three blocks: the RF front end, MCHEM, and RF Scenario. The SRNs are part of the RF front end. For our experimentation, we utilize SRNs in multiples of 2 (in accordance with our assumptions stated before). We use two SRNs (a transmitter and a receiver) to create an SU pair. Each of the two SRNs consists of an individual USRP device.

Colosseum has four Internet-facing interactive components as follows [76]:

1. *SSH Gateway*: The gateway address is: '192.10.14.202', which acts as the door for the user to access all of Colosseum's resources.

2. *User website*: 'https://experiments.colosseum.net': Used for setting up Colosseum resource reservations.

3. *File-Proxy server*: From the gateway, users can access their Colosseum network storage, including image directory. If a custom SRN image needs to used, it should be uploaded using File-Proxy server.

4. *SRNs*: These are the actual USRP X310 radio devices which can be allocated to users during their reservations with specific pre-loaded Linux container.

Wireless channel emulation is done by the MCHEM. It contains its own set of 128 USRPs,

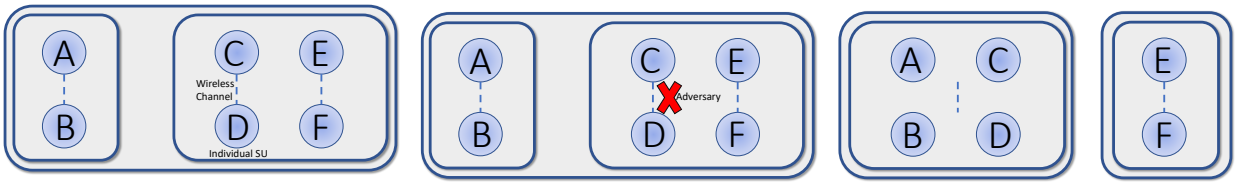

(a) Two coalitions **(b)** Adv. attacks bigger coalition **(c)** Link C-D switches coalition

Figure 3.8: Representation of Emulated CRN in Cognisseum

connected in a one-to-one fashion with those in the RF front end. Apart from the USRPs, MCHEM also contains Field Programmable Gate Array (FPGA) modules which process the digital signals generated by the RF front end. During an RF transmission, the signals generated by the USRPs in the front end gets transmitted to the corresponding USRPs in the MCHEM that convert the RF signals to baseband. Finite Impulse Response (FIR) filters on the FPGAs process the signals. The Channel Impulse Response (CIR) between any two SRNs is captured using the 512 FIR filter taps. These channel taps are then applied to signal x through a convolution operation. The effects of the wireless channels are made possible by the scenarios that include path loss and fading. The RF scenario server maintains a catalog of all Colosseum RF scenarios and feeds their channel taps to the channel emulator at run time.

Hardware-Based Emulation in Colosseum

We build up on the software-based approach during emulation on Colosseum. Here, we work with a limited set size of coalitions already-formed and assumed to have allocated channels. We achieve this by reserving individual Software-defined Radio Nodes (SRNs) and grouping them in a pairwise basis - a transmitter and a receiver. Coalitions are represented by grouping such pairwise transceivers. The channel conditions of the SRNs are based on [77] and we do

not modify them. In order to signify a pair utilizing a sub-channel, we use a channel that has the least amount of permissible pathloss (0 dB pathloss) in Colosseum. In order to signify a coalition having to share its resources (channel(s)) after getting merged with another coalition, we use a channel with higher pathloss. During the experiments on Colosseum, although the radios have a transmit power, we do not consider the power radii of the radios as in the simulation, because we assume the coalitions to be already formed. We start with a predetermined coalition structure and see how the overall network throughput varies for various changes that we make to the coalition structure after introducing the adversaries. As mentioned above, a good channel is one with 0dB pathloss and increasing the pathloss of a channel makes it progressively worse, making it suitable to use for sub-optimal cases like a coalition having to share its resources.

In the simulation setting, we consider the legitimate SU pairs and adversaries are using different channels and forming coalitions and, at the same time, being attacked by the adversaries. The adversaries, as well, may opt to use a smart or naive approach as discussed earlier.

Setting up Experimental Parameters

Fig. 3.8 shows the high-level picture of our emulation setup to experiment with the concept of SU coalitions under attack(s) from adversaries (PU presence is assumed but not emulated as our experiments deal with SUs). We start our experiment with a total of six SRNs acting as three SU pairs. Initially, we have two coalitions (see Fig. 3.8a). Nodes A and B communicate with each other over a single channel and they form a single coalition. On the other hand, user pairs A-D and E-F form a bigger coalition; each link gets one channel each. For 300 seconds, we let this setup continue communicating among themselves. We measure

the data rates of individual links and compute the sum rate of all the links for 300 seconds.

In our setup, initially, all SU pairs use 0dB path loss channels (using the 0dB path loss scenario on Colosseum) and we have three channels in total. We use network performance measurement tool `iPerf3` to generate TCP traffic between the transmitters and receivers of the SU pairs. In each of the SU pairs, one acts as the iperf server while the other acts as the iperf client. At 300th second, the adversary joins the network. Unlike the legitimate SU pairs, the adversaries do not work in pairs, rather, they are equipped with a transmitter blasting away AWGN in a specific channel, rendering it useless.

Emulation Results

In this section, we discuss and analyze the results that we get from the emulation part of our Cognisseum framework. Fig. 3.8b illustrates an adversary with a red cross. The adversarial node decides to block channel 2, which is being used by the SU pair C-D. After being attacked, the SU pair C-D has two options: either join the coalition containing A-B

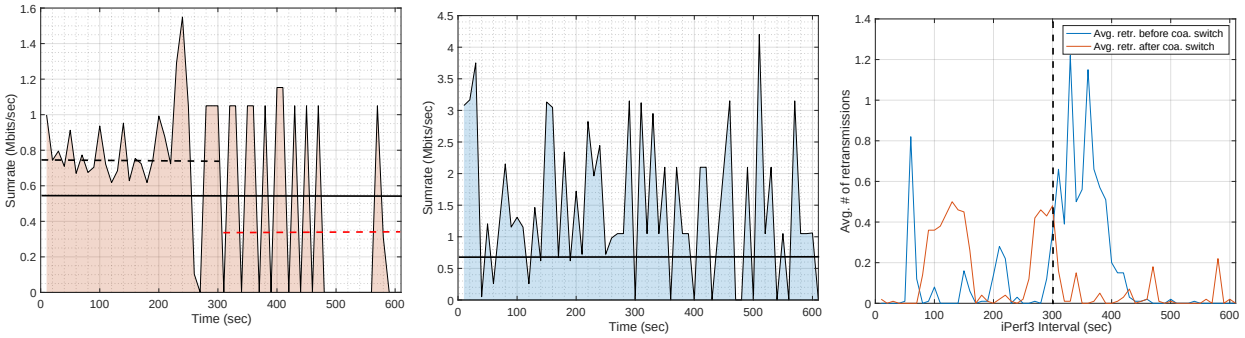

(a) Sumrate before pair C-D switches coalition

(b) Sumrate after pair C-D switches coalition

(c) Avg. retransmissions before and after attack

Figure 3.9: Cognisseum Emulation Results

or be singleton. For our experimental setup, we have programmed the pair C-D to join A-B. Fig. 3.8c shows the coalition set after C-D joins A-B. Here, A-B and C-D pairs communicate over the same channel and the E-F pair has its own channel. The channel originally used by C-D is now blocked by the adversary. After the coalition switch by C-D, the SU pairs keep communicating for another 300 seconds. To emulate two links communicating over the same channel, we have chosen a different scenario ID in Colosseum that emulates a channel with 20 dB path-loss. Hence, we use 20 dB path-loss channel for the bigger coalition consisting of the A-B and C-D pairs and the smaller coalition consisting of the E-F pair continues to use a 0dB path-loss channel.

TCP throughput of the coalition set degrades significantly after the attacker joins. As shown in Fig. 3.9a, the dashed black line signifies the sum rate before the adversary attacks the channel used by pair C-D (before the 300 seconds mark). The dashed red line signifies the sum rate after the attack (after the 300 seconds mark). The solid black line denotes the overall average sum rate of all the three pairs in the whole duration of 600 seconds. We have set the `iPerf3` software to record the individual link rate (in Mbits/sec) in intervals of 0.1 second. We have chosen a small interval to better understand how the linkwise rate varies in a sub-second interval when the experiment runs for a long time. Then, we analyze the results after a 10-minute run on Colosseum. During analysis, we take the average of 10 second intervals and plot the results for a total of 600 seconds. Sum rate of each of the 10-second interval is marked by the individual spikes in the line plot. The final plots are made after averaging several 600-second runs on Colosseum.

Now, we study how the sum rate of the coalition set varies after the link C-D switches coalition. Fig. 3.9b shows the overall sum rate of all the three SU pair after the C-D pair has switched coalition. The data has been collected in the same way as in Fig. 3.9b. Here, the solid black line indicates overall sum rate of three SU pairs. Comparing the two figures,

we see the overall sum-rate is indeed higher after the SU pair C-D has switched coalition, when compared to that before the switch (marked by the dashed red line in Fig. 3.9a).

We also look into the number of retransmitted packets using `iPerf3`. Fig. 3.9c is about the average number of retransmitted data packets in the TCP protocol used in the `iPerf3` software. Before adversary attack (till the the 300 sec. mark), the average number of retransmissions before the coalition switch is (blue line) shows a lower number. After the adversary attacks the bigger coalition, the total number of retransmissions shoots up, signifying the channel between pair C-D getting blocked. Once the switch is made the plot showing the total retransmissions in orange is overall lower.

Observation 5 *The overall study presented in the emulation corroborates the fact that the adversary can be a deterrent in the ongoing communication among legitimate SU pairs in a CRN. Due to the limited number of channel resources present in a coalition, when an additional SU pair joins and starts utilizing the resource of the coalition after being attacked by the adversary, the SU pair is able to attain a higher link capacity and the sum rate of the coalitions improve when compared to that before the SU pair switches to the new coalition (See Figs. 3.9a and 3.9b).*

Summary

In this chapter, we have devised two distinct approaches as part of Cognisseum: software simulation and hardware-based emulation using the large scale wireless channel emulator called Colosseum.

In the simulation, we showed how SU pairs in an ad-hoc CRN can create coalitions autonomously in the absence of base stations to increase their payoffs. We presented an intelligent coalition

formation algorithm and formulated the payoff function for the calculation of the utilities of the SU pairs in terms of throughput/sum rate. We have devised a coalition formation algorithm which can be used by SUs in the CRN to find potential partners for coalition formation. Using these potential coalitions, we have come up with the final coalition model. We also introduced adversaries in the proposed framework and modelled an algorithm for adversarial attack against the legitimate SUs. Next, we presented the data which shows percentage decrease in the average utilities with varying number of adversaries, keeping the number of SUs and channels constant. Then, we showed the increase in coalition utility with increasing number of channels, keeping the number of SUs and number of adversaries as constant along with the difference in coalition utilities for smart and naive adversarial attack strategies.

In the emulation part, we have shown a novel approach towards the calculation of coalitional sum rate before and after adversarial attack using our proposed coalition structure. We have used a variety of channel scenarios to emulate the SU pairs being singleton or part of a coalition. We even modeled a hardware-based adversary and discussed how that hampers communication within a coalition and showed ways by which an SU pair can protect itself by switching coalitions. We have also provided insight into the `iPerf3` software that we have used to record network activity and provided details on packet retransmissions in the TCP framework.

Overall, we believe that this piece of work is the first of its kind to merge a software based simulation solution with the Colosseum platform that models a CRN along with adversarial presence. We envision that this research will serve as a benchmark in the future endeavour of implementing a functioning and complex CRN using Colosseum.

CHAPTER 4: DIRECTIONAL RADIO COALITION FORMATION (CENTRALIZED AND DECENTRALIZED METHODS)

Introduction

Emerging mobile 5G-and-beyond communication technologies rely on mmWave bands (28-300GHz), which provide higher data rates and bandwidth. Highly directional antennas are necessary for practically accessing these frequencies as the transmissions are vulnerable to path loss and atmospheric absorption. Substantial work [78] has been done to address these issues like designing high gain antennas with appropriate beamforming for mitigating propagation loss. However, due to the line-of-sight and alignment requirements of directional transmission, integrating these antennas into mobile and ad-hoc settings is a challenge. Further, in settings with no or minimal infrastructure support (e.g., battlefield or emergency communication), nodes need to form coalitions to attain successful and efficient transmissions [36].

A key benefit of coalitions is higher spatial and frequency reuse. Without coalitions, all inter-node communication has to go through a base station (BS), which limits the aggregate throughput. On the other hand, many nodes participating in a single coalition can use as few as one channel (assigned to the entire coalition) to communicate among themselves and one node in the coalition can forward the message to the BS using one channel. Coalitions of omni-directional radios have been studied heavily for higher throughput [79], higher spectrum efficiency [80], or stronger security against attackers [81]. However, understanding how directionality changes the establishment of coalitions among radios has not been explored

well.

In this chapter, we explore the concept of 'directional coalitions' among radios utilizing mmWave bands. We consider a collection of highly directional mmWave radio nodes scattered randomly on a 2-dimensional plane. Each node is initialized with its field-of-view (FoV), which limits what other nodes it could potentially talk to. The scheduling of data transmission among the nodes is assumed to be regulated by the BS in phases of downlink and relay. During these phases, the nodes use an optimized set of steering angles and follow randomly scheduling for transmission. Under this phased random scheduling assumption, we formulate achievable rate of a directional coalition. Considering various aspects such as roles of the nodes within a coalition, proximity of the nodes and coalitions to each other, and size of the coalitions, we devise heuristics that aim to maximize the sum rate of all coalitions. We theoretically study our framework and numerically evaluate its heuristics in terms of solving the problem of forming a set of coalition that maximizes the sum rate while making sure all nodes are included in a coalition. Our work's key novelty lies in role categorization of directional nodes and using these roles to guide development of fast coalition formation heuristics, both centralized and decentralized/ad-hoc. We make the following contributions [82, 83]:

- A step-by-step formal method to categorize directional antenna nodes based on their FoVs and illustration of the method on networks of nodes of varying sizes.
- Formulations of directional link capacities when transmissions are randomly scheduled.
- Calculation of coalitional sum rate or throughput using the scheduling methods and channel allocation schemes.
- Heuristics for forming coalition sets (in both centralized and decentralized manners)

that place all/some network nodes to a coalition set, and exploring possibilities of merging coalitions to improve the network sum rate.

- Simulation-based evaluations of the centralized/ad-hoc coalition set formation heuristics in terms of sum rate of all coalitions.

System Model and Problem Statement

Consider mmWave nodes spread over a fixed two dimensional region, that wish to communicate using a channel with bandwidth B. Our goal is to structure them into disjoint and autonomous coalitions. The coalition formation is assumed to be coordinated by a base station (BS) using a secure and interference-free Common Control Channel (CCC). Each node in a coalition is equipped with a half-duplex beam-steerable directional antenna, and hence is capable of steering its beam within the range of its field-of-view (FoV). Given the location and FoV of each node, our goal is find the optimal coalition set formation such that the sum-rate of all coalitions is maximized.

All-Covering Max-Throughput Coalition Set (For Centralized and Decentralized Approaches)

Let $\mathcal{A} = \{\mathcal{A}_1, \mathcal{A}_2, ..\mathcal{A}_A\}$ represent the set of mmWave nodes with directional antennas, where node $\mathcal{A}_i$ is located at Cartesian location (x_i, y_i) for $i = 1, .., A$. The nodes are partitioned into C disjoint coalitions, denoted as $\text{coa}_1, \text{coa}_2, .., \text{coa}_C$ such that $\text{coa}_q \subseteq \mathcal{A}$ for $q = 1, .., C$ and $\text{coa}_k \cap \text{coa}_l = \emptyset$ for all k, l. Due to limited FoV, some nodes in $\mathcal{A}$ cannot establish a communication link with other nodes. These nodes will be isolated and cannot be part of any coalition, which means the union of coalitions may not be equal to $\mathcal{A}$, i.e., $\bigcup_{n=1}^{C} \text{coa}_n \subseteq \mathcal{A}$.

Let set $\Omega = \{\text{coa}_1, \text{coa}_2, ..., \text{coa}_C\}$ be an all-covering coalition set, ensuring all nodes in $\mathcal{A}$, except the isolated nodes, are included in different coalitions. The structure of nodes within a coalition and the feasible links for intra-coalition communication are determined based on the FoVs of the nodes. Let $R(\text{coa}_n)$ denote the achievable communication rate of nodes in coalition coa_n and $R(\Omega)$ be the sum-rate across all coalitions. Then, we have $R(\Omega) = \sum_{n=1}^{C} R(\text{coa}_n)$.

Given that Ω consists of C coalitions, the problem of finding the optimal coalition set Ω that maximizes $R(\Omega)$ can be formulated as the following:

$$\begin{aligned} \text{Given } C, \qquad & \Omega^* = \arg\max R(\Omega) \\ & s.t. \;\; \text{coa}_q \subseteq \mathcal{A}, \forall q; \qquad \text{coa}_k \cap \text{coa}_l = \emptyset, \forall k, l; \\ & \bigcup_{n=1}^{C} \text{coa}_n \subseteq \mathcal{A}; \qquad \bigcup_{n=1}^{C} \text{coa}_n \equiv \mathcal{A}' \end{aligned} \tag{4.1}$$

where $\mathcal{A}'$ is the set of nodes in $\mathcal{A}$ that can form a link with at least one other node. Since it assumes a fixed count of coalitions, the problem in (4.1) is a simpler version of the main problem we aim to solve where C can be any integer in $[1, A]$. To analyze the computational complexity of the main problem, we define C empty sets, denoted as $\text{coa}_1, \text{coa}_2, ..., \text{coa}_C$. Let the binary variable a_i^n indicate whether or not node $\mathcal{A}_i$ is in the set coa_n, i.e., if $a_i^n = 1$ then $\mathcal{A}_i$ is in the set coa_n, and if $a_i^n = 0$ then $\mathcal{A}_i$ is not in the set coa_n. Given C, finding Ω^* requires solving a_i^n for $i = 1, ..., A, n = 1, ..., C$, i.e., solving AC binary variables. Finding Ω^* requires solving the above problem for each C values, where $C = 1, ..., A$. Hence, the computational complexity of finding Ω^* is upper bounded by the solution search space, i.e., $\mathcal{O}(A2^{A^2})$. Exhaustively scanning this search space to find the optimum partitioning of the nodes to coalitions is prohibitive as it is known to be an NP-complete problem [84]. Hence, we resort to designing effective heuristics to form coalition sets.

Partially-Covering Coalition Set (For Decentralized Approach Only)

With the set of assumptions mentioned before, the problem of decentralized coalition set formation can be written as an optimization problem. The problem of finding the set of coalitions Ω which maximizes R can be written as follows:

$$\begin{aligned} \text{Given } C, \qquad & \Omega^* = \arg\max R(\Omega) \\ & \text{s.t.} \;\; \text{coa}_q \subseteq \mathcal{N}, \forall q; \\ & \text{coa}_i \cap \text{coa}_j = \emptyset, \forall i, j. \end{aligned} \tag{4.2}$$

Here, set Ω^* is the coalition set that maximizes the coalitional sum rate R. Also, any coalition consisting of nodes become a subset of set of nodes $\mathcal{N}$ and no two coalitions are overlapping. Since we assume a fixed count of coalitions, the problem in (4.2) is a simpler version of the main problem we aim to solve where C can be any integer in $[1, N]$. Here, we are not enforcing any constraint such that all nodes present in set Ω^* must be present in set $\mathcal{N}$, and hence we call this 'partially-covering coalition set'.

All-Covering Coalition Set (For both Decentralized and Centralized Approaches)

We use the same set of assumptions as before. However, the problem of finding the best set of coalitions Ω that maximizes R becomes as follows:

$$\text{Given } C, \qquad \Omega^* = \arg\max R(\Omega) \tag{4.3}$$

$$\text{s.t. } \text{coa}_q \subseteq \mathcal{N}, \forall q;$$

$$\text{coa}_i \cap \text{coa}_j = \emptyset, \forall i, j;$$

$$\bigcup_{n=1}^{C} \text{coa}_n \equiv \mathcal{N}' \tag{4.4}$$

where $\mathcal{N}'$ is the set of nodes that can establish a link with at least one other node. This version of the problem is called 'all-covering coalition set' problem because other than the isolated nodes, we enforce the additional constraint (4.4) which enforces that all nodes that can form a link with another node are included in a coalition.

The computational complexity of finding Ω^* is upper bounded by the solution search space, i.e., $\mathcal{O}(A2^{A^2})$ for $|\mathcal{N}| = A$ nodes. Exhaustively scanning this search space to find the optimum partitioning of the nodes to coalitions is prohibitive. Further, the problem of finding Ω^* is known to be NP-complete [82, 84]. Henceforth, we design novel and effective coalition set formation heuristics that are able to form all-covering coalition sets as well as partial-covering coalition sets that maximize R.

Structure of Nodes within a Coalition

Potential Coalition Partners (PCPs). Recall the set of nodes $\mathcal{A}$ has A elements, i.e., $|\mathcal{A}| = A$. We associate each node $\mathcal{A}_i \in \mathcal{A}$ with a set $\text{PCP}_{\mathcal{A}_i}$ consisting of the nodes in $\mathcal{A}$ that

$\mathcal{A}_i$ can potentially establish a directional wireless link with, and hence they are "Potential Coalition Partners (PCPs)" of $\mathcal{A}_i$. A node $\mathcal{A}_j \in \mathcal{A}$ belongs to set $\text{PCP}_{\mathcal{A}_i}$ if and only if $\mathcal{A}_j$ and $\mathcal{A}_i$ are within FoVs of each other. We denote the communication link between $\mathcal{A}_i$ and $\mathcal{A}_j$ by $(\mathcal{A}_i, \mathcal{A}_j)$. We note the following:

- If two nodes are within FoVs of each other, their PCPs must include each other. Therefore, two nodes can form a link iff they fall within each other's PCPs.
- If $|\text{PCP}_{\mathcal{A}_i}| = 0$, $\mathcal{A}_i$ cannot communicate with any other node and hence cannot be part of any coalition.

Isolated Nodes, Primary Antenna, and Secondary Antenna. We call the nodes with empty PCPs *isolated nodes*. Excluding the isolated nodes from the set $\mathcal{A}$, we categorize the remaining nodes in $\mathcal{A}$ as *Primary Antenna (PA)* or *Secondary Antenna (SA)* nodes. Node $\mathcal{A}_i \in \mathcal{A}$ is a PA if $|\text{PCP}_{\mathcal{A}_i}| > 1$, i.e., a PA node can potentially establish links with more than one other nodes. Node $\mathcal{A}_i \in \mathcal{A}$ is an SA if $|\text{PCP}_{\mathcal{A}_i}| = 1$, i.e., an SA node can potentially establish a link with only one other node. Let $\mathcal{A}^p = \{\mathcal{A}^p_1, \mathcal{A}^p_2, ..., \mathcal{A}^p_D\}$ and $\mathcal{A}^s = \{\mathcal{A}^s_1, \mathcal{A}^s_2, ..., \mathcal{A}^s_V\}$ signify the sets of PAs and SAs, respectively, and $\mathcal{A}^p_i$ and $\mathcal{A}^s_j$ be the ith PA and the jth SA, respectively. Clearly, $\mathcal{A}^p \subseteq \mathcal{A}$, $\mathcal{A}^s \subseteq \mathcal{A}$, and $\mathcal{A}^s \cap \mathcal{A}^p = \emptyset$. Let $\{\mathcal{X}\}^s$ and $\{\mathcal{X}\}^p$ represent the sets of SAs and PAs in set $\mathcal{X}$, respectively. Then, $\{\text{PCP}_{\mathcal{A}_i}\}^s$ and $\{\text{PCP}_{\mathcal{A}_i}\}^p$ represent, respectively, the sets of SAs and PAs that node $\mathcal{A}_i$ can potentially form a link with. Table 4.1 shows a summary of our notations.

The classification of nodes into SA or PA categories enables the following interesting observations regarding forming of an all-covering coalition set:

1. *An SA-only coalition can have only two nodes.*

2. *An SA-PA coalition must have least one PA and at least two SAs.* In a coalition including PA(s) and SA(s) nodes, there must be at least two SAs. For the PA node, there will have to be at least two SAs otherwise the PA would not be a PA.

3. *A PA-only coalition has at least three PAs.*

These observations enable design of very fast heuristics for forming coalition sets out of directional radios.

Table 4.1: List of symbols and their descriptions

Symbol	Description
$\mathcal{A}$	Set of all nodes in the network
$\mathcal{A}_n$	nth node
$\mathcal{A}^p$	Set of all PA nodes
$\mathcal{A}^p_u$	uth PA
$\mathcal{A}^s$	Set of all SA nodes
$\mathcal{A}^s_v$	vth SA
$\mathcal{A}(\mathcal{A}_n)$	Set of nodes in FoV of $\mathcal{A}_n$
$\text{PCP}_{\mathcal{A}_n}$	Set of nodes that $\mathcal{A}_n$ can form a link with
$(\mathcal{A}_m, \mathcal{A}_n)$	Link between $\mathcal{A}_m$ and $\mathcal{A}_n$
$\{\mathcal{X}\}^s$	Set of SAs in the node set $\mathcal{X}$
$\{\mathcal{X}\}^p$	Set of PAs in the node set $\mathcal{X}$

All-Covering Coalition Set Examples. Consider the all-covering coalition set $\Omega = \{\text{coa}_1, \text{coa}_2, ..., \text{coa}_C\}$. Figs. 4.1 and 4.2 provide two examples of an all-covering coalition sets. Without showing the SA nodes in these sets, they can be respectively written as $\Omega_1 = \{\{\mathcal{A}^p_1, \mathcal{A}^p_2, \mathcal{A}^p_3\}, \{\mathcal{A}^p_4, \mathcal{A}^p_5, \mathcal{A}^p_6\}, \{\mathcal{A}^p_7\}, \{\mathcal{A}^p_8, \mathcal{A}^p_9, \mathcal{A}^p_{10}\}$ and $\Omega_2 = \{\{\mathcal{A}^p_1, \mathcal{A}^p_2, \mathcal{A}^p_3\}, \{\mathcal{A}^p_4, \mathcal{A}^p_5, \mathcal{A}^p_8, \mathcal{A}^p_9\}, \{\mathcal{A}^p_6, \mathcal{A}^p_7, \mathcal{A}^p_{10}\}$. We see that, on the same set of nodes, the coalition set formed can be different. The PA nodes along with their SA nodes are marked by blue lines and coalitions are marked by green lines. There is a PA-only coalition in Fig. 4.1 comprised of $\mathcal{A}^p_8$, $\mathcal{A}^p_9$ and $\mathcal{A}^p_{10}$. It is possible that these PAs can join other coalitions and form a different coalition set, as

shown in Fig. 4.1. It is clear from this example that categorizing the nodes into PAs and SAs significantly reduces the number of possible coalition sets. Fig. 5.3 shows the dynamics inside a coalition in more details by zooming into the bottom-left coalition in Figs. 4.1 and 4.2, which is comprised of $\mathcal{A}_1^p$, $\mathcal{A}_2^p$ and $\mathcal{A}_3^p$ and their SA nodes. In Fig. 5.3, the FoV of each node is shown with dashed lines and the feasible links among them with solid lines along with the full list of nodes within each node's FoV.

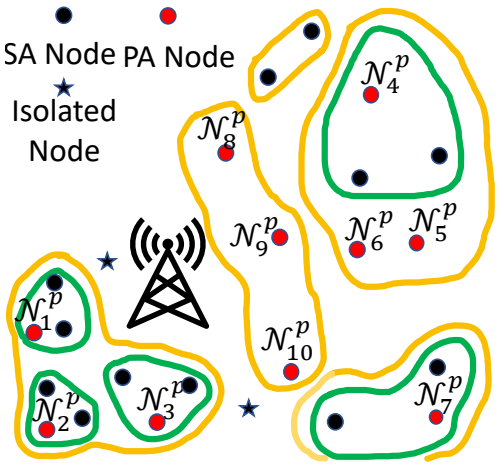

Figure 4.1: Coalition example 1

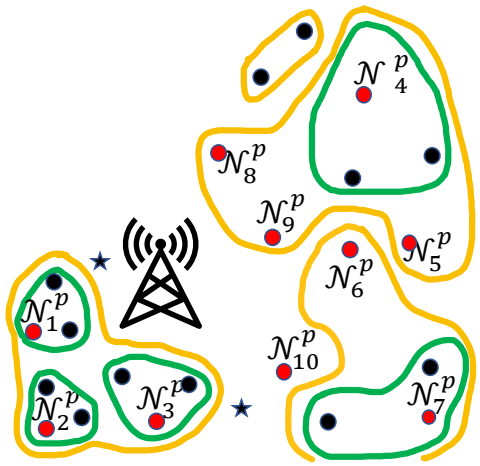

Figure 4.2: Coalition example 2

Scheduling and Bandwidth Allocation

The BS is responsible for finding the best coalition set Ω via solving the coalition formation optimization problem, a simpler version of which is formulated in (4.1). Then, BS informs the nodes to which coalition they belong through the CCC. Once the coalitions are formed, each coalition operates autonomously based on a time-slotted communication mechanism, where time is divided into sub-frames of duration T_f sec, and the nodes in a coalition schedule intra-coalition communication themselves without relying on the BS. We assume intra-coalition communication consists of two consecutive phases: the Downlink Phase and the PA-PA

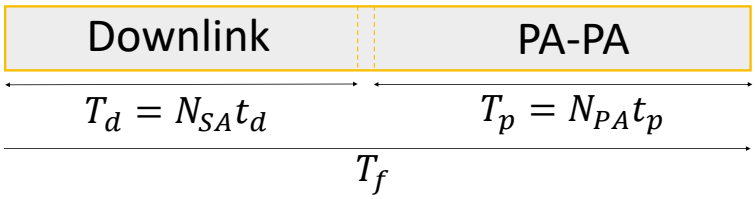

Figure 4.3: Two phases corresponding to a time frame

Phase, with duration T_d and $T_p = T_f - T_d$ sec, respectively (see Fig. 4.3). We define the transmission scheduling of nodes within a coalition in each phase as follows:

Downlink Phase. During this phase, all PA nodes in coa_n are in transmitting mode and all SA nodes in coa_n are in receiving mode. Each PA node acts independently and divides T_d sub-frame equally among the SA nodes in its PCP and transmits data to them during their corresponding allocated time fraction in a deterministic manner. This scheduling does not depend on how other PA nodes utilize their Downlink phase.

PA-PA Phase. During this phase, the SA nodes in coa_n do not transmit or receive, and the PA nodes talk among themselves. Each PA node can be in transmitting or receiving mode with equal probability. Consider $\mathcal{A}_i^p \in \text{coa}_n$ and the set of PA nodes represented by $\{\text{PCP}_{\mathcal{A}_i^p}\}^p$, some of which may be in coa_n. If $\mathcal{A}_i^p$ is in transmitting mode, it randomly chooses a PA node in its PCP that is also in coa_n and transmits data to the chosen PA node. If $\mathcal{A}_i^p$ is in receiving mode, it randomly chooses a PA node in its PCP that is also in coa_n and receives data from the chosen PA node. Suppose $\mathcal{A}_i^p, \mathcal{A}_j^p \in \text{coa}_n$. To establish the link $(\mathcal{A}_i^p, \mathcal{A}_j^p)$, the following three conditions must be met: (i) $\mathcal{A}_i^p$ and $\mathcal{A}_j^p$ are in transmitting and receiving modes, respectively, (ii) $\mathcal{A}_i^p \in \{\text{PCP}_{\mathcal{A}_j^p}\}^p$ and $\mathcal{A}_j^p \in \{\text{PCP}_{\mathcal{A}_i^p}\}^p$, and (iii) $\mathcal{A}_i^p$ chooses to transmit to $\mathcal{A}_j^p$ and $\mathcal{A}_j^p$ chooses to receive from $\mathcal{A}_i^p$ simultaneously.

We let $R(\text{coa}_n)$ be the overall communication rate of nodes in coalition coa_n. Since in this scheduling scheme only PAs transmit, the corresponding communication rate of an SA-only

coalition is zero. Hence, we allocate bandwidth B to PA-only and SA-PA coalitions. Consider the all-covering coalition set $\Omega = \{\text{coa}_1, \text{coa}_2, ..., \text{coa}_C\}$. Suppose $\Omega' \subseteq \Omega$ where Ω' excludes SA-only coalitions and consists of C' PA-only and SA-PA coalitions, and C' is less than or equal to the total number of PA nodes, i.e., $C' \leq D$. Given a total bandwidth B, we devise the following scheme to split B to sub-channels:

Bandwidth Allocation Scheme. B is divided into C' sub-channels with bandwidth $w_1 = \frac{B}{C'}$. During the Downlink Phase, all PA nodes in a coalition transmit simultaneously over the same channel and cause co-channel interference.

During the PA-PA Phase, all transmitting PA nodes in a coalition transmit simultaneously over the same channel and cause co-channel interference. Suppose, $\mathcal{A}_i^p, \mathcal{A}_j^p \in \text{coa}_n$. When the link ($\mathcal{A}_i^p$,$\mathcal{A}_j^p$) is established, $\mathcal{A}_j^p$ is susceptible to interference from other transmitting PA nodes in coa_n that $\mathcal{A}_j^p$ is in their FoVs. Also, $\mathcal{A}_i^p$ imposes interference on other receiving PA nodes in coa_n that are in its FoV. Consider Fig. 5.3 and suppose the network is in Downlink phase. In coa_n four PA nodes are transmitting simultaneously. For example, $\mathcal{A}_1^p$ imposes interference on SA nodes associated with $\mathcal{A}_2^p, \mathcal{A}_3^p, \mathcal{A}_4^p$ that fall within the FoV of $\mathcal{A}_1^p$. Similarly, $\mathcal{A}_2^p$ imposes interference on SA nodes associated with $\mathcal{A}_1^p, \mathcal{A}_3^p, \mathcal{A}_4^p$ that fall within the FoV of $\mathcal{A}_2^p$. This interference will affect the signal-to-interference-plus-noise ratio (SINR) calculation of the links in which the receiving SA node is subject to interference from other transmitting PA nodes in the coalition.

Directional Antenna Model

Consider node $\mathcal{A}_i$ and let Γ_i represent the initial inclination angle of node $\mathcal{A}_i$ with reference to the x-axis, and θ_i denote the steering angle corresponding to the central line of the beam of node $\mathcal{A}_i$ with reference to the positive x-axis. We let node $\mathcal{A}_i$ to freely choose its beam

steering angle θ_i. Let β_i denote the FoV of node $\mathcal{A}_i$, which defines the maximum angular sweeping range of the main beam of $\mathcal{A}_i$. A representation of the deployment of directional nodes along with the parameters of node $\mathcal{A}_i$ is shown in Fig. 5.1. The deviation angle $\psi_{i\to j}$ indicates the digression of the center of the beam of node $\mathcal{A}_i$ away from the straight line connecting two nodes: $\mathcal{A}_i$ and $\mathcal{A}_j$.

A reference directional antenna model with side lobe for IEEE 802.15.3c. is considered. However, in this paper, we focus on the main lobe (without side lobe), applicable for line-of-sight (LoS) transmission that uses high frequency signals like 60 GHz or above, and safely ignore the side lobe gain [85]. Let us assume $G_i(\theta_i)$ is the directional antenna gain of node $\mathcal{A}_i$. Then,

$$G_i(\theta_i) = e^{-(\ln 2)(\frac{\theta_i}{\alpha_i})^2}, \qquad \beta_i^{\min} \leq \theta_i \leq \beta_i^{\max} \tag{4.5}$$

where $\beta_i^{\min} = \Gamma_j - \beta_j/2$ and $\beta_i^{\max} = \Gamma_j + \beta_j/2$ are the minimum and maximum beam steering angles allowed within the FoV of $\mathcal{A}_i$, assuming $\Gamma_j > 2\beta_j$.

SINR Formulation with Directional Antenna

Consider the link $(\mathcal{A}_i, \mathcal{A}_j)$ between two nodes $\mathcal{A}_i \in \mathcal{A}$ and $\mathcal{A}_j \in \mathcal{A}$. Suppose d_{ij} signifies the distance separating the two nodes $\mathcal{A}_i$ and $\mathcal{A}_j$. Also, assume that $\mathcal{A}_i$ is steered towards $\mathcal{A}_j$ with a beam steering angle θ_i. Given the coordinates of $\mathcal{A}_i$ and $\mathcal{A}_j$,the deviation angle $\psi_{i\to j}$ is found (see Fig. 5.1). Let P_t and $P_r(\mathcal{A}_i, \mathcal{A}_j)$ be the transmit power of $\mathcal{A}_i$ and the received power at $\mathcal{A}_j$. Using THz communication channel model in [86], $P_r(\mathcal{A}_i, \mathcal{A}_j)$ can be expressed in terms of P_t as follows:

$$P_r(\mathcal{A}_i, \mathcal{A}_j) = \frac{P_t}{d_{i,j}^{\alpha}} G_i(\theta_i - \psi_{i\to j}) G_j(\theta_j - \pi - \psi_{i\to j}) \tag{4.6}$$

where α is the path-loss exponent, and G_i and G_j are the directional antenna gains of nodes $\mathcal{A}_i$ and $\mathcal{A}_j$, respectively.

Coalition Set Formation: Formal Problem

Consider $\Omega' = \{\text{coa}_1, \text{coa}_2, ..., \text{coa}_{C'}\}$, which is obtained from an all-covering coalition set Ω after removing SA-only coalitions, i.e., Ω' consists of C' PA-only and SA-PA coalitions, and C' is less than or equal to the total number of PA nodes, i.e., $C' \leq D$, where the equality can hold only when no PA-only coalition exists and all coalitions in Ω' are SA-PA coalitions. The sum-rate across all coalitions in Ω' is $R(\Omega') = \sum_{n=1}^{C'} R(\text{coa}_n)$.

We define the binary optimization variable a_ℓ^n to indicate whether or not $\mathcal{A}_\ell^p$ is in coa_n, i.e., if $\mathcal{A}_\ell^p \in \text{coa}_n$ then $a_\ell^n = 1$, and if $\mathcal{A}_\ell^p \notin \text{coa}_n$ then $a_\ell^n = 0$.

Sum Rate Calculations. Let $R_\ell^d(\text{coa}_n)$ denote the contribution of $\mathcal{A}_\ell^p$ during Downlink phase to $R(\text{coa}_n)$ if $\mathcal{A}_\ell^p \in \text{coa}_n$. In particular, $R_\ell^d(\text{coa}_n)$ is the total amount of data (measured in bits/sec) transmitted by $\mathcal{A}_\ell^p$ and received by its associated SA nodes during Downlink phase. In Section 4 we characterize $R_\ell^d(\text{coa}_n)$ in terms of the binary optimization variables a_ℓ^n's.

Let $R_\ell^p(\text{coa}_n)$ denote the contribution of $\mathcal{A}_\ell^p$ during PA-PA phase to $R(\text{coa}_n)$ if $\mathcal{A}_\ell^p \in \text{coa}_n$. $R_\ell^p(\text{coa}_n)$ is the total amount of data (measured in bits/sec) received by $\mathcal{A}_\ell^p$ and transmitted by some other PA nodes in coa_n during PA-PA phase. In Sec. 4 we characterize $R_\ell^d(\text{coa}_n)$ in terms of the binary optimization variables a_ℓ^n's.

Using the binary optimization variables a_ℓ^n's, we can write $R(\text{coa}_n)$ in terms of $R_\ell^d(\text{coa}_n)$ and

$R_\ell^p(\text{coa}_n)$ as the following

$$R(\text{coa}_n) = \sum_{\mathcal{A}_\ell^p \in \mathcal{A}^p} a_\ell^n (R_\ell^d(\text{coa}_n) + R_\ell^p(\text{coa}_n)). \tag{4.7}$$

Therefore, $R(\Omega')$ becomes

$$R(\Omega') = \sum_{n=1}^{C'} \sum_{\mathcal{A}_\ell^p \in \mathcal{A}^p} a_\ell^n (R_\ell^d(\text{coa}_n) + R_\ell^p(\text{coa}_n)). \tag{4.8}$$

Optimization. The problem of finding the best coalition formation in (4.1) becomes equivalent to putting PA nodes into C' disjoint sets, denoted as $coa_1, coa_2, ..., coa_{C'}$, i.e., finding the binary optimization variables a_ℓ^n for $\ell = 1, ..., D, n = 1, ..., C'$, such that $R(\Omega')$ is maximized.

$$\begin{aligned}
&\text{Given } C',\ \Omega^* = \arg\max \sum_{n=1}^{C'} R(\Omega') \\
&\text{s.t.} \quad \sum_{n=1}^{C'} a_\ell^n = 1, \text{for } \ell = 1, ..., D \\
&\sum_{\ell=1}^{D} a_\ell^n \geq 3, \text{if coa}_n \text{ is a PA-only coalition} \\
&\sum_{\ell=1}^{D} a_\ell^n \geq 1, \text{if coa}_n \text{ is an SA-PA coalition}
\end{aligned} \tag{4.9}$$

It is clear that all three constraints in (4.1) are satisfied, i.e., $\text{coa}_q \subseteq \mathcal{A}$ for $q = 1, ..., C'$, $\text{coa}_k \cap \text{coa}_l = \emptyset$ for all k, l, and $\bigcup_{n=1}^{C'} \text{coa}_n \subseteq \mathcal{A}$. The first constraint in (4.9) ensures that Ω^* is a viable coalition set with no overlapping coalitions. The second and third constraints in (4.9) assure that the solution Ω^* includes legitimate coalitions only.

Achievable Channel Rate

Recall $R_i^d(\text{coa}_n)$ denote the contribution of $\mathcal{A}_i^p$ during Downlink phase to $R(\text{coa}_n)$ if $\mathcal{A}_i^p \in \text{coa}_n$. In this phase, we assume that SA nodes steer their beams directly towards their respective PA node for data reception. Also, recall $R_i^p(\text{coa}_n)$ denote the contribution of $\mathcal{A}_i^p$ during PA-PA phase to $R(\text{coa}_n)$ if $\mathcal{A}_i^p \in \text{coa}_n$. In this phase, we assume that PA nodes steer their beams directly towards each other for data communication. Further, recall the binary optimization variables a_i^n's, which indicate whether or not $\mathcal{A}_i^p$ is in coa_n. In the following, we use Bayesian rule and conditional probability to formulate $R_i^d(\text{coa}_n)$ and $R_i^p(\text{coa}_n)$ in terms of a_i^n's for the bandwidth allocation scheme in Section 4.

Rate Formulation in Downlink Phase

Consider a PA node in coa_n, denoted as $\mathcal{A}_i^p$. Recall $\{\text{PCP}_{\mathcal{A}_i^p}\}^s$ is the set of SA nodes that are in coa_n and $\mathcal{A}_i^p$ can form a directional link with. Suppose $\mathcal{A}_j^s \in \{\text{PCP}_{\mathcal{A}_i^p}\}^s$, and consider the link $(\mathcal{A}_i^p, \mathcal{A}_j^s)$ in coa_n, where $\mathcal{A}_i^p, \mathcal{A}_j^s$ are transmitter and receiver, respectively. The capacity of this link, measured in bits/sec, is

$$R_{ij}^d(\text{coa}_n) = \frac{w_1}{|\{\text{PCP}_{\mathcal{A}_i^p}\}^s|} \log_2 \left(1 + \frac{P_r(\mathcal{A}_i^p, \mathcal{A}_j^s)}{N_0 w_1 + I_{\mathcal{A}_j^s}(\text{coa}_n)}\right), \quad n = 1, ..., C' \tag{4.10}$$

where $I_{\mathcal{A}_j^s}(\text{coa}_n)$ is the interference imposed on $\mathcal{A}_j^s$. This interference is imposed by other PA nodes in coa_n that $\mathcal{A}_j^s$ is in their FoVs. In other words

$$I_{\mathcal{A}_j^s}(\text{coa}_n) = \sum_{\mathcal{A}_k^p : \mathcal{A}_k^p \neq \mathcal{A}_i^p, \mathcal{A}_k^p \in \text{coa}_n, \mathcal{A}_j^s \in \mathcal{A}(\mathcal{A}_k^p)} P_r(\mathcal{A}_k^p, \mathcal{A}_j^s). \tag{4.11}$$

Note that the set $\{\text{PCP}_{\mathcal{A}_i^p}\}^s$ in (4.10) does not depend on the optimization variables a_i^n's, since the nodes in this set are always in the same coalition as $\mathcal{A}_i^p$. However, $I_{\mathcal{A}_j^s}(\text{coa}_n)$ in (4.11) depends on a_i^ns. To characterize $I_{\mathcal{A}_j^s}(\text{coa}_n)$ in terms of a_i^ns, we introduce another binary variable $b(\mathcal{A}_m, \mathcal{A}_k)$ to indicate whether or not node $\mathcal{A}_m$ is within FoV of node $\mathcal{A}_k$, i.e., if $b(\mathcal{A}_m, \mathcal{A}_k) = 1$ then $\mathcal{A}_m \in \mathcal{A}(\mathcal{A}_k)$, and if $b(\mathcal{A}_m, \mathcal{A}_k) = 0$ then $\mathcal{A}_m \notin \mathcal{A}(\mathcal{A}_k)$. Now, we can rewrite $I_{\mathcal{A}_j^s}(\text{coa}_n)$ in (4.11) as the following

$$I_{\mathcal{A}_j^s}(\text{coa}_n) = \sum_{\mathcal{A}_k^p \in \mathcal{A}^p \setminus \{\mathcal{A}_i^p\}} a_k^n b(\mathcal{A}_j^s, \mathcal{A}_k^p) P_r(\mathcal{A}_k^p, \mathcal{A}_j^s) \tag{4.12}$$

We note that $R_{ij}^d(\text{coa}_n)$ in (4.10) depends on a_i^ns through the interference $I_{\mathcal{A}_j^s}(\text{coa}_n)$ in (4.12). Recall $R_i^d(\text{coa}_n)$ is the total amount of data transmitted by $\mathcal{A}_i^p$ and received by its associated SA nodes. In other words

$$R_i^d(\text{coa}_n) = \sum_{\mathcal{A}_j^s \in \{\text{PCP}_{\mathcal{A}_i^p}\}^s} R_{ij}^d(\text{coa}_n). \tag{4.13}$$

Recall that the set $\{\text{PCP}_{\mathcal{A}_i^p}\}^s$ in (4.13) does not depend on a_i^ns. Hence, $R_i^d(\text{coa}_n)$ in (4.13) depends on a_i^ns only through $R_{ij}^d(\text{coa}_n)$.

Rate Calculation in PA-PA Phase

Consider a PA node in coa_n, denoted as $\mathcal{A}_i^p$. Recall $\{\text{PCP}_{\mathcal{A}_i^p}\}^p$ is the set of PA nodes that $\mathcal{A}_i^p$ can potentially form a directional link with. These PA nodes may or may not be part of coa_n. Node $\mathcal{A}_i^p$ can be in transmitting or receiving mode, with equal probability. Also, if in transmitting (receiving) mode, $\mathcal{A}_i^p$ chooses randomly another PA node from the set $\{\text{PCP}_{\mathcal{A}_i^p}\}^p$ that is also in coa_n to transmit to (receive from). Suppose $\mathcal{A}_j^p \in \{\text{PCP}_{\mathcal{A}_i^p}\}^p$ and also $\mathcal{A}_j^p \in coa_n$. To form the link $(\mathcal{A}_i^p, \mathcal{A}_j^p)$, node $\mathcal{A}_i^p$ needs to be in transmitting

mode, and chooses to transmit to $\mathcal{A}_j^p$. Also, node $\mathcal{A}_j^p$ needs to be in receiving mode, and chooses to receive from $\mathcal{A}_i^p$. Let $R_i^p(\text{coa}_n)$ be the total amount of data (measured in bits/sec) received by $\mathcal{A}_i^p$ and transmitted by some other PA nodes in coa_n. Let set $\mathcal{Y}_{\mathcal{A}_i^p}^{(\text{coa}_n)} = \{\mathcal{A}_k^p | \mathcal{A}_k^p \neq \mathcal{A}_i^p, \mathcal{A}_k^p \in \text{coa}_n \text{ and } \mathcal{A}_k^p \in \{\text{PCP}_{\mathcal{A}_i^p}\}^p\}$. We can express $R_i^p(\text{coa}_n)$ as below

$$\begin{aligned} R_i^p(\text{coa}_n) &= \frac{w_1}{4 \times |\mathcal{Y}_{\mathcal{A}_j^p}^{(\text{coa}_n)}| \times |\mathcal{Y}_{\mathcal{A}_i^p}^{(\text{coa}_n)}|} \\ &\times \sum_{\mathcal{A}_j^p \in \{\text{PCP}_{\mathcal{A}_i^p}\}^p} a_j^n \log_2 \left(1 + \frac{P_r(\mathcal{A}_j^p, \mathcal{A}_i^p)}{N_0 w_1 + I_{\mathcal{A}_i^p}(\text{coa}_n)}\right) \end{aligned} \tag{4.14}$$

where $I_{\mathcal{A}_i^p}(\text{coa}_n)$ is the interference imposed on $\mathcal{A}_i^p$. The sum in (4.14) is over all PA nodes in PCP of $\mathcal{A}_i^p$ that are also in coa_n. The fraction outside the sum in (4.14) stems from the facts that (1) $\mathcal{A}_i^p$ and $\mathcal{A}_j^p$ should be in transmitting and receiving modes, respectively, (2) $\mathcal{A}_j^p$ chooses randomly $\mathcal{A}_i^p$ from the nodes in $\{\text{PCP}_{\mathcal{A}_j^p}\}^p$ that are also in coa_n. Also, $\mathcal{A}_i^p$ chooses randomly $\mathcal{A}_j^p$ from the nodes in $\{\text{PCP}_{\mathcal{A}_i^p}\}^p$ that are also in coa_n. Hence, this fraction is equal to $\frac{1}{2} \times \frac{1}{2} \times \frac{1}{|\mathcal{Y}_{\mathcal{A}_i^p}^{(\text{coa}_n)}|} \times \frac{1}{|\mathcal{Y}_{\mathcal{A}_j^p}^{(\text{coa}_n)}|}$. The interference $I_{\mathcal{A}_j^p}(\text{coa}_n)$ is imposed by other transmitting PA nodes in coa_n that $\mathcal{A}_j^p$ is in their FoVs:

$$I_{\mathcal{A}_j^p}(\text{coa}_n) = \frac{1}{2} \sum_{\mathcal{A}_k^p : \mathcal{A}_k^p \neq \mathcal{A}_i^p, \mathcal{A}_k^p \in \text{coa}_n, \mathcal{A}_j^p \in \mathcal{A}(\mathcal{A}_k^p)} P_r(\mathcal{A}_k^p, \mathcal{A}_j^p) \tag{4.15}$$

where $\frac{1}{2}$ in (4.15) comes from the fact that $\mathcal{A}_k^p$ is transmitting and thus interfering with $\mathcal{A}_j^p$ only with probability $\frac{1}{2}$. The set cardinalities $|\mathcal{Y}_{\mathcal{A}_i^p}^{(\text{coa}_n)}|, |\mathcal{Y}_{\mathcal{A}_j^p}^{(\text{coa}_n)}|$ in (4.14) as well as $I_{\mathcal{A}_j^s}(\text{coa}_n)$ in (4.15) depend on the optimization variables a_i^n's. Using the same binary variables we used

in Section 4 we can rewrite $I_{\mathcal{A}_j^p}(\text{coa}_n)$ in (4.15) as

$$I_{\mathcal{A}_j^p}(\text{coa}_n) = \sum_{\mathcal{A}_k^p \in \mathcal{A}^p \setminus \{\mathcal{A}_i^p\}} a_k^n a_j^n b(\mathcal{A}_j^p, \mathcal{A}_k^p) P_r(\mathcal{A}_k^p, \mathcal{A}_j^p). \tag{4.16}$$

Also, we can characterize the set cardinalities as below

$$|\mathcal{Y}_{\mathcal{A}_i^p}^{(\text{coa}_n)}| = \sum_{\mathcal{A}_k^p \in \{\text{PCP}_{\mathcal{A}_i^p}\}^p} a_k^n, \;\; |\mathcal{Y}_{\mathcal{A}_j^p}^{(\text{coa}_n)}| = \sum_{\mathcal{A}_k^p \in \{\text{PCP}_{\mathcal{A}_j^p}\}^p} a_k^n \tag{4.17}$$

We note that $R_i^p(\text{coa}_n)$ in (4.14) depends on the optimization variables a_i^n's through the interference $I_{\mathcal{A}_j^p}(\text{coa}_n)$ in (4.16) and the set cardinalities $|\mathcal{Y}_{\mathcal{A}_i^p}^{(\text{coa}_n)}|, |\mathcal{Y}_{\mathcal{A}_j^p}^{(\text{coa}_n)}|$ in (4.17).

Centralized Coalition Set Formation Heuristics (Centralized Approach)

The main problem we aim to solve is the generic version of (4.9), where C' is not fixed; i.e., we need to look at the ways in which coalitions can be formed such that the overall sum rate $R^d + R^p$ is maximized. In Sec. 4, we detailed how R can be calculated for a coalition as well as for the entire network. These achievable R values give us a way to compare the efficacy of coalition sets, which we use steer our heuristic search towards a better coalition set. Further, the insights obtained from the classification of directional radio antennas in Section 4 allows us to reduce the search space significantly as can eliminate infeasible coalitions based on whether or not a node is an SA or PA. Next, we first present a technique (Heuristic 1) that yields an *all-covering* initial coalition set, composed of smallest possible coalitions. We, then, design two heuristics (Heuristics 2 and 3) that attempt to merge the small coalitions in the initial coalition set with hopes to improve the sum rate.

Heuristic 1: Minimalist Coalitions (MC)

We first start with composing the list of PCPs for A nodes, the complexity of which is $\mathcal{O}(A^2)$. Then, we initialize the coalition set $\Omega \leftarrow \emptyset$, and inspect PCP of all nodes. If $|\text{PCP}_{\mathcal{A}_i}| = 0$, $\mathcal{A}_i$ cannot be part of a coalition and is excluded from $\mathcal{A}$. If $|\text{PCP}_{\mathcal{A}_i}| = 1$, then $\mathcal{A}_i$ is an SA and it will have to be in coalition with the node in its PCP. We first check if there exists a specific coalition that already contains the PCP member of $\mathcal{A}_i$. If so, then, $\mathcal{A}_i$ gets merged into that coalition and removed from $\mathcal{A}$. Otherwise, we form a coalition $coa_i = \{\mathcal{A}_i\} \cup \{\text{PCP}_{\mathcal{A}_i}\}$, and add this coalition to the set of coalitions, i.e., $\Omega \leftarrow \Omega \cup coa_i$. Once the above steps are applied to all nodes in $\mathcal{A}$, there will be no SA left alone, as all of them will be placed to a coalition. However, there will be isolated PA nodes as the above initialization does not add nodes with |PCP| >1 to a coalition. We create a set Δ to store the outstanding PAs in increasing order of their PCP sizes. We also move all 2-node coalitions to set $\Omega_{\text{SA-SA}}$. All the other coalitions stay in Ω. This process is detailed in Algo. 3 as the InitialCoalitionSet($\mathcal{A}$) function which returns the coalitions with one PA and one or more PAs, the coalitions with only two SAs, and the set of PAs left alone, i.e., Ω, $\Omega_{\text{SA-SA}}$, and Δ.

To satisfy the all-covering property, we, next, focus on placing the outstanding PAs, Δ, that got left alone after the InitialCoalitionSet($\mathcal{A}$) procedure. Our approach here exploits the fact that none of the PAs in Δ has an SA in its PCP. This is the due to the fact that InitialCoalitionSet($\mathcal{A}$), once it is done, places all SAs to a coalition. Hence, the PCPs of all PAs in Δ must only be composed of one PA or more PAs. Given this, the essence of our approach is to place the outstanding PAs in the same coalition as the PA with minimum PCP size. So, for a PA $\mathcal{A}_i^p$, we place $\mathcal{A}_i^p$ in the same coalition as the PA in $\text{PCP}_{\mathcal{A}_i}$ that has the smallest PCP size. The ConsumeOutstandingPAs(Ω, Δ) procedure in Algo. 4 details the steps for merging outstanding PAs to the coalition set Ω.

Execution of InitialCoalitionSet($\mathcal{A}$) and ConsumeOutstandingPAs(Ω, Δ) guarantees a feasible solution, Ω, to the all-covering coalition set formation problem. However, it may be possible to further improve the sum rate of the coalition set by merging some of the coalitions in Ω. The next two sections will detail heuristics for this purpose. the MC heuristic has a complexity of $\mathcal{O}(A^2)$.

Algorithm 3 Generate and Sort Initial Coalitions

function InitialCoalitionSet($\mathcal{A}$)
  Generate $\text{PCP}_{\mathcal{A}_1..\mathcal{A}_A}$
  $\Omega \leftarrow \emptyset$ *Coalition Set *\
  coaCount $\leftarrow 0$
  for $\mathcal{A}_i = 1 : A$ **do**
    if $|PCP_{\mathcal{A}_i}| = 0$ **then**
      Exclude $\mathcal{A}_i$ from $\mathcal{A}$
    end
    else if $|PCP_{\mathcal{A}_i}| = 1$ **then**
      foundPA $\leftarrow$ FALSE **for** $j = 1 : coaCount$ **do**
        if coa_j *contains* $PCP_{\mathcal{A}_i}$ **then**
          foundPA $\leftarrow$ TRUE $\text{coa}_j \leftarrow \text{coa}_j \cup \{\mathcal{A}_i\}$ Exclude $\mathcal{A}_i$ from $\mathcal{A}$ break
        end
      end
      if *not foundPA* **then**
        coaCount ++ $\text{coa}_{\text{coaCount}} = \{\mathcal{A}_i\} \cup \{\text{PCP}_{\mathcal{A}_i}\}$ $\Omega \leftarrow \Omega \cup \text{coa}_{\text{coaCount}}$ Exclude $\mathcal{A}_i$ and $\text{PCP}_{\mathcal{A}_i}$ from $\mathcal{A}$
      end
    end
  end
  $\Delta \leftarrow \mathcal{A}$ *Outstanding PA set*\
  Sort Δ in ascending order of $|\text{PCP}_{\mathcal{A}_k}|$, $\forall \mathcal{A}_k \in \Delta$
  $\Omega_{SA-SA} \leftarrow \emptyset$
  Move all $\text{coa}_i \in \Omega$ with two nodes (i.e., $|\text{coa}_i| = 2$) to Ω_{SA-SA}
  Sort Ω in ascending order of $\text{coa}_j, \forall j \in \Omega$ **return** $\Omega, \Omega_{SA-SA}, \Delta$
end function

Heuristic 2: Smaller Coalitions (SC)

The possibility of merging two coalitions is possible only if they have PAs that are in the PCP of each other. Since $\Omega_{\text{SA-SA}}$ does not include coalitions with a PA, it is excluded from this merging process. We start from the coalition set Ω found by Heuristic 1, i.e., first call the functions InitialCoalitionSet($\mathcal{A}$) and ConsumeOutstandingPAs(Ω, Δ). Then,

Algorithm 4 Merge Outstanding PAs to Coalition Set

```
1: function ConsumeOutstandingPAs(Ω, Δ)
2:     while Δ ≠ ∅ do
         for k = 1 : |Δ| do
           c ← PCP_k   c ← c\{j}, ∀j ∈ Δ
           if c ≠ ∅ then
             u ← u ∈ c : |PCP_u| = min{|PCP_{j∈c}|}
           else
             u ← u ∈ PCP_k : |PCP_u| = min{|PCP_{j∈Δ}|}
           end
           if coa_u = ∅ then
             Ω ← Ω ∪ {k, u};
           else
             coa_u ← coa_u ∪ {k}, coa_u ∈ Ω
           end
           Δ ← Δ\{k}
         end
         end
3:     return Ω
4: end function
```

we pick two coalitions from Ω with a probability inversely proportional to the sizes of the coalitions The intuition is that by merging smaller coalitions earlier in the process, a larger portion of the search space is left untried, which increased the likelihood of finding a better solution eventually. If merging the two coalitions results in a larger R, we merge them. If not, we retract. If no improvement on R is observed after stopCount=3 merger trials, the process stops. Assuming that the probability of finding mergeable coalitions is high, The complexity of this heuristic is $\mathcal{O}(\text{stopCount} \times A^3)$.

Heuristic 3: Smaller & Closer Coalitions (SCC)

This heuristic is a finer tuned version of SC using the intuition that merging coalitions closer to each other should yield a better outcome. Basically, we run SC three times and gather the smaller coalition pairs that are mergeable and those that yield a higher R. Then, for each of these coalition pairs, we calculate the relative distance separating them. For this, we apply the process of finding the center of gravity of each coalition and then, find the

Table 4.2: Simulation Parameters

Parameter	**Value**
B	1 GHz
N_0	-110dBm [49]
α	2
HPBW	15°
Γ_i	$[0^\circ, 360^\circ]$

Euclidean distance separating them. We check if SCC yields a higher R over SC and if it does, we report that, otherwise, no improvement is made. Since this heuristic simply runs Heuristic 2 a constant number of times, its worst-case complexity follows the same behavior as Heuristic 2.

Centralized Coalition Set Formation Heuristics (Decentralized Approach)

We design three decentralized approaches while forming coalition sets. In the first approach, we focus on creating an all-covering coalition set. In other words, we create coalition set in an *unguided method* without necessarily guaranteeing maximization of the coalitional sum rate. This method acts as a baseline upon which we improve and enforce sum rate maximization bringing us to the second and third approaches, where we come up with our *semi-guided* and *guided* approaches respectively. The semi-guided approach also enables formation of all-covering coalition set while maximizing sum rate, and the guided approach may create a partially-covering coalition set while guaranteeing sum rate maximization.

Algorithm 5 Unguided Method (UM) - Merge Outstanding PAs to Coalition Set (Heuristic 1)

```
function UM(Ω, Δ)
for k = 1 : |Δ| do
        c = random member (RM) from PCP_k  if c in Ω then
    |       Joinable coa = coalition containing c  Joinable coa ← k
        else
    |       Create empty coa ec = {}  ec ← {k, c}  Ω ← ec
        end
        Δ ← Δ\{k}
        end
    return Ω
end function
```

Algorithm 6 Semi-guided Method (SM) - Merge Outstanding PAs to Coalition Set (Heuristic 2)

```
function SM(Ω, Δ)
for k = 1 : |Δ| do
        Initialize empty list distance vector dv = []  for p in PCP_k do
    |       dist = Cartesian distance (k, p)  dv ← dist
        end
        min_dist = min(dv)  c = PCP_min_dist  if c in Ω then
    |       Joinable coa = coalition containing c  Joinable coa ← k
        else
    |       Create empty coa ec = {}  ec ← {k, c}  Ω ← ec
        end
        Δ ← Δ\{k}
        end
    return Ω
end function
```

Heuristic 1: Unguided Method (UM)

Now, our focus is on merging the outstanding PAs given by set Δ which are left out after the bootstrapping phase. We follow an unguided, randomized method to merge these outstanding PA nodes to existing coalitions. The essence of our approach here is basically to iterate over set Δ and randomly merge each outstanding PA node with their PCP members. If the randomly chosen PCP member 'RM' of outstanding PA Δ_k already belongs to a coalition formed during the bootstrapping phase, then Δ_k gets itself merged into that coalition, else it creates a new coalition along with its chosen PCP member. This process will

Algorithm 7 Guided Method (GM) - Merge Outstanding PAs to Coalition Set (Heuristic 3)

function GM(Ω, Δ)
for $k = 1 : |\Delta|$ **do**
    Initialize empty rate improvement vector: $riv = []$ Initialize empty rate vector: $rv = []$ Initialize empty vector: in_coa = [] Initialize empty vector: not_in_coa = [] **for** p *in* PCP_k **do**
        if $p \in \Omega$ **then**
            in_coa $\leftarrow p$
        else
            not_in_coa $\leftarrow p$
        end
    end
    for i *in in_coa* **do**
        potential = Ω_i $R^{\mathrm{w/o}} = R^{\mathrm{potential}}$ potential $\leftarrow k$ $R^{\mathrm{w}} = R_k^{\mathrm{potential}}$ $R^{\mathrm{diff}} = R^{\mathrm{w}} - R^{\mathrm{w/o}}$ $riv_i \leftarrow R^{\mathrm{diff}}$
    end
    for n *in not_in_coa* **do**
        Create empty coa $ec = \{\}$ $ec \leftarrow \{k, n\}$ Calculate R^{ec} $rv_n \leftarrow R^{ec}$
    end
    if *not_in_coa* $\neq \emptyset$ **then**
        if *max[rv]* > *max[riv]* **then**
            $\Omega \leftarrow ec^{\max[rv]}$
        else
            $\Omega \leftarrow \Omega_k^{\max[riv]}$ $\Delta \leftarrow \Delta \backslash \{k\}$
        end
    else
        if *max[riv]* > 0 **then**
            $\Omega \leftarrow \Omega_k^{\max[riv]}$
        else
            $\Delta \leftarrow \Delta \backslash \{k\}$
        end
    end
    end
    return Ω
end function

continue until set Δ gets exhausted. This approach, although is able to generate coalition set Ω extremely fast, it does not always guarantee the maximum coalitional sum rate R. If a very quick, robust coalition formation method is sought after with lower priority towards maximizing R, this heuristic might be a good choice. Algo. 5 details how this heuristic is simulated.

Heuristic 2: Semi-guided Method (SM)

Our next fast heuristic method to merge the outstanding PA nodes in set Δ is a semi-guided approach where nodes assume that joining a closeby coalition is beneficial as it would allow establishment of high SNR links. The differentiating factor from heuristic 1 is that this time, instead of randomly choosing the PCP members for every outstanding PA node in set Δ, the PA nodes merge themselves with their closest PCP members. In Algo. 6, we detail the semi-guided method in a simulation. Like heuristic 1, after bootstrapping, each member of Δ iterates over their PCP members and append the Cartesian distances between themselves and their PCP members to the *distance vector* list. Then, they choose the PCP members that are closest to them. Now, if the outstanding PAs find that their chosen members already belong to a coalition, then they add themselves to that coalition. Otherwise, they form a new coalition with their PCP member and join set Ω.

Heuristic 3: Guided Method (GM)

In this heuristic, the outstanding PAs go through a more rigorous merging process to create the final coalition set Ω. The details are presented in Algo. 7. Every outstanding PA node initializes four empty vectors: 1. rate improvement vector riv, 2. rate vector rv, 3. in_coa, and 4. not_in_coa. As before, after the bootstrapping, each outstanding PA node k starts iterating over its PCP members. It checks which of those PCP members are already part of a coalition and places them in the list in_coa, which is local to the PA node k. Those that are not part of a coalition, are placed into the list not_in_coa. For those nodes that are in in_coa, k communicates with the PA of the coalition that it wishes to join (because that coalition contains its PCP member) and asks about its current sum rate R. It stores this value in variable $R^{\text{w/o}}$. On a trial basis, it temporarily merges itself with that coalition and

computes the new coalitional R including itself and stores this value in variable R^{w}. Then, it computes $R^{\text{w/o}} - R^{\text{w}}$ and stores the difference in vector riv. For those nodes that are in list not_in_coa, k adds itself in a temporary coalition and calculates R and stores the value in vector rv. These processes are repeated for all members in the vectors rv and riv. The vector riv now contains differences and the values can be negative (since the R^{w} can be less than $R^{\text{w/o}}$) whereas the minimum possible value within vector rv can be 0 (since R of a coalition in the absolute worst case is 0). It might happen that for k, all of its PCP members are part of Ω. In that case, vector not_in_coa is empty. Then k looks at its riv and chooses the corresponding PCP member that, when joined, would yield a better coalitional R. In other words, k joining that coalition would prove beneficial for the entire coalition set Ω. It must be noted here that the values within riv could be negative signifying k will steer away from joining those coalitions that yield a worse R.

An interesting case is when the outstanding PA k is detrimental to all coalitions it can join to. If all values within riv are negative, that signifies k is unable to improve the R for any coalition it wishes to join and altruistically removes itself from the entire process. On the other hand, if vector not_in_coa is not empty, then k compares maximum value of rv with that of riv and if the former is greater, then k proceeds with adding itself with its PCP member, and creating a new coalition. Otherwise, it joins with its PCP member that is already part of a coalition. This process continues until set Δ gets exhausted.

In this heuristic, each outstanding PA node is sensitive to the state of Ω in terms of overall R and selflessly acts in favor of the greater good by removing itself from the system if it sees that it causes more harm by joining the system. Hence, this heuristic may create a partially-covering coalition set that maximizes overall R but results in some PA nodes to be alone.

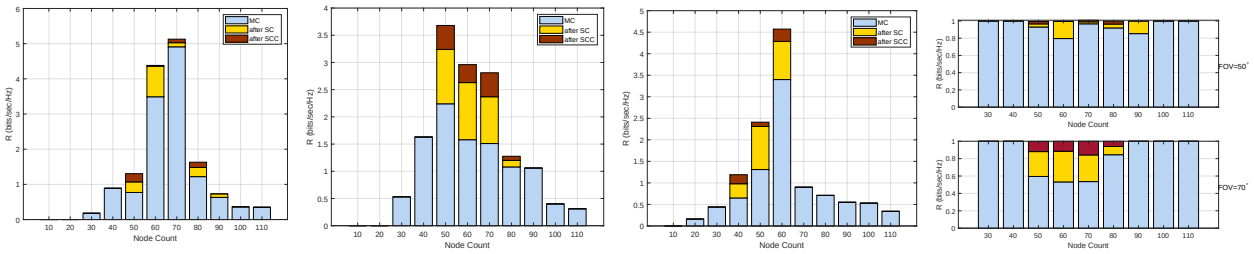

(a) FoV = 50° **(b)** FoV = 70° **(c)** FoV = 90° **(d)** Heuristic comparison

Figure 4.4: Impact of heuristics SC and SCC on R for a dense network

Simulation Results and Discussion (Centralized Approach)

We present and discuss various coalition formation and sum-rate related results for the centralized approach. The simulation parameters are shown in Table 4.2. We have repeated each simulation three to ten times, with randomly scattered nodes, within a fixed geographical area, from which we generated coalition sets. All nodes are assumed to have the same FoV, β_i, and a randomly generated inclination angle, Γ_i. The isolated nodes are excluded from the simulation. We evaluate our heuristics for dense (10×10 m^2) networks.

We capped transmit power of the overall coalition set to a maximum of 1 mW. This means that the 1 mW is split into the total number of coalitions formed and nodes within each coalition equally share the coalitional power. Fig. 4.4 shows how the sum rate behaves w.r.t. network density and FoV using the proposed power allocation scheme for the dense network case. MC attains a peak in R (e.g., at 80 nodes for FoVs 50°) as more nodes are added, indicating that the number of nodes in the network plays a critical role. The transmit power is not simply added up, rather interference plays a major role. Also limiting the area of node deployment helps us in observing the peak in R.

Since their complexity is higher, a critical question to answer is whether or not there is a need

for the SC and SCC heuristics that try to merge small coalitions for improving the sum rate. Figs. 4.4a, 4.4b and 4.4c show R w.r.t node density and FoV. We see significant improvement for medium node density, and beyond a certain limit, the SC and SCC heuristics make little sense due to increased interference. This is more clear in the Fig. 4.4d that shows the percentage of R attained by each heuristic for the cases with FoVs 50° and 70°. Also, we have not shown results beyond FoV = 90° because, in the smaller area, SC and SCC with such wide FoVs rarely provide any improvement due to added interference.

Simulation Results and Discussion (Decentralized Approach)

In this section, we have presented and discussed various coalition formation and sum rate related results for the decentralized approach. The simulation parameters are as in Table 4.2. Each simulation run is repeated three to ten times, with randomly scattered directional radio nodes, enclosed within a fixed geographical area, from which coalitional sets are generated. All nodes are assumed to have the same FOV, β_i, and a randomly generated inclination angle, Γ_i. The isolated nodes are excluded from the simulation. The heuristics are evaluated for dense (20×20 m^2) networks. The transmit power of the overall coalition set is capped to a maximum of 1 mW. This means that the 1 mW is split into the total number of coalitions formed and nodes within each coalition equally share the coalitional power. Fig. 4.5 shows how the sum rate R in bits/sec/Hz varies w.r.t. network density (in terms of node count) and FOV using the proposed power allocation scheme. Heuristic UM (denoted by light green bars) attains a peak in R (e.g., at 80 nodes for FOVs 50°). For nodes fewer than 80, R is lower and for very few node count like 10 or 20, there are not enough nodes to form coalition set. The overall plot has a 'hump'-like structure because after node count of 80, the node density becomes too high and individual nodes within a coalition end up receiving more interference

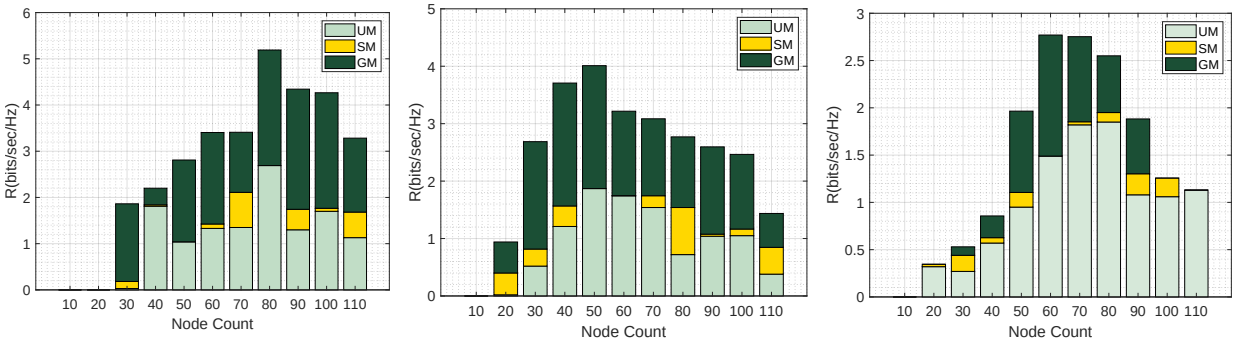

(a) FOV = 50° **(b)** FOV = 70° **(c)** FOV = 90°

Figure 4.5: R attained by Unguided, Semi-Guided and Guided heuristics

from others and that results in lower R. Similar trend is noticeable across the board in Figs. 4.5b and 4.5c. It must be noted here that the maximum R achievable for the latter two cases are lower than that of Fig. 4.5a. This is because of higher FOV values (signifying a wider 'eye' for every node which means every node can see more nodes outside of its PCP list and is susceptible to more interference), which in turn invites more interference for each node in the system. Overall, in general, we can say that limiting the area of node deployment helps us in observing these peaks in R.

Heuristic SM (in golden bars) on top of heuristic UM for FOV values 50°, 70° and 90° in Figs. 4.5a, 4.5b and 4.5c show the improvement that we can expect when we switch to semi-guided method. As described in section 4, the outstanding PA nodes are more careful in choosing their PCP members while merging to Ω. The overall trends for all three FOV values are preserved. In the same figure, using deep green bars representing R attained by GM on top of SM, we show the attainable R for the three FOV values and same node densities. From these deep green bar plots we can see that the overall attainable R in general is much higher than those attainable by the prior heuristics. This is because the heuristic GM, in terms of overall coalitional R is much more strict in terms of outstanding PA nodes merging

themselves to set Ω, as discussed in section 4. The gains are clearly visible in terms of peaks in each of the FOV values when compared to other heuristics. For FOV value 90° in Fig. 4.5c, we see very minor improvement for node count 100 and 110 using GM. This is because for such FOV value and high node density, GM provides negligible improvement. In general, for higher FOV values like 70° and 90° we observe that R tapers off faster than lower FOV values like 50°. This is because as we increase the node count, higher FOV values result in higher interference within coalitions.

Summary

For ultra-high speed 5G-and-beyond communication mmWave antenna equipped radios are becoming a necessity. The keys to designing a successful 5G-and-beyond infrastructure are proper resource allocation and throughput management systems. In this piece of work, mmWave directional nodes are characterized into SAs and PAs and we have used this characterization to present an extensive all-covering as well as partially-covering coalition set formation. Using the SA and PA categorization of nodes, decentralized, fast, robust and novel heuristics are designed and are shown to have proven beneficial for maximizing the sum rate of coalition set. We studied the trade-off between guaranteeing placement of all nodes in a coalition (i.e., all-covering coalition set) and maximizing the sum rate of the coalition set. For networks with too few or too many nodes, the trade-off did not show to be strong; while for networks with mediocre number of nodes, the relaxation of the requirement of covering all nodes showed significant benefits in terms of sum rate.

In the future, we aim at extending our decentralized heuristics approach by exploring additional methods of transmission scheduling and bandwidth allocation schemes. Here, we focused on the sum rate of the coalition set, however, it will be interesting to study

the fairness among coalitions in terms of achievable data rate. Another key aspect is the inter-coalition transmission rate. In our work, we did not consider data transmissions among coalitions. Incorporating the inter-coalition data rate to the sum rate will assure full end-to-end connectivity among all nodes regardless of which coalition they belong to. More research is needed in this direction. Finally, introducing adversarial presence to the coalition set and understanding node mobility will be interesting directions to take.

CHAPTER 5: BEAMSTEERING OPTIMIZATION

Introduction

Compared to traditional sub-6 GHz radio networks, mmWave and Terahertz communication employ higher frequency bands and their antennas are highly directional in terms of their beam propagation. Due to this directionality, this technology is able to provide a higher throughput, but at the same time, suffers from severe environmental attenuation [87]. In such directional communication at high frequencies, line-of-sight (LOS) alignment is practically necessary to establish links as the side lobes and multipath signals are too weak [88]. Understanding the capacity of networks formed from such emerging directional LOS wireless links is of importance for the wireless community.

We consider a group of mmWave/Terahertz phased array antennas (or nodes) in the form of a network and examine the overall network channel capacities. For every node, we have the Field-of-View (FOV) and that is one of the factors that decide how many other nodes it could potentially talk to, resulting in viable links. A node can potentially establish links with as many other nodes as possible, as long as they are within the FOV of each other. We assume random scheduling, i.e., there is no central entity to govern network communication. We investigate the capacity of the individual directional links and, through a beamsteering optimization, figure out the best steering angles for antennas talking to multiple other antennas, such that network capacity is maximized. The optimization of the steering angles is based on an exhaustive search method that scans the whole range within the FOV of an antenna.

Directional (mmWave/Terahertz) communication offers new features to utilize for improving

network capacity. Recent research have studied how beamsteering aids in achieving higher throughput [46], e.g., by optimizing channel resource allocation [47] or coalition formation [33]. These studies did not consider the impact of scheduling in the optimality of beamsteering angles. In a more relevant study, optimizing beamsteering of directional antennas in a mobile fronthaul [48] was performed for uplink or downlink transmissions. The authors in [49, 54] show how beam steering in cognitive radio setup affects the achievable channel rate. Unlike prior work, we tackle the problem from the perspective of optimizing steering angles of multiple nodes talking to multiple other nodes, all at the same time, to come up with the highest network capacity. Going beyond the fronthaul settings where a base station organizes the uplink/downlink transmission schedule, we model the network capacity to mobile and more ad-hoc settings where nodes may randomly form links and decide their transmissions schedules in a distributed manner.

Key novelties and contributions of our work are: **(1)** A formal method to categorize directional nodes based on their FOVs and illustration of the method on networks of nodes of varying sizes.**(2)** Extraction of links and formation of the nodes into groups, for which three different types of transmission becomes possible: uplink, downlink and ad-hoc. **(3)** Formulations of directional uplink, downlink and ad-hoc link capacities when transmissions are randomly scheduled. **(4)** Calculation of average network throughput by optimizing beamsteering angles of all nodes for uplink, downlink, or ad-hoc transmission, jointly or separately. **(5)** Exhaustive and Genetic Algorithm (GA) solutions to optimize the beamsteering angles. **(6)** Study of the average network throughput for varying FOVs.

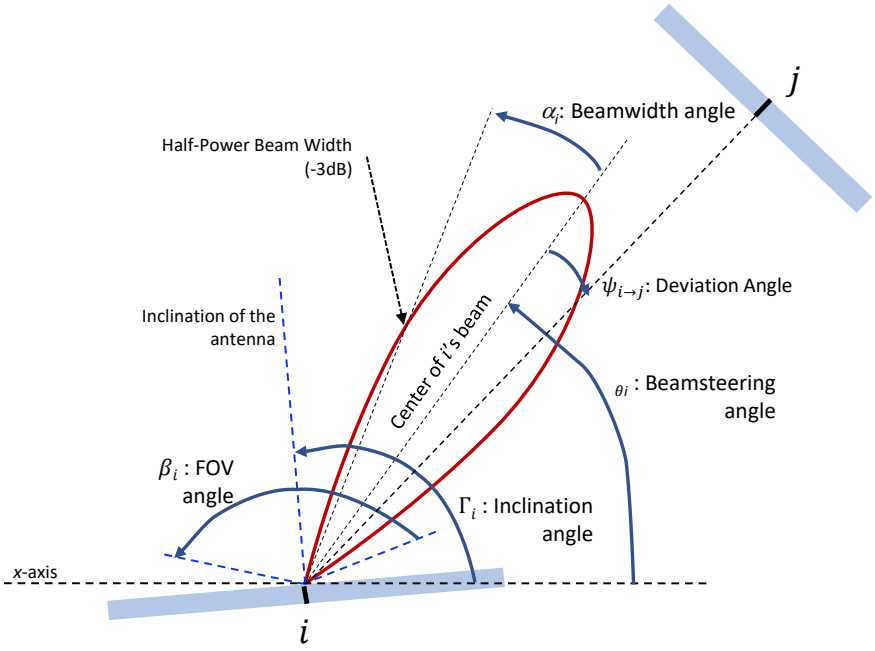

Figure 5.1: Antenna array of $\mathcal{A}_i$

System Model

Directional Antenna Model

We contemplate a two-dimensional geographical plane wherein randomly positioned mmWave transceivers, each outfitted with a directional antenna array, operate in a half-duplex manner, utilizing a shared radio channel for communication. These transceivers, also referred to as "nodes," are characterized as follows: Let $\mathcal{A} = \{\mathcal{A}_1, \mathcal{A}_2, ..., \mathcal{A}_A\}$ represent the set of antenna arrays, with $\mathcal{A}_i$ positioned at the Cartesian coordinates (x_i, y_i) for $i = 1, ..., A$. The initial inclination angle of node $\mathcal{A}_i$ relative to the x-axis is denoted as Γ_i, while θ_i signifies the steering angle corresponding to the center of the beam emitted by node $\mathcal{A}_i$, referenced from the positive x-axis. Node $\mathcal{A}_i$ possesses the flexibility to select its beamsteering angle θ_i. The field of view (FOV) of node $\mathcal{A}_i$, represented by β_i, defines the maximum span of angle

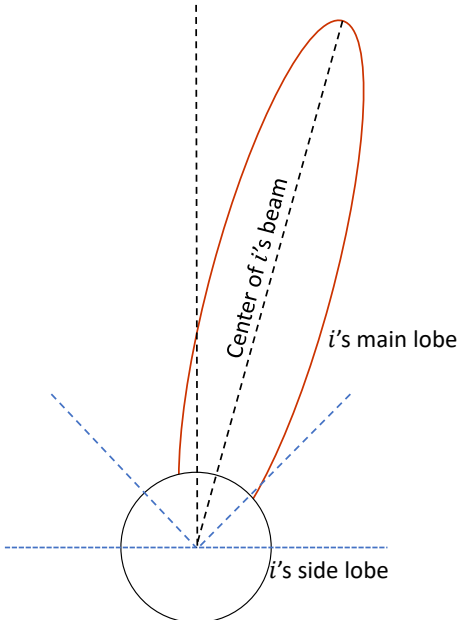

Figure 5.2: Antenna array $\mathcal{A}_i$ along with side-lobe

θ_i. An essential parameter in the characterization of node $\mathcal{A}_i$ is its half-power beamwidth (HPBW), also known as the divergence angle, denoted by α_i. Thus, the combination $\mathcal{A}_i(x_i, y_i, \Gamma_i, \theta_i, \beta_i, \alpha_i)$ provides a distinct specification for the antenna array attributes of node $\mathcal{A}_i$ as well as its present beam orientation. A visual depiction of the node distribution, accompanied by the key directional antenna parameters of node $\mathcal{A}_i$, is presented in Fig. 5.1. In this context, the transmitter is denoted as $\mathcal{A}_i$, while the receiver is labeled as $\mathcal{A}_j$. lie in each others' FOV, and both can steer their beams to each other. The deviation angle $\psi_{i\to j}$ indicates the deviation of receiver $\mathcal{A}_j$ from the center of the beam of the transmitter node $\mathcal{A}_i$, away from the line connecting nodes $\mathcal{A}_i$ and $\mathcal{A}_j$.

A directional antenna with side lobe is shown in Fig. 5.2. We consider a reference directional antenna model with side lobe for IEEE 802.15.3c. In this work, we use only the main lobe for LOS communications and side lobe is only considered for NLOS interference, which is applicable for LOS transmission using high frequency signals such as 60 GHz or above. For

LOS communications, we can safely ignore the side lobe gain [85]. Let $G_i(\theta_i)$, in units of dB, be the directional antenna gain of node $\mathcal{A}_i$. Then, the gain of the directional antenna is

$$G_i(\theta_i) = \begin{cases} G^i_{\text{ml}} - 3.01 \cdot \left(\frac{2\theta_i}{\alpha_i}\right)^2, & |\alpha_i| \geq |\psi_{i\to j}| \\ G^i_{\text{sl}}, & \text{otherwise} \end{cases} \tag{5.1}$$

where G^i_{ml} is the main lobe antenna gain and G^i_{sl} is the side lobe gain. When numerically simulating the channel, we use $G^i_{\text{ml}} = 10\log(1.6162/\sin(\alpha_i/2))^2$ and $G^i_{\text{sl}} = -0.4111\log(\alpha_i) - 10.579$ [33]. The main lobe gain applies when the receiver is within the HPBW of the transmitter, i.e., $|\alpha_i| \geq |\psi_{i\to j}|$. The units of all angles are in degrees. Regardless of the position of the receiver and for both the main the side lobe propagation in (4.5), the beamsteering angle must be within the FOV limits of the antenna. This is expressed as $\beta_i^{\min} \leq \theta_i \leq \beta_i^{\max}$, where $\beta_i^{\min} = \Gamma_i - \beta_i/2$ and $\beta_i^{\max} = \Gamma_i + \beta_i/2$ are the minimum and maximum beamsteering angles allowed within the FOV of $\mathcal{A}_i$.

Network of Nodes

In Fig. 5.3, we present an example node network under consideration. We posit that node $\mathcal{A}_i \in \mathcal{A}$ possesses the capability to engage in communication with node $\mathcal{A}_j \in \mathcal{A}$ (in other words, nodes $\mathcal{A}_i$ and $\mathcal{A}_j$ can establish a viable communication connection) exclusively when they both reside within the overlapping regions of their transmission ranges and FOVs. For simplicity, we assume that each node $\mathcal{A}_i \in \mathcal{A}$ has a fixed transmission range[1]. Along with the FOV, this transmission range plays a role in determining the characteristics of each $\mathcal{A}_i \in \mathcal{A}$. In cases where nodes $\mathcal{A}_i$ and $\mathcal{A}_j$ fall within each other's transmission ranges, if $\mathcal{A}_i$ is positioned within the FOV of node $\mathcal{A}_j$, while the reverse is not accurate, the possibility

[1]To obtain our simulation-based evaluations in Section 5 we assume the fixed transmission range is 1 m.

of establishing a communication link between these two nodes becomes null. We make the assumption that all nodes $\mathcal{A}$ are capable of establishing a connection with at least one other node; in other words, there are no isolated nodes that lack the ability to communicate with another node. Our conceptualized network is formed through a combination of valid links spanning all nodes. Each node can be classified as either a *Primary Antenna* (PA) or a *Secondary Antenna* (SA). A PA node holds the capability to establish connections with multiple other nodes, whereas an SA node is limited to establishing a connection with just one other node.

To enhance clarity and brevity, we introduce the following formal notations. Let $\mathcal{A}^p = \{\mathcal{A}^p_1, \mathcal{A}^p_2, ..., \mathcal{A}^p_U\}$ and $\mathcal{A}^s = \{\mathcal{A}^s_1, \mathcal{A}^s_2, ..., \mathcal{A}^s_V\}$ represent the sets of PA (Primary Antenna) nodes and SA (Secondary Antenna) nodes, respectively, where $U = |\mathcal{A}^p|$ and $V = |\mathcal{A}^s|$. The u-th PA node is denoted as $\mathcal{A}^p_u$, while the v-th SA node is $\mathcal{A}^s_v$. It follows that $\mathcal{A}^p \subseteq \mathcal{A}$, $\mathcal{A}^s \subseteq \mathcal{A}$, $\mathcal{A}^s \cap \mathcal{A}^p = \emptyset$, and the total number of nodes is given by $A = U + V$. Let $\mathcal{A}(\mathcal{A}_i) \subset \mathcal{A}$ signify the set of nodes within the field of view (FOV) of $\mathcal{A}_i$, excluding the node $\mathcal{A}_i$ itself. Moreover, the communication link between nodes $\mathcal{A}_i$ and $\mathcal{A}_j$ is represented as $(\mathcal{A}_i, \mathcal{A}_j)$. A comprehensive overview of the employed notations can be found in Table 5.1. We make the following observations:

1. *Two nodes can form a link iff they fall within each other's FOVs*: $\exists(\mathcal{A}_i, \mathcal{A}_j) \iff \mathcal{A}_i \in \mathcal{A}(\mathcal{A}_j) \wedge \mathcal{A}_j \in \mathcal{A}(\mathcal{A}_i) \wedge i \neq j$.

2. *A node is an SA if it can form a link with only one other node*: $\mathcal{A}_i \in \mathcal{A}^s \iff \exists(\mathcal{A}_i, \mathcal{A}_j) \wedge \nexists(\mathcal{A}_i, \mathcal{A}_k), \forall \mathcal{A}_k \in \mathcal{A}(\mathcal{A}_i) \setminus \mathcal{A}_j \wedge i \neq j \neq k$.

3. *A node is a PA if it can form a link with multiple other nodes*: $\mathcal{A}_i \in \mathcal{A}^p \iff \exists(\mathcal{A}_i, \mathcal{A}_j) \wedge \exists(\mathcal{A}_i, \mathcal{A}_k), \mathcal{A}_k \in \mathcal{A}(\mathcal{A}_i) \setminus \mathcal{A}_j \wedge i \neq j \neq k$.

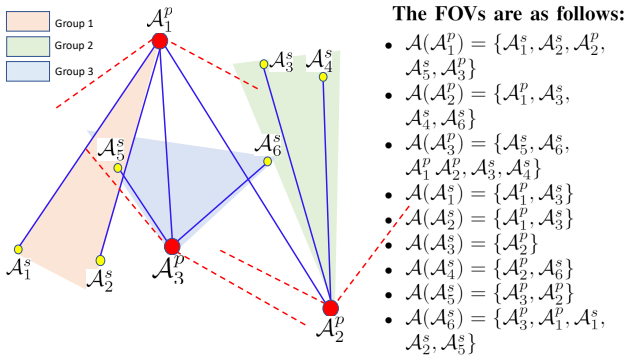

Figure 5.3: Example of network of nodes with grouping

Link Formations Between SAs-PA and Among PAs

We proceed with the assumption that both the location and the FOV for each node within the network are mutually known among the other nodes. Following the classification of nodes into SA and PA categories, as elaborated in Section 5, the network can be conceptualized as a series of distinct node groupings. Specifically, group i is composed of a single PA node, denoted as $\mathcal{A}_i^p$, along with its corresponding set of SA nodes (refer to Fig. 5.3). The SA

Table 5.1: List of Symbols

Symbol	Explanation
$\mathcal{A}$	Set of all nodes in the network
$\mathcal{A}_n$	nth node
$\mathcal{A}^p$	Set of all PA nodes
$\mathcal{A}_u^p$	uth PA
$\mathcal{A}^s$	Set of all SA nodes
$\mathcal{A}_v^s$	vth SA
$\mathcal{A}(\mathcal{A}_n)$	Set of nodes in FOV of $\mathcal{A}_n$
$\{\mathcal{A}\|\mathcal{A}_n\}$	Set of nodes that $\mathcal{A}_n$ can form a link with
$(\mathcal{A}_m, \mathcal{A}_n)$	Link between $\mathcal{A}_m$ and $\mathcal{A}_n$
$\{\mathcal{X}\}^s$	Set of SAs in the node set $\mathcal{X}$
$\{\mathcal{X}\}^p$	Set of PAs in the node set $\mathcal{X}$

nodes situated within group i engage in communication with $\mathcal{A}_i^p$. Furthermore, PA nodes from diverse groups establish communication links amongst themselves.

In the same figure, where the set of nodes is $\mathcal{A} = \{\mathcal{A}_1^s, \mathcal{A}_2^s, \mathcal{A}_3^s, \mathcal{A}_4^s, \mathcal{A}_5^s, \mathcal{A}_6^s, \mathcal{A}_1^p, \mathcal{A}_2^p, \mathcal{A}_3^p\}$, the sets of nodes that are within the FOV of each node are listed, and the FOVs of PAs are in dotted red lines. We note that node $\mathcal{A}_1^p$ forms links (blue lines) with $\mathcal{A}_1^s$, $\mathcal{A}_2^s$, $\mathcal{A}_2^p$, $\mathcal{A}_3^p$, node $\mathcal{A}_2^p$ forms links with $\mathcal{A}_1^p$, $\mathcal{A}_3^s$ $\mathcal{A}_4^s$, and node $\mathcal{A}_3^p$ forms links with $\mathcal{A}_5^s$, $\mathcal{A}_6^s$.

Consider $\mathcal{X}^s$ and $\mathcal{X}^p$ as representations of the sets of SAs and PAs within the node collection $\mathcal{X}$, respectively. Additionally, denote by $\mathcal{A}|\mathcal{A}_i$ the set of nodes with which node $\mathcal{A}_i$ can establish a communication link. Consequently, $\mathcal{A}|\mathcal{A}_i{}^s$ and $\mathcal{A}|\mathcal{A}_i{}^p$ signify the subsets of SAs and PAs, respectively, that node $\mathcal{A}_i$ holds the capability to create a link with. At this point, we proceed to make the following observations:

1. *An SA can form a link with only one other node*: $|\{\mathcal{A}|\mathcal{A}_i\}| = 1 \iff \mathcal{A}_i \in \mathcal{A}^s$.
2. *A PA can form a link with multiple other nodes*: $|\{\mathcal{A}|\mathcal{A}_i\}| > 1 \iff \mathcal{A}_i \in \mathcal{A}^p$.
3. *An SA can form a link with only one PA*: $|\{\mathcal{A}|\mathcal{A}_i\}^p| = 1 \iff \mathcal{A}_i \in \mathcal{A}^s \wedge \nexists(\mathcal{A}_u, \mathcal{A}_v), \forall \mathcal{A}_u, \mathcal{A}_v \in \mathcal{A}^s$.

Transmission Schedule of Nodes

We operate within a slotted communication framework where time is partitioned into frames, each lasting T_f seconds. In this context, a central entity, often represented by a base station (BS), further segments each time frame into three distinct sub-frames, depicted in Fig. 4.3. These sub-frames, designated as Uplink, Downlink, and PA-PA phases, possess durations of T_u, T_d, and T_p seconds, respectively. The information regarding this time

frame division is disseminated to all nodes within the network via a secure and interference-free Common Control Channel (CCC). The central entity, typically the BS, undertakes the responsibility of addressing the constrained optimization problem detailed in Section 5, culminating in the determination of optimized beamsteering angles for the PAs. The BS also communicates these optimized angles to the relevant Primary Antenna (PA) nodes. However, it is noteworthy that the task of scheduling transmissions is not managed by the BS; instead, this responsibility is entrusted to the individual nodes themselves. The transmission scheduling of nodes in each phase follows.

Within the Uplink and Downlink phases, the nodes in group i independently manage the scheduling of their transmissions across the designated time interval. Specifically, during the Uplink phase, the Primary Antenna (PA) node $\mathcal{A}_i^p$ allocates the sub-frame of duration T_u equally among its associated Secondary Antennas (SAs). This scheduling is executed without regard to the strategies employed by neighboring groups. During this phase, PA node $\mathcal{A}_i^p$ assumes the role of the receiver, while the SAs engage in transmission. Each SA within group i communicates with $\mathcal{A}_i^p$ exclusively during its designated sub-frame. Similarly, in the Downlink phase, PA node $\mathcal{A}_i^p$ allocates the sub-frame of duration T_d equally among its corresponding SAs. This allocation is carried out independently of the actions of other groups. During this phase, PA node $\mathcal{A}_i^p$ transitions into the transmitting mode, while the SAs within group i act as receivers. PA node $\mathcal{A}_i^p$ communicates individually with each SA during its allotted sub-frame. The PA-PA phase is distinct, with SAs remaining idle and PAs engaging in inter-PA communication. In this phase, each PA node can choose to be in either transmitting or receiving mode, each with equal probability. Additionally, when transmitting, a PA node selects another PA node randomly as the recipient of its transmission. To recap, the Uplink and Downlink phases witness PAs and SAs operating in varying modes, communicating according to their designated time slots, while the PA-PA

phase is characterized by inter-PA communication and a stochastic choice of transmitting and receiving modes.

It's important to emphasize that, during both the Uplink and Downlink phases, the transmission scheduling of nodes within group i remains private and is only accessible to the nodes within the same group. Consequently, from the viewpoint of group i, the transmission scheduling of nodes not affiliated with the group appears as a form of *random scheduling*. This distinction highlights the inherent lack of knowledge about the transmission plans of nodes external to the group. Moreover, it's noteworthy that during either the Uplink or Downlink phase, the act of transmitting within group i has the potential to introduce interference to the nodes in other groups that are in the process of receiving transmissions. This interaction between different groups can lead to instances of interference that need to be carefully managed and mitigated.

Certainly, the described scenario presents a complex interplay of interference and signal-to-noise ratios (SNR) in different phases of the network operation. Allow me to elaborate further on the points you've raised.

Consider Fig. 5.3 and assume the network is in the Downlink phase. For the link $(\mathcal{A}_2^p, \mathcal{A}_3^s)$ within group 2, it's observed that $\mathcal{A}_3^s$ falls within the field of view (FOV) of $\mathcal{A}_3^p$ from group 3. Consequently, when $\mathcal{A}_3^p$ transmits during this phase, it introduces interference on the receiving end of $\mathcal{A}_3^s$. This interference significantly impacts the signal-to-interference-plus-noise ratio (SINR) calculation for the link $(\mathcal{A}_2^p, \mathcal{A}_3^s)$ during this phase. Now, if we shift our focus to the Uplink phase, specifically examining the link $(\mathcal{A}_6^s, \mathcal{A}_3^p)$ within group 3, it's apparent that $\mathcal{A}_1^p$ from group 1 lies within the FOV of $\mathcal{A}_6^s$. As a result, when $\mathcal{A}_6^s$ transmits during this phase, it introduces interference on the receiving end of $\mathcal{A}_1^p$ from group 1. These instances of interference and SNR variations across different links and phases must

be accounted for when assessing the achievable channel rates in the network. To address this complexity, a Bayesian approach involving conditional probabilities can be employed to formulate the achievable channel rate for each link. This would allow for a comprehensive evaluation of the communication performance, considering the effects of interference and the stochastic nature of transmission scheduling.

SINR Calculation and Achievable Link Rate

Let's delve into the expression for the received power between nodes $\mathcal{A}_i$ and $\mathcal{A}_j$ in the context of the given parameters and channel model. Given the distance d_{ij} separating the nodes $\mathcal{A}_i$ and $\mathcal{A}_j$, and assuming that $\mathcal{A}_i$ is pointing toward $\mathcal{A}_j$ with a beamsteering angle θ_i, we can determine the deviation angle $\psi_{i\to j}$ as illustrated in Fig. 5.1. Furthermore, let P_t denote the transmit power of $\mathcal{A}_i$ and $P_r(i,j)$ represent the received power at $\mathcal{A}_j$ from $\mathcal{A}_i$. Employing the THz communication channel model described in [86], characterized by a path-loss exponent of 2, we can express $P_r(i,j)$ in relation to P_t as follows:

$$P_r(i,j) = \frac{P_t}{d_{i,j}^2} G_i(\theta_i - \psi_{i\to j}) G_j(\theta_j - \pi - \psi_{i\to j}) \tag{5.2}$$

where G_i and G_j are the directional antenna gains of nodes $\mathcal{A}_i$ and $\mathcal{A}_j$, respectively. We can now calculate the SINR at node $\mathcal{A}_j$ as follows:

$$\text{SINR}_{i\to j} = \frac{P_r(i,j)}{N_0 W + I} \tag{5.3}$$

where $N_0 W$ is the cumulative thermal noise power and I is the interference power at $\mathcal{A}_j$. The achievable rate over the link $(\mathcal{A}_i, \mathcal{A}_j)$ during each time (sub-)frame, measured in bit/sec/Hz,

is

$$R_{i\to j} = \log_2(1 + \text{SINR}_{i\to j}). \tag{5.4}$$

Achievable Network Sum Rate

To derive the optimal beamsteering angles for a network of mmWave radio nodes, it's essential to quantify the total achievable sum-rate that the nodes can collectively attain. This is achieved by formulating the achievable rates, namely, R^u for the Uplink phase, R^d for the Downlink phase, and R^p for the PA-PA phase. In our approach, we assume that during the Uplink and Downlink phases, the SA nodes within each group direct their beams towards their corresponding PA nodes for data transmission and reception respectively. This approach ensures that maximum transmit gain is achieved by the SAs. Nevertheless, achieving maximum network capacity requires the adjustment of beamsteering angles for all PA nodes across the network. Additionally, we operate under the assumption that during the Uplink (Downlink) phase, each PA node within a group employs a single fixed beamsteering angle for reception (transmission) from (to) various SA nodes. In other words, the beamsteering angles of the PA node remain consistent throughout the given phase, regardless of the SA node it's interacting with.

Finding Rate R^u in Uplink Phase

Consider group j with its PA node, denoted as $\mathcal{A}_j^p$, and its set of SA nodes, denoted as $\{\mathcal{A}|\mathcal{A}_j^p\}^s$. The links within group j in this phase are represented as $(\mathcal{A}_i^s, \mathcal{A}_j^p)$, where $\mathcal{A}_i^s \in \{\mathcal{A}|\mathcal{A}_j^p\}^s, \mathcal{A}_j^p$ are the transmitting SA and the receiving PA nodes, respectively. Note that transmitting SA nodes in other groups may impose interfere on $\mathcal{A}_j^p$, depending on their FOVs.

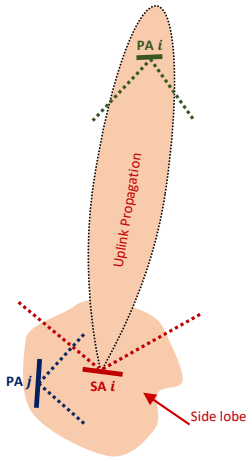

Figure 5.4: PA node j receiving side lobe interference

Let $R^u_{\mathcal{A}^s_i \to \mathcal{A}^p_j}$ denote the achievable channel rate over all links within group j in this phase. We have

$$R^u_{\mathcal{A}^s_i \to \mathcal{A}^p_j} = \frac{1}{|\{\mathcal{A}|\mathcal{A}^p_j\}^s|} \sum_{\mathcal{A}^s_i \in \{\mathcal{A}|\mathcal{A}^p_j\}^s} \log_2 \left(1 + \frac{P_r(\mathcal{A}^s_i, \mathcal{A}^p_j)}{N_0 W + I_{\mathcal{A}^p_j}}\right) \tag{5.5}$$

where $I_{\mathcal{A}^p_j}$ denotes the interference power imposed on $\mathcal{A}^p_j$. Before expressing $I_{\mathcal{A}^p_j}$ mathematically, we note that the sum in (5.5) is over all SA nodes in group j. The fraction outside the sum in (5.5) comes from the fact that the SA nodes in each group are time sharing the channel. Each SA node in group j transmits only during a fraction of sub-frame T_u, and this fraction is equal to $\frac{1}{|\{\mathcal{A}|\mathcal{A}^p_j\}^s|}$, where $|\{\mathcal{A}|\mathcal{A}^p_j\}^s|$ is the number of SA nodes in group j. The interference power $I_{\mathcal{A}^p_j}$ in (5.5) can be expressed as follows

$$I_{\mathcal{A}^p_j} = \sum_{\mathcal{A}^p_i \in \mathcal{A}^p, i \neq j} \frac{1}{|\{\mathcal{A}|\mathcal{A}^p_i\}^s|} \sum_{\mathcal{A}^s_k \in \mathcal{I}^s_{i \to j}} P_r(\mathcal{A}^s_k, \mathcal{A}^p_j) \tag{5.6}$$

The inner sum in (5.6) is over the interfering SA nodes belonging to the set $\mathcal{I}^s_{i \to j}$. The SA nodes in this set, defined as $\mathcal{I}^s_{i \to j} = \{\mathcal{A}^s_k : \mathcal{A}^s_k \in \{\mathcal{A}|\mathcal{A}^p_i\}^s\}$, can impose interference on $\mathcal{A}^p_j$ in

this phase. The interference on $\mathcal{A}_j^p$ from the SA nodes in other group i can be from the main lobe or the side lobe. If $\mathcal{A}_j^p$ lies within the main lobe of an SA node in group i, then, it will be subject to main lobe interference, otherwise, it will be subject to side lobe interference. The main lobe and side lobe interference gain expressions will be governed by (4.5). In Fig. 5.4, we have provided an illustration of the side lobe interference being received by PA node j (in blue) from SA node i (in red), belonging to group i. In group i, SA node i is transmitting data to PA node i (in green) during the uplink phase. PA j does not fall within the main lobe of SA i and hence, during this phase, it is being subject to side lobe interference from SA i.

To recap, it's important to note that the transmission scheduling of group i is perceived as random by group j. This means that the likelihood of an SA node within $\mathcal{I}_{i\to j}^s$ having a simultaneous transmission with the link $(\mathcal{A}_i^s, \mathcal{A}_j^p)$ of group j is uniform and is given by $\frac{1}{|\{\mathcal{A}|\mathcal{A}_i^p\}^s|}$, where $|\{\mathcal{A}|\mathcal{A}_i^p\}^s|$ represents the count of SA nodes in group i. Consequently, this implies that the average interference power introduced by group i is the total sum of interference power originating from the SA nodes within $\mathcal{I}_{i\to j}^s$, divided by the number of SA nodes within group i. Consequently, the overall interference power imposed on $\mathcal{A}_j^p$, as (5.6) shows, is the sum of average interference power imposed by other groups. The aggregate data transmission rate during Uplink phase is

$$R^u = \sum_{j=1}^{U} R_j^u. \tag{5.7}$$

As a numerical example, consider Fig. 5.3, where we have:

$$R_1^u = \frac{1}{2}\left[\log_2\left(1+\frac{P_r(\mathcal{A}_1^s,\mathcal{A}_1^p)}{N_0+I_{\mathcal{A}_1^p}}\right)+\log_2\left(1+\frac{P_r(\mathcal{A}_2^s,\mathcal{A}_1^p)}{N_0+I_{\mathcal{A}_1^p}}\right)\right],$$
$$R_2^u = \frac{1}{2}\left[\log_2\left(1+\frac{P_r(\mathcal{A}_3^s,\mathcal{A}_2^p)}{N_0+I_{\mathcal{A}_2^p}}\right)+\log_2\left(1+\frac{P_r(\mathcal{A}_4^s,\mathcal{A}_2^p)}{N_0+I_{\mathcal{A}_2^p}}\right)\right],$$
$$R_3^u = \frac{1}{2}\left[\log_2\left(1+\frac{P_r(\mathcal{A}_5^s,\mathcal{A}_3^p)}{N_0+I_{\mathcal{A}_3^p}}\right)+\log_2\left(1+\frac{P_r(\mathcal{A}_6^s,\mathcal{A}_3^p)}{N_0+I_{\mathcal{A}_3^p}}\right)\right].$$

The interferences are $I_{\mathcal{A}_1^p} = \frac{1}{2}P_r(\mathcal{A}_6^s,\mathcal{A}_1^p)$, $I_{\mathcal{A}_2^p} = \frac{1}{2}P_r(\mathcal{A}_5^s,\mathcal{A}_2^p)$, and $I_{\mathcal{A}_3^p} = 0$, since no SA node is imposing interference on $\mathcal{A}_3^p$. The factor $1/2$ in $I_{\mathcal{A}_1^p}$ is because the interfering SA node $\mathcal{A}_6^s$ belongs to to group 3, and there are 2 SA nodes in group 3. The factor $1/2$ in $I_{\mathcal{A}_2^p}$ is because the interfering SA node $\mathcal{A}_5^s$ belongs to to group 3, and there are 2 SA nodes in group 3. We have $R^u = R_1^u + R_2^u + R_3^u$.

Finding Rate R^d in Downlink Phase

Consider an SA node, denoted as $\mathcal{A}_j^s$, and its corresponding PA node, denoted as $\mathcal{A}_i^p$, where $\mathcal{A}_i^p \in \{\mathcal{A}|\mathcal{A}_j^s\}^p$. The link between these two nodes in this phase is represented as $(\mathcal{A}_i^p, \mathcal{A}_j^s)$, where $\mathcal{A}_i^p$ and $\mathcal{A}_j^s$ are the transmitting PA and the receiving SA nodes in group i, respectively. Note that other transmitting PA nodes that their FOVs contain $\mathcal{A}_j^s$ will impose interfere on $\mathcal{A}_j^s$. Let $R^d_{\mathcal{A}_j^s}$ denote the achievable rate over the link $(\mathcal{A}_i^p, \mathcal{A}_j^s)$ in this phase. We have

$$R^d_{\mathcal{A}_i^p \to \mathcal{A}_j^s} = \frac{1}{|\{\mathcal{A}|\mathcal{A}_i^p\}^s|}\log_2\left(1+\frac{P_r(\mathcal{A}_i^p,\mathcal{A}_j^s)}{N_0W+I_{\mathcal{A}_j^s}}\right) \tag{5.8}$$

where $I_{\mathcal{A}_j^s}$ denotes the interference power imposed on $\mathcal{A}_j^s$. The fraction outside the $\log_2$ in (5.8) comes from the fact that $\mathcal{A}_i^p$ transmits to $\mathcal{A}_j^s$ only during a fraction of sub-frame T_d,

and this fraction is equal to $\frac{1}{|\{\mathcal{A}|\mathcal{A}_i^p\}^s|}$. The interference power $I_{\mathcal{A}_j^s}$ in (5.8) can be expressed as follows

$$I_{\mathcal{A}_j^s} = \sum_{\mathcal{A}_k^p : \mathcal{A}_k^p \neq \mathcal{A}_i^p} P_r(\mathcal{A}_k^p, \mathcal{A}_j^s) \tag{5.9}$$

The sum in (5.9) is over all the interfering PAs from other groups and hence they can impose both main lobe and side lobe interference on $\mathcal{A}_j^s$ in this phase. If the interfering PA nodes from other groups contain $\mathcal{A}_j^s$ within their main lobes, then they impose main lobe interference, otherwise they impose side lobe interference. The main lobe and side lobe interference gains are governed by (4.5). The aggregate data transmission rate during Downlink phase is

$$R^d = \sum_{\mathcal{A}_j^s \in \mathcal{A}^s} R^d_{\mathcal{A}_i^p \to \mathcal{A}_j^s}. \tag{5.10}$$

Finding Rate R^p in PA-PA Phase

Let's examine a PA node, denoted as $\mathcal{A}_i^p$, and consider the set of PA nodes with which $\mathcal{A}_i^p$ can establish a connection, denoted as $\{\mathcal{A}|\mathcal{A}_i^p\}^p$. During this specific phase, it is assumed that $\mathcal{A}_i^p$ can operate in either transmitting or receiving mode, with both options having an equal probability. Furthermore, when $\mathcal{A}_i^p$ is in the transmitting (receiving) mode, it randomly selects another PA node from the set $\{\mathcal{A}|\mathcal{A}_i^p\}^p$ to send data to (receive data from). Now, consider two PA nodes, $\mathcal{A}_i^p, \mathcal{A}_j^p$. Our statement above implies that, to form the link $(\mathcal{A}_i^p, \mathcal{A}_j^p)$, node $\mathcal{A}_i^p$ needs to be in transmitting mode, and chooses to transmit to $\mathcal{A}_j^p$. Also, node $\mathcal{A}_j^p$ needs to be in receiving mode, and chooses to receive from $\mathcal{A}_i^p$. Let $R_{\mathcal{A}_i^p \to \mathcal{A}_j^p}$ denote the achievable channel rate over all the links that $\mathcal{A}_j^p$ is the receiving node in this phase. We

have

$$R_{\mathcal{A}_i^p \to \mathcal{A}_j^p} = \frac{1}{4 \times |\{\mathcal{A}|\mathcal{A}_i^p\}^p| \times |\{\mathcal{A}|\mathcal{A}_j^p\}^p|} \times \sum_{\mathcal{A}_i^p \in \{\mathcal{A}|\mathcal{A}_j^p\}^p} \log_2 \left(1 + \frac{P_r(\mathcal{A}_i^p, \mathcal{A}_j^p)}{N_0 W + I_{\mathcal{A}_j^p}}\right) \tag{5.11}$$

where $I_{\mathcal{A}_j^p}$ denotes the interference power imposed on $\mathcal{A}_j^p$. Before expressing $I_{\mathcal{A}_j^p}$ mathematically, we note that the sum in (5.11) is over all PA nodes that can form a link with $\mathcal{A}_j^p$. The fraction outside the sum in (5.11) stems from the facts that (1) $\mathcal{A}_i^p$ and $\mathcal{A}_j^p$ should be in transmitting and receiving modes, respectively, (2) $\mathcal{A}_i^p$ should be randomly chosen from the set $\{\mathcal{A}|\mathcal{A}_j^p\}^p$ by $\mathcal{A}_j^p$. And, $\mathcal{A}_j^p$ should be randomly chosen from the set $\{\mathcal{A}|\mathcal{A}_i^p\}^p$ by $\mathcal{A}_i^p$. Hence, this fraction is equal to $\frac{1}{2} \times \frac{1}{2} \times \frac{1}{|\{\mathcal{A}|\mathcal{A}_i^p\}^p|} \times \frac{1}{|\{\mathcal{A}|\mathcal{A}_j^p\}^p|}$, where $|.|$ of a set indicates the cardinality of the set.

$$I_{\mathcal{A}_j^p} = \frac{1}{2} \sum_{\mathcal{A}_k^p : \mathcal{A}_k^p \neq \mathcal{A}_i^p} P_r(\mathcal{A}_k^p, \mathcal{A}_j^p) \tag{5.12}$$

The sum in (5.12) is over the PA nodes, other than $\mathcal{A}_i^p$ and hence they can impose interference on $\mathcal{A}_j^p$, only if they are in transmitting mode, in this phase. The factor 1/2 outside the sum in (5.12) reflects that the fact that $\mathcal{A}_k^p$ interferes with $\mathcal{A}_j^p$ only if it is transmitting. If $\mathcal{A}_j^p$ lies in the main lobe of $\mathcal{A}_k^p$ then it will receive main lobe interference otherwise it will be subject to side lobe interference. The aggregate data transmission rate during PA-PA phase is

$$R^p = \sum_{\mathcal{A}_j^p \in \mathcal{A}^p} R_{\mathcal{A}_i^p \to \mathcal{A}_j^p}. \tag{5.13}$$

Problem Formulation

Given the network of directional links as detailed in the previous sections, we focus on maximizing the network capacity by tuning the beamsteering angles of all directional nodes. We assume that each SA node $\mathcal{A}_k^s$ in a group has chosen its beamsteering angle θ_k such that the center of its beam is exactly aligned with its associated PA node, and hence there is no need to optimize the beamsteering angles of SAs. We assume the transmit power P_t is given such that it satisfies the hardware constraints, and hence, we do not optimize it. Let R^u, R^d, R^p denote the achievable rates over the links during Uplink, Downlink, and PA-PA phases, respectively. The constrained problem of sum rate maximization (SRM), where the sum rate R is $R = R^d + R^u + R^p$, via tuning the beamsteering angles of all PAs can be expressed as the following.

(P1): Sum Rate Maximization (SRM)

$$\max_{\mathbf{\Theta}} \; R \tag{5.14}$$

$$\text{s.t. } \beta_j^{\min} \leq \theta_j \leq \beta_j^{\max}, j = 1, ..., U, \tag{5.15}$$

where $\mathbf{\Theta}$ is the set of beamsteering angles of all PA nodes, i.e., $\mathbf{\Theta} = \{\theta_j : \mathcal{A}_j^p \in \mathcal{A}^p, j = 1, ..., U\}$. We optimize the beamsteering angles of all PA nodes such that R in (5.14) is maximized, subject to the FOV constraint in (5.15). This optimized set of beamsteering angles will make each PA node point toward a direction such that, as transceivers, they would contribute towards maximization of R.

The SRM problem assumes that each of the three transmission phases within a time frame has equal importance. This assumption may not work well for certain applications. For instance, if this network is supporting voice communication among nodes participating in

it, some nodes will have to work as relays which will result in a situation where Uplink, Downlink, and PA-PA phases need to be given a different share of the time. The inspiration to tune the time in each phase as weights comes from the unique ways ad-hoc wireless communications systems in military and emergency public safety tactical communication systems [15, 89] are implemented. In such scenarios, a *tactical bubble* is created off of the 5G infrastructure meant for civilian usage. This bubble helps in maintaining data privacy of the tactical network traffic, while using the BSs for civilian networks. Hence, we consider a constrained weighted sum rate maximization (WSRM) problem with the assumption that PAs will act as relays. To design a low-latency setup for end-to-end communication among SAs, we allocate equal time for the Uplink and Downlink phases. Since the PA-PA phase is only for relaying, the time allocated for that phase is less than or equal to the summation of that allocated to the Uplink and Downlink phases. This new problem can be written as follows.

(P2): Weighted Sum Rate Maximization (WSRM)

$$\max_{\boldsymbol{\Theta},\boldsymbol{W}} \; w_d R^d + w_u R^u + w_p R^p \tag{5.16}$$

$$\text{s.t. } \beta_j^{\min} \leq \theta_j \leq \beta_j^{\max}, j = 1, ..., U, \tag{5.17}$$

$$w_d + w_u + w_p = 1, \tag{5.18}$$

$$w_d, w_u, w_p \in (0, 1), \tag{5.19}$$

$$w_d = w_u, \tag{5.20}$$

$$w_p \leq w_d + w_u, \tag{5.21}$$

where $\boldsymbol{W}$ is the set of weights for tuning the time duration for each phase, i.e., $\boldsymbol{W} = \{w_d, w_u, w_p\}$, and $w_d = \frac{T_d}{T_f}$, $w_u = \frac{T_u}{T_f}$, $w_p = \frac{T_p}{T_f}$, respectively. The constraint (5.20) guarantees that $T_u = T_d$. The constraint (5.21) assures that $T_p \leq T_d + T_u$. This formulation assumes

that the communication is taking place only between SAs, e.g., in terms of voice or end-to-end data/video transfers. The constraints (5.20) and (5.21) can be customized for other network application scenarios. Our proposed solution approaches in the following sections can still be applied to these other scenarios.

Solution Approaches

Solving the constrained problems in (5.14) and (5.16) requires non-linear optimization methods. Directional antenna configurations in practice requires discrete inputs, e.g., phases of a phased array mmWave antenna, to steer the beam, are discrete values. Hence, to comply with the directional antenna configurations the authors in [90] discretize each of the optimization variables in the set $\mathbf{\Theta}$, i.e., they assume θ_j is discretized into N_j values, for $j = 1, ..., U$. This implies that the search space of SRM and WSRM problems to find the best beamsteering angles consists of $\prod_{j=1}^{U} N_j$ discrete points. In other words, the computational complexity of finding the solution using exhaustive search grows exponentially w.r.t. U when $N_j = N$. In this paper, we follow similar discretization of each optimization variable in the set $\mathbf{\Theta}$. To avoid the prohibitive computation complexity of the exhaustive search solution, a heuristic algorithm (Genetic Algorithm or GA) has been designed in [90] for large networks and the authors compare their GA solutions to the exhaustive search solution for small networks. In this paper, we take those results and compare them to a new heuristic approach, presented in this paper, called Recursive Random Search (RRS). This comparison is done with the exhaustive and the tuned GA results as presented in in [90].

Algorithm 8 Beamsteering angle optimization of PAs

Input: $\mathcal{A}^p$
Output: S^*
Function `OptimizeAngle(`$\mathcal{A}^p$`):`
  $\{\mathcal{A}|\mathcal{A}_i^p\}$ = set of nodes that $\mathcal{A}_i^p$ can form link with, $\forall \mathcal{A}_i^p \in \mathcal{A}^p$;

  for $\mathcal{A}_i^p \in \mathcal{A}^p$ **do**
    $\beta_i^{\min} = \Gamma_i - \beta_i/2$; $\beta_i^{\max} = \Gamma_i + \beta_i/2$;
    Trim β_i into $[\beta_i^{\min}, (\beta_i^{\min} + 1^\circ), ..., \beta_i^{\max}]$;
    $\beta_i^p \leftarrow \beta_i^{\text{trimmed}}$;
  end
  $C \leftarrow 0$;
  for S *in* ***CartesianProduct***(β^p) **do**
    $C_{temp} \leftarrow 0$;
    for $\mathcal{A}_i^p \in \mathcal{A}^p$ **do**
      for $\mathcal{A}_n \in \{\mathcal{A}^p|\mathcal{A}_i^p\}$ **do**
        $C_{temp} += \log_2(1 + \frac{P_r(\mathcal{A}_i^p, \mathcal{A}_n)}{N_0 + \sum_{\mathcal{A}_j : \mathcal{A}_n \in \mathcal{A}(\mathcal{A}_j)} P_r(\mathcal{A}_j, \mathcal{A}_n)/2})$;
      end
    end
    if $C_{temp} > C$ **then**
      $S^* \leftarrow S$;
      $C \leftarrow C_{temp}$;
  end
  return S^*
End Function

Solving (P1)

Exhaustive Search

The exhaustive search for beamsteering optimization has been summarized in Algorithm 8. For every PA node $\mathcal{A}_i^p \in \mathcal{A}^p$, based on their $\beta_i^{\min}$ and $\beta_i^{\max}$, we trim the unnecessary parts of the whole beamwidth β_i. For example, if the FOV of $\mathcal{A}_i^p$ is 170°, but the two extreme nodes within that FOV span 85°, then we work with $\beta_i^{\text{trimmed}} = 85^\circ$. The two new extremities now become $\beta_i^{\min} = \Gamma_i - 42.5^\circ$ and $\beta_i^{\max} = \Gamma_i + 42.5^\circ$. For all PAs, we store the beamsteering range in a vector, denoted as β^p. Hence, β^p becomes a set of trimmed FOVs for all PAs. Next, we invoke the function to calculate Cartesian Product of sets and pass β^p as the input parameter to this function. The output is the set of all possible beamsteering angles for all

PAs. We then loop through these sets of beamsteering angles and do the following: (1) For all PAs, using the current set of beamsteering angle S, find the received power at every node belonging to the set of nodes that can form links with $\mathcal{A}_i^p, \forall \mathcal{A}_i^p \in \mathcal{A}^p$. For this, we use the angles that each of the node makes with $\mathcal{A}_i^p$. Recall, we are using current set of beamsteering angles S. Then, we use the absolute values of the differences of these two angles to find the divergence angle $\psi_{\mathcal{A}_i^p \to \mathcal{A}_n}, \forall \mathcal{A}_n \in \{\mathcal{A} | \mathcal{A}_i^p\}$. (2) Calculate the interference power affecting the link $(\mathcal{A}_i^p, \mathcal{A}_n)$. (3) Calculate the achievable channel rate over the link $(\mathcal{A}_i^p, \mathcal{A}_n)$. Following this procedure we calculate the achievable channel rate over all the links in the network. Once we have the channel rates for current set S, the next set of beamsteering angles are applied to PAs. This procedure is repeated till the last set in the set β^p is reached. Finally, we compare R values resulted from all sets of beamsteering angles and declare that set as the best set of beamsteering angles which provides the highest value of R.

Genetic Algorithm (GA)

To overcome the computational complexity of the exhaustive search, we design a GA for solving (5.14). We first compare the GA results to the exhaustive search results, and tune the GA configuration for a good tradeoff between optimality of its solution and the time it takes to compute the solution. Then, we use the tuned GA configuration to solve (5.14) for large networks, which are intractable with the exhaustive search. The GA steps involve the followings:

- Individual (Chromosome): An individual chromosome is essentially a vector of beamsteering angles, i.e., $\hat{\theta}$ in (5.14), and represents a solution to (5.14). A gene in a chromosome are randomly chosen real values as they correspond to A steering angles, one for each node in the network.

- Population Size: We set the population of size to kA, where $k = 10$ or 100. For larger networks (i.e., large A), the population size is increased accordingly.

- Fitness Value: Fitness value of an individual (chromosome) is R, achieved as a result of the chosen set of steering angles, $\hat{\theta}$.

- Fit Population: Fit population is the top $x\%$ of the current population. We tried fit population sizes from $x = 20$ to $x = 90$.

- Selection and Crossover: From the fit population, we randomly select two parents for crossover. Then, the child is generated by performing weighted average of genes of the two selected parents. This is repeated to generate kA children, that form the next generation, which is then fed back as inputs to our GA. This is repeated until the convergence criterion is met.

- Convergence Criterion: If the current generation is g_0 and the next generation is g_1, then the fittest individual of g_1 cannot be fitter than that of g_0 by more than 0.3% (we decide this). This low percentage value shows that the next generation does not show a significant fitness improvement over the current one, which is a safe assumption that GA has converged to an optima.

Recursive Random Search (RRS)

Although GA overcomes the computational complexity of exhaustive search while offering solutions close to the optimum, it still is not fast enough for very large networks with tens to hundreds of nodes. The fine tuned GA in in [90], does provide good results for network size of around 32, however, optimizing the steering angles for networks consisting of 50 or more nodes, we need a faster algorithm. This leads us to RRS algorithm, which converges

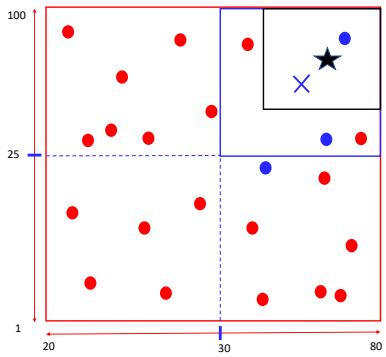

Figure 5.5: 2-dimensional RRS search space $\mathcal{S}$

much faster and was shown [17] to outperform conventional evolutionary algorithms like GA for most optimization problems. Like other evolutionary algorithms, RRS comprises of exploration and exploitation phases.

For exploration, RRS randomly samples Q_1 points and during the exploitation phase, it samples Q_2 points. In our case, RRS randomly samples $Q_1 = 40$ points[2] from the entire search space $\mathcal{S}$. This allows it to "inspect" the overall form of the objective function and identify promising areas in $\mathcal{S}$. RRS was described generically in [17] with several tunable parameters. We describe our implementation of it. Let us consider a 2-dimensional search space $\mathcal{S}$, defined by parameters x and y as shown in Fig. 5.5. RRS samples the search space (defined by the red box) by randomly selecting x ranging from 20 to 80 and y from 1 to 100) and picks 40 such samples (only 20 red points showed for illustration purpose) within the boundaries of $\mathcal{S}$. Then, RRS selects the sample (marked in blue cross) yielding the best result out of all the 40 samples tried, and starts its exploitation phase.

In exploitation, RRS continues to search only within the identified promising area using recursive random sampling. Recursion is implemented by two operations: *re-center* and

[2] [17] shows that this many points is the empirically best for most objective functions.

shrink. RRS iteratively performs *re-centering* around the initial best solution and then shrinks the search space around it before applying random sampling again. After the first shrink, the number of random samples taken reduces from $Q_1 = 40$ to $Q_2 = 3$ in the subsequent searches. In the example at Fig. 5.5, RRS, after initially sampling 40 points, finds the one marked with "×" as the best. Then, it uses 3 random samples to try and find a better "×"; let us call it "⋆". If it is indeed able to find a "⋆", then it re-centers the search space around "⋆". The initial re-centered search space for "×" is found (marked with blue square) within the red square. This new search space gets updated as RRS successfully finds better "×"s, i.e., "⋆" in this case, shifting the search space gradually towards north-east, represented by the black square within the blue square.

When we say 'RRS is impossible to shrink', we mean that we are left with only one set of beamsteering angle for every node in the network. Our shrinking factor $s = 0.5$. If we consider a 2-dimensional search space, as shown in Fig. 5.5, we calculate the area of the search space as, say, A. After shrinking, the length and width each reduces by half. Hence, the area reduces by 1/4. This means the number of shrinking steps to reduce the search space size to 1 is characterized by the logarithm of the initial search space, A. So we can write the complexity of shrinking the search space until it becomes impossible to search as $\log_{2^k} \beta^k$, where k is the total number of nodes and β is the FOV of each node. In simplified form, This becomes $\log_{2^k} \beta^k = \log_2 \beta$. Ignoring the base, we can write the computational complexity of shrinking the search space is $\log_2 \beta$. For shrinking factor $0 < s < 1$, this complexity can be written as $\log_{1/s} \beta = -\log_s \beta$. If RRS is unable to find the "⋆" or a solution better than the original "×" after three consecutive tries, then it shrinks the new search space (marked by the black box) by halving each parameter range, effectively reducing the search space exponentially. RRS keeps re-centering and shrinking until it becomes impossible to shrink the search space, which means that we have arrived at the solution. Although RRS can

stop at this point, we run the whole procedure repeatedly to generate "multiple optima" and stop when the current optimum is better than the previous by less than 0.01%. Worst case complexity for our RRS setup is is: $\mathcal{O}(Q_2 Q_1^2 z \log_2 \beta)$.

We showed how RRS works by principle with a 2-dimensional example. However our SRM problem in (5.14) has a search space with multiple parameters given in $\hat{\theta}$ and $\hat{w}$. Hence, we implemented RRS over this multi-dimensional search space.

Solving (P2)

In the case of WSRM in (5.16), the scheduling is also being optimized in addition to the beamsteering. We solve (P2) in two stages. In (5.16), given the set of beamsteering angles of all PA nodes $\mathbf{\Theta}$, the optimization of the weights, $\hat{w}$, for each transmission phase is a convex problem. Hence, we solve WSRM in two stages: First, starting with equal weights (i.e., $\hat{w_d} = \hat{w_u} = \hat{w_p} = 1/3$) for the scheduling, we use the RRS as detailed in the previous section to optimize $\hat{\theta}$. Then, we use a convex optimizer to find the optimum $\hat{w}$ for the $\hat{\theta}$ values from the first stage. We, then, repeat these two stages until the objective in (5.16) does not improve.

Simulation Results and Discussion

Throughout our simulation, we have used $N_0 = -87$dBm [91]. We assume all the nodes have the same FOV and the same half-power beamwidth, i.e., $\beta_i = \beta, \alpha_i = 15°, \forall i$, and the nodes are within each other's transmission ranges. The inclination angles Γ_i are randomly generated such that $0° \leq \Gamma_i \leq 360°, \forall i$. The simulation was repeated with randomly generated networks (PAs and SAs are determined at runtime) within a fixed geographic

area and averaged over 3 to 30 runs. In each run, the nodes that are not within the FOV of any other node, are excluded from our simulation, since such nodes are isolated and are not communicating. Hence, the networks that we consider in our simulation are formed by connected nodes only.

Solving SRM

Inspecting very large networks with hundreds of nodes is not tractable with exhaustive or GA methods. We first show that RRS can attain results similar to GA for large networks and use RRS to inspect very large networks. In Fig. 5.6a, we show how R varies when RRS, GA, and exhaustive methods are used for optimizing beamsteering angles of the PAs in the network. Compared to exhaustive and GA (using various fit population sizes), single pass RRS offers good results. For the small network shown in the figure, single pass RRS is better than GA with 50% fit population. If we run RRS for multiple passes, then accuracy improves significantly, bringing it on par with 70% fit population GA. Although in terms of accuracy, RRS does not (and cannot) offer better results than the exhaustive approach, Fig. 5.6b shows us the amount of time (T), in terms of the total number of times we compute the summation of the individual link throughputs of the said network. We see that even for 70% fit population for small networks, convergence time of GA is an order of magnitude higher than multi pass RRS. In fact, 70% fit population GA offers around a 1.6% better R than single pass RRS, while consuming around 600% more computation time than the same, for a 4-node network. This means that RRS offers a great trade-off between accuracy and computation time, and RRS becomes more advantageous for larger networks.

A key question regarding efficacy of RRS is whether or not it can attain close-to-optimal results as the network is getting larger. Fig. 5.6c shows R attained by GA and RRS for

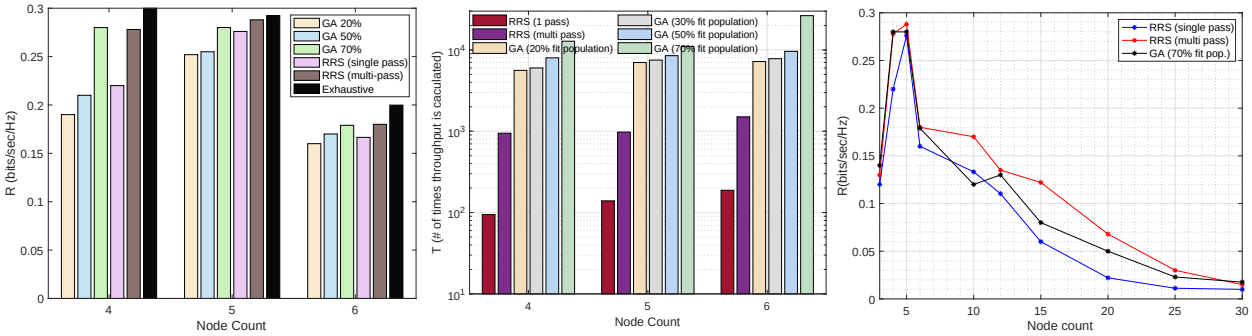

(a) R for various θ optimizing approaches **(b)** Convergence times for small networks **(c)** R for various θ optimizing approaches

Figure 5.6: Sum rate and computation time comparison among GA, exhaustive and RRS approaches

large networks with tens of nodes. We use a high fit population size (i.e., 70%) for GA to get results closer to the optimum and use that as a basis for evaluating the performance of RRS for large networks. The figure shows that single-pass RSS can attain close-to-optimum results while multi-pass RRS can even beat the GA in many cases. This clearly shows that RRS is well suited for solving the SRM (P1) and WSRM (P2) problems for very large networks.

Using RRS, we explore the attainable throughput for small, large and very large networks as the HPBW (α) and the FOV (β) vary. To better visualize the trend in R, we use node density as the x-axis parameter. To calculate the density for given network of nodes on a plane, we draw the 'bounding box' around the nodes. This is found by taking the spatially outermost nodes and drawing an imaginary rectangular area using their x and y coordinates. Dividing the number of nodes in the network by the bounding box area gives us the density of nodes per square meter area. Then, to plot average R vs. the density, we generate multiple such networks (each confirmed to be connected) and group them based on their density values. While generating the networks randomly, we classify the networks among the different density

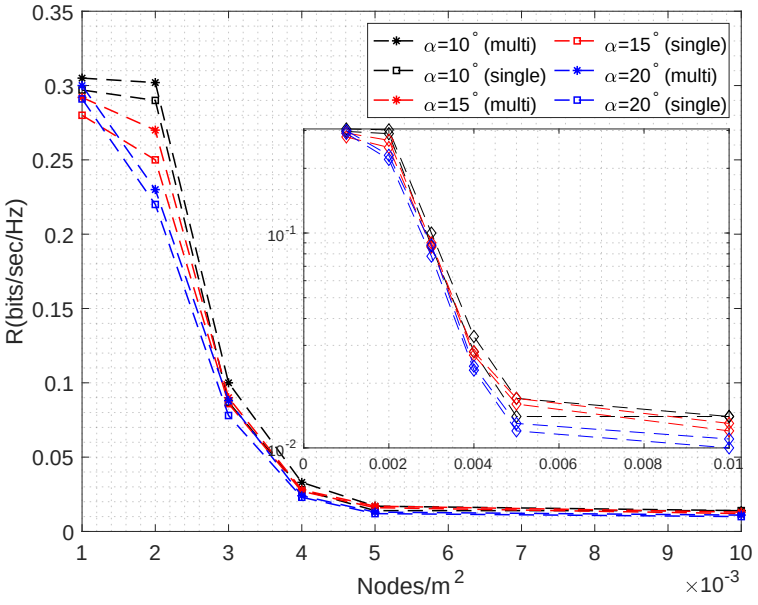

Figure 5.7: R for various α values; Nodes randomly scattered over an area of 200 $\times$ 200 m^2

values presented in Fig. 5.7 and 5.8. In these figures, we show R for specific node density values, such as 0.001, 0.002, and 0.003, each corresponding to a bin. However, since the network generation is random in our setup, we do not always get networks with densities exactly equal to these bins. To resolve this, we placed the randomly generated network to the closest bin. Fig. 5.7 shows R when α is 10°, 15°, or 20°, for both single-pass and multi-pass RRS optimization methods for θ_i (the x-axis is in log scale and the y-axis is in linear scale). As expected, when the node density is high, the network with wider beamwidths suffer from more interference. R is higher for low-to-medium node density. For a network with around 0.001 nodes/m^2 it remains a peak. After that, R exponentially decays (observed in the inner plot with x-axis in logarithmic scale) as the node density increases. This same trend is observable for single- and multi-pass RRS methods and the latter consistently yields higher R than the former throughout the presented node density range. Fig. 5.8 shows R when β is 50°, 70°, or 90°, for both single- and multi-pass RRS optimization methods for θ_i. Here as well, with higher node density, the network with wider FOVs result in lower R due

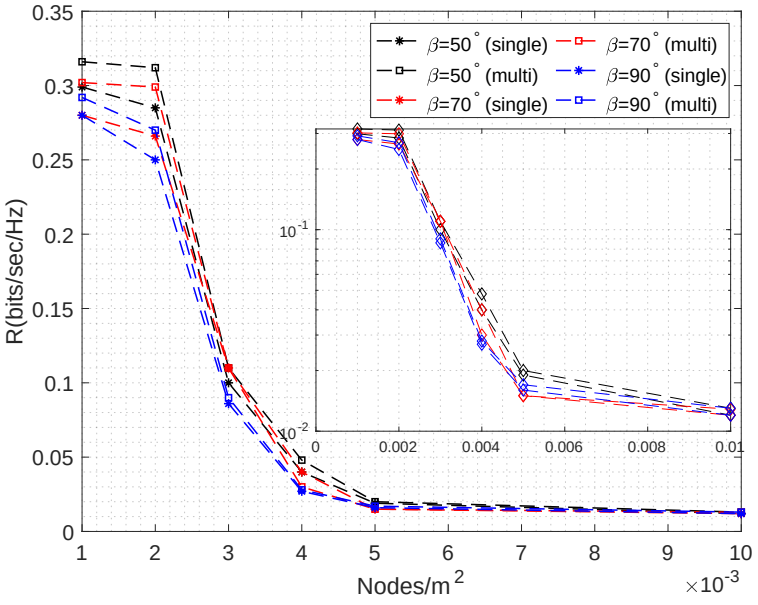

Figure 5.8: R for various β values; Nodes randomly scattered over an area of 200v $\times$ 200 m^2

to increasing amount of interference. There is a steady decay in R as we reach a high node density. Finally, for very high node density of around 0.01 nodes/m^2, network interference becomes a major hindrance resulting in near-zero sum rate. The inner plot with x-axis in logarithmic scale reiterates this trend. Just like Fig. 5.7, multi-pass RRS yields better R throughout the node density range.

In Fig. 5.9, we show how close RRS results get to 70% fit population GA for various node densities. With increasing density values, we observe the exponential decay in R for all three optimization techniques (made clearer with the inner plot with logarithmic y-axis). We see that both single and multi-pass RRS methods provide satisfactory results, close to GA, throughout the density range.

In Fig. 5.10, we show the improvement achieved by multi-pass RRS over single-pass RRS. With reference to the the left y-axis, we plot the ratio of R attained by multi-pass and single-pass RRS. On the right y-axis, we show the ratio of T that multi-pass RRS takes

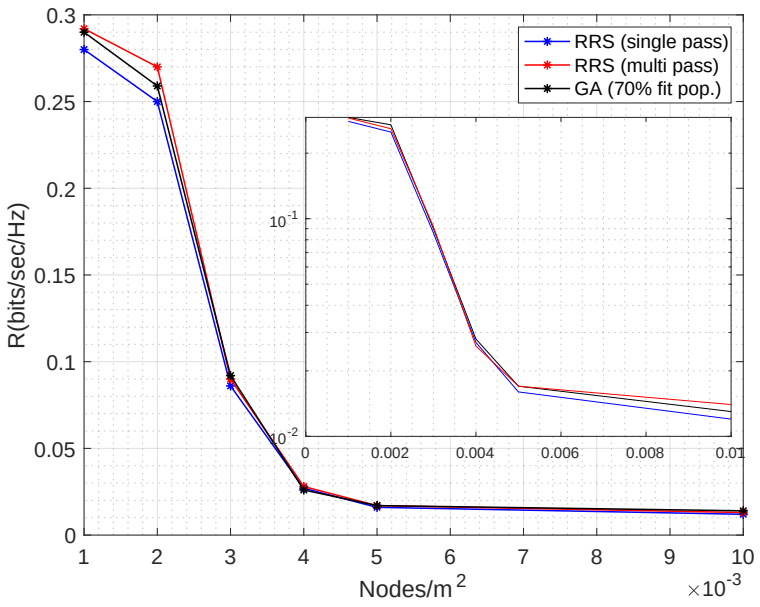

Figure 5.9: R for various θ optimization approaches; Nodes randomly scattered over 200 × 200 m^2

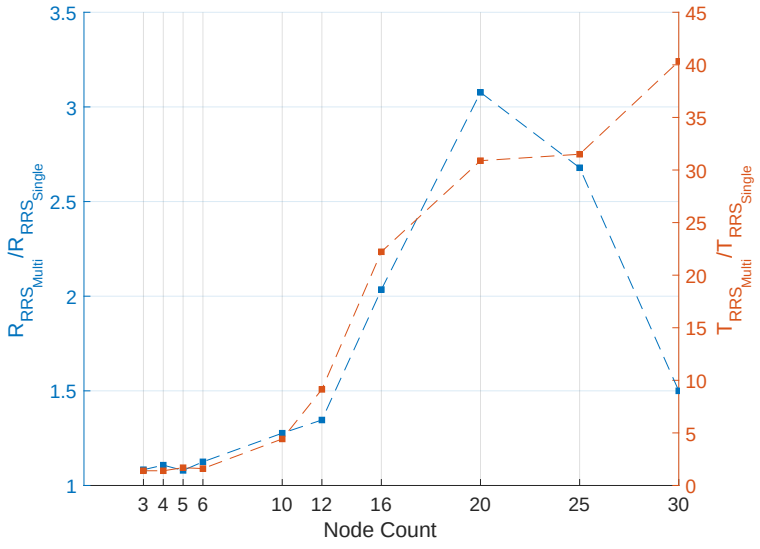

Figure 5.10: Ratios of changes in R and T by single and multi-pass RRS

over single-pass RRS. Over a variety of node counts, we see that multi-pass RRS does indeed perform better than single-pass RSS, but the margin of improvement diminishes as we approach bigger networks like a 25-node network. However, in contrast, the trade-off of multi-pass RRS in terms of the time T (in seconds) increases with bigger network sizes. From this, we can conclude that the time trade-off is far too great if multi-pass RRS is used over single-pass RRS. Hence, it can be concluded that single-pass RRS serves its purpose and can be safely used for bigger networks.

Solving WSRM

So far, we have optimized the steering angles, $\hat{\theta}$, of the PA nodes in a network to solve the SRM problem in (5.14) where the time allotment for each phase (i.e., Uplink, Downlink, or PA-PA) is assumed equal. Solving the WSRM problem in (5.16) requires optimization of the weights, $\hat{w}$, for each phase in addition to the steering angles. In Section 5, we designed a two-stage method to iteratively optimize the weights using a convex optimizer after optimizing the steering angles using multi-pass RRS. To simultaneously optimize $\hat{\theta}$ and $\hat{w}$, we adapt RRS by letting it pick a random w_p following the constraints in (5.18), (5.20) and (5.21); and then calculate w_d and w_u from the aforementioned constraints.

For varied network densities, Fig. 5.11 shows R when using RRS to solve the SRM (i.e., equal weights for the time schedule) problem (shown with 'RRS – SRM') and the WSRM problem (shown with 'RRS – WSRM'), and the two-stage method for solving the WSRM problem with one iteration (shown with 'Two-stage (single iter.)') or multiple iterations (shown with 'Two-stage (multi-iter.)'). The stacked amounts on the graph shows the additional R attained by these methods on top of RRS – SRM.

In Fig 5.12, we show how the maximum convergence times for two stage (single and multi

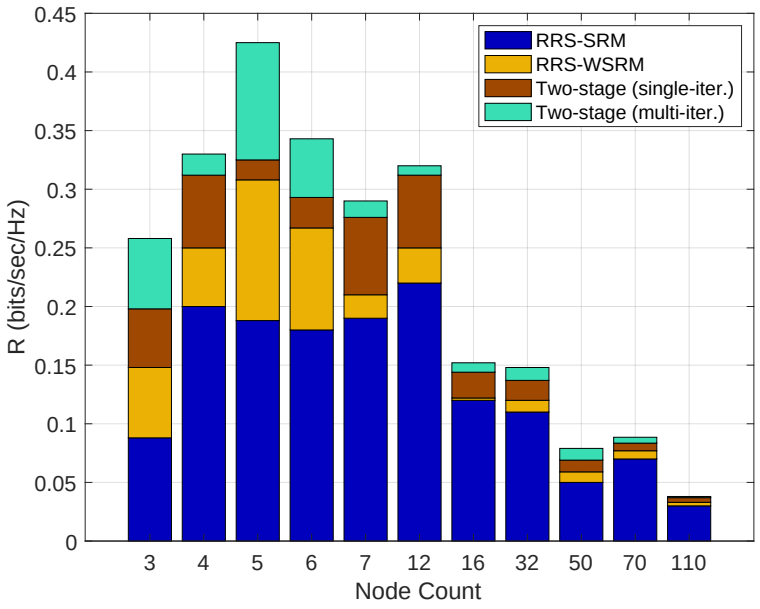

Figure 5.11: Attainable R by various scheduling optimization techniques

iteration) optimizations for $\hat{w}$ for a variety of node counts. Here, as we keep increasing the node counts, we see that the maximum convergence time increases. Moreover, as expected, the time for multi-iteration method is more than that of single-iteration. The inner plot with the x-axis in logarithmic scale clarifies the trend further. Fig. 5.13 shows the empirical time taken (for a 110 node network) for all transmission schedule optimization methods used so far. When run on an Intel™ Core™ i7™ CPU @ 4.0 GHz, RRS optimized transmission schedule takes a huge hit on performance while providing worse R than two-stage optimization. Fine-tuned multi-iteration two-stage optimization provides even better R than the single-iteration two-stage method, albeit at a slightly higher computation cost. In conclusion, the two-stage optimization with multiple iterations provides the best results, when taken into account the factor of time complexity while maximizing R.

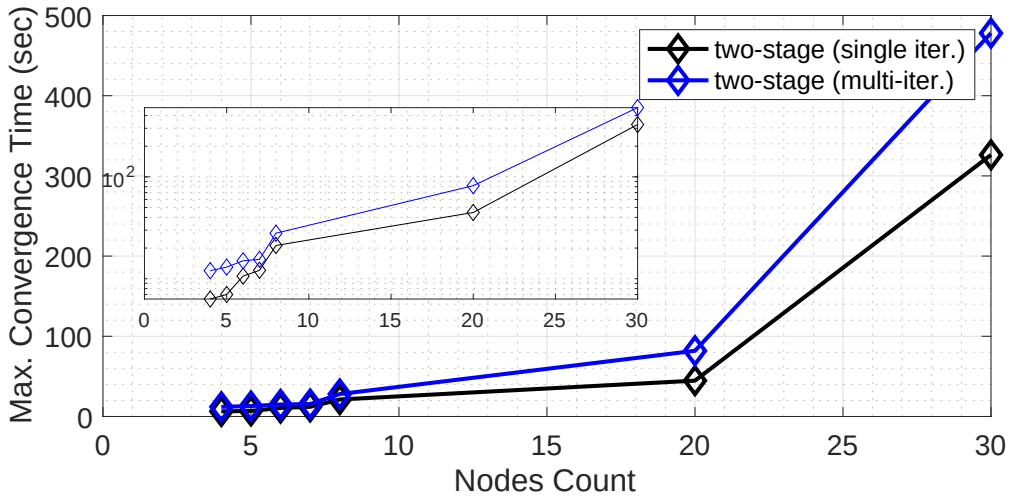

Figure 5.12: Two-stage optimization times for varying node counts

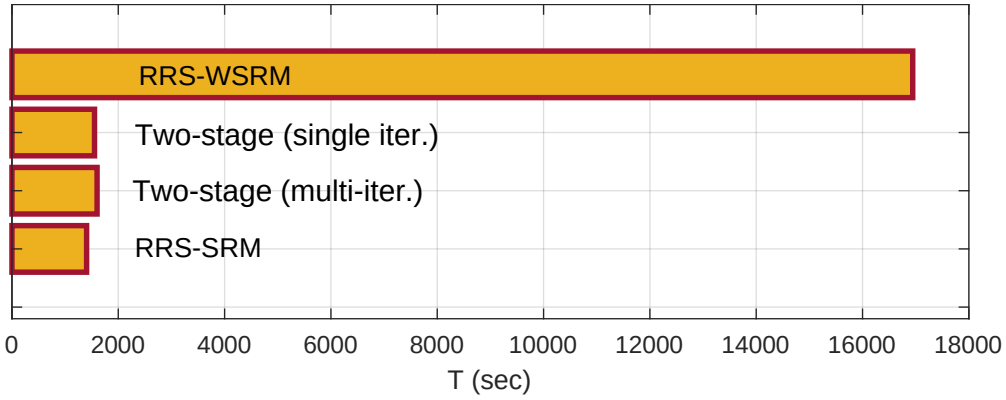

Figure 5.13: $\hat{w}$ optimization time for 110 nodes

Summary

We conducted an investigation into the enhancement of beamsteering for directional line-of-sight (LOS) millimeter-wave (mmWave) links while operating under the assumption of random transmission schedules. Our approach involves categorizing nodes as either secondary or primary directional nodes. We further segment wireless transmissions into three distinct phases: Uplink (from secondary to primary), Downlink (from primary to secondary), and PA-

PA (between primary nodes). Utilizing this devised scheduling framework, we formulated expressions for the attainable sum-rates, taking careful consideration of interference and noise present within the network. By leveraging evolutionary techniques, we delved into the optimization of the nodes' steering angles to effectively align their directional beams.

We utilized the results of exhaustive search solution that explored the relationship between network capacity and both Field of View (FOV) and transmit power within Line-of-Sight (LOS) directional wireless networks in [90]. Our comprehensive analysis encompassed RRS methods for optimizing the beamsteering angles of directional nodes and detailed comparisons with exhaustive search, GA methods in [90].

We conducted a thorough comparison of the network's sum-rate denoted as R across all three approaches. Notably, we observed that GA achieves precision akin to the exhaustive search, albeit with a relatively larger population size for fitness evaluation, while also converging at a significantly faster pace. The integration of GA enabled us to delve into larger networks. We illustrated how the network sum-rate R behaves as we vary the node count from a few to a more substantial quantity (tens of nodes). However, for networks with hundreds of nodes, we highlighted the pivotal role of scalability in fast evolutionary algorithms, as exemplified by RRS, in accurately optimizing the beamsteering angles of PAs to determine R. Upon comparing the outcomes of RRS with those of GA and exhaustive methods, it became evident that both single and multi-pass RRS approaches yield exceptional results in terms of both achieved rate and convergence precision. We also tackled the Weighted Sum-Rate Maximization (WSRM) problem, where each phase is assigned a distinct weight to accommodate voice applications. This was addressed using both RRS and a two-stage approach involving convex optimization. Our findings revealed that the latter method yields superior results within a significantly shorter timeframe when compared to the RRS-only approach.

The results in this paper have shown the effectiveness of our beamsteering algorithm and WSRM approaches, along with sum-rate comparison with different transmit powers. A key takeaway is that beamsteering optimization is a necessary component for the emerging mmWave and Terahertz networks, and that effective heuristics that can find close-to-optimal solutions with minimal help from infrastructure are heavily needed.

CHAPTER 6: CONCLUSION

In this dissertation, we have shown in detail why coalition formation among directional SDR nodes is essential. We have provided thorough and rigorous technical discussion of various cutting-edge technology available in terms of wireless communication in general, including cognitive radio devices, directional antennas, and high-frequency radio channels suitable for mmWave 5G and THz applications. Using dedicated chapters, we presented:

- A coalition formation approach for cognitive radio networks, in adversarial presence (in Chapter 3).
- An omni-directional coalition formation approach prototyped on a large-scale wireless channel emulator: Cognisseum(in Chapter 3).
- Two types of attack strategies on cognitive radio systems and ways to evade them (in Chapter 3).
- First-of-its-kind scalable, centralized, decentralized, and fast coalition formation heuristics for directional radios, along with sum-rate maximization techniques (in Chapter 4).
- Robust sum-rate maximization techniques by optimizing beamsteering angles of directional radios using evolutionary algorithms (in Chapter 5).

From the various studies presented in this dissertation, there are multiple takeaways. First, there exist scalable ways to form coalition structures rapidly in centralized or decentralized manner among directional or omni-directional software radio nodes. In addition to sclability, such coalitions enable better utilization of legacy as well as super-6 GHz spectrum bands. A binary categorization of the directional wireless nodes (e.g., primary or secondary nodes)

enables efficient and scalable heuristics for such coalition formation. Second, there are ways to understand the intuition of adversaries in a coalitional radio network and how they can work together to block legitimate radio nodes. This knowledge can then be utilized by the legitimate nodes and coalition structures can be strategized to evade attackers. And finally, our fast converging beamsteering angle optimization for directional mmWave nodes can improve overall network throughput efficiently for small, medium and large networks.

This dissertation opens up avenues for future ventures like expanding the decentralized coalition formation heuristics by investigating additional methods for transmission scheduling and bandwidth allocation strategies. Currently, the focus has been on the collective data rate of coalition groups. However, it would be intriguing for the research community to explore the fairness in terms of achievable data rates among these coalitions. Also, it would be interesting to see the impact on coalition formation if the directional nodes do not possess neighboring node information in the form of PCP lists. Additionally, it would be fascinating for researchers to delve into the introduction of adversarial elements within the directional node coalition groups and to comprehend how node mobility factors into the equation. It would also be interesting to tackle the single coalition beamsteering optimization problem in the case of multiple coalitions and jointly optimize the beamsteering angles for the entire coalition set. Introduction of node mobility would enable researchers to see how the optimization heuristics perform in more stringent real-world scenarios. Finally, it would be interesting to implement machine learning frameworks for coalition formation and beamsteering optimization heuristics and compare the findings with the ones presented in this dissertation.

PUBLICATIONS

Following is the list of published papers:

- S. Seth, D. Roy, M. Yuksel, Spectrum Sensing Secondary Users in Presence of Multiple Adversaries, in International Conference on NETwork Games, Control and Optimisation, 2020.
- S. Seth, H Yazdani, M. Yuksel, A. Vosoughi, Rate Optimizing Beamsteering for Line-of-Sight Directional Radios with Random Scheduling, in IEEE International Symposium on Dynamic Spectrum Access Networks, 2021.
- S. Mustafa, S. Seth, M. Yuksel, M. Rahman, Cellular Service with Settlement-Free Peering, in IEEE International Symposium on Dynamic Spectrum Access Networks, 2021.
- H Yazdani, S. Seth, A. Vosoughi, M. Yuksel, Throughput-Optimal D2D mmWave Communication: Joint Coalition Formation, Power, and Beam Optimization, in IEEE Wireless Communications and Networking Conference, 2021.
- S. Seth, M. Yuksel, A. Vosoughi, Forming Coalition Sets from Directional Radios, in IEEE Military Communications Conference, 2022.
- S. Seth, M. Yuksel, A. Vosoughi, Ad-hoc Coalition Set Formation among Directional Radios, in IEEE International Conference on Mobile Ad-Hoc and Smart Systems, 2023.

Following is the list of submitted papers:

- S. Seth, D. Roy, M. Yuksel, Cognisseum: Cognitive Radios on Colosseum Facing Adversaries, in Computer Networks Journal, 2023.
- S. Seth, M. Yuksel, A. Vosoughi, Beamsteering Optimization for Line-of-Sight MillimeterWave Radios, in IEEE Transactions on Vehicular Technology, 2023.

LIST OF REFERENCES

[1] W. Hassan. State of iot 2022: Number of connected iot devices growing 18% to 14.4 billion globally. [Online]. Available: https://iot-analytics.com/number-connected-iot-devices/

[2] 3GPP, "Digital cellular telecommunications system (Phase 2+) (GSM); Universal Mobile Telecommunications System (UMTS); LTE; 5G; Release description; Release 15 (3GPP TR 21.915 version 15.0.0 Release 15) ," 3rd Generation Partnership Project (3GPP), Technical Specification (TS) 21.915, 10 2019, version 15.0.0. [Online]. Available: https://portal.3gpp.org/desktopmodules/Specifications/SpecificationDetails.aspx?specificationId=3389

[3] Colosseum the world's most powerful wireless network emulator. [Online]. Available: https://www.northeastern.edu/colosseum//

[4] J. Howington. 25 companies switching to permanent remote work-from-home jobs. [Online]. Available: https://www.flexjobs.com/blog/post/companies-switching-remote-work-long-term/

[5] J. Myers. This is how much data we're using on our phones. [Online]. Available: https://www.weforum.org/agenda/2021/08/how-the-pandemic-sparked-a-data-boom/

[6] X. Wang, L. Kong, F. Kong, F. Qiu, M. Xia, S. Arnon, and G. Chen, "Millimeter wave communication: A comprehensive survey," *IEEE Communications Surveys & Tutorials*, vol. 20, no. 3, pp. 1616–1653, 2018.

[7] S. Sathyanarayan. Standalone (sa) and non-standalone (nsa) 5g architectures: The various paths to 5g revenues and profitability. [Online]. Available: https://www.affirmednetworks.com/sa-and-nsa-5g-architectures-the-path-to-profitability/

[8] R. Rofougaran. Understanding the challenges of 5g mmwave. [Online]. Available: https://www.electronicproducts.com/understanding-the-challenges-of-5g-mmwave/

[9] X. Yu, J. Zhang, M. Haenggi, and K. B. Letaief, "Coverage analysis for millimeter wave networks: The impact of directional antenna arrays," *IEEE Journal on Selected Areas in Communications*, vol. 35, no. 7, pp. 1498–1512, 2017.

[10] G. Brown, O. Koymen, and M. Branda. Is mmwave viable for mobile 5g applications? yes. here's how. Youtube. [Online]. Available: https://www.youtube.com/watch?v=2_ubCLvqBqo&t=9s&ab_channel=SherifHanna

[11] H.-J. Song and N. Lee, "Terahertz communications: Challenges in the next decade," *IEEE Transactions on Terahertz Science and Technology*, vol. 12, no. 2, pp. 105–117, 2022.

[12] Cisco. What is iot (internet of things)? [Online]. Available: https://www.cisco.com/c/en/us/solutions/internet-of-things/what-is-iot.html/

[13] FCC, "Public safety spectrum." [Online]. Available: https://www.fcc.gov/public-safety/public-safety-and-homeland-security/policy-and-licensing-division/public-safety-spectrum/

[14] D. Elliott, "Hurricane michael's damage to communications systems has slowed recovery." [Online]. Available: https://www.npr.org/2018/10/22/659611105/hurricane-michaels-damage-to-communications-systems-has-slowed-recovery/

[15] J. Suomalainen, J. Julku, M. Vehkaperä, and H. Posti, "Securing public safety communications on commercial and tactical 5g networks: A survey and future research directions," *IEEE Open Journal of the Communications Society*, vol. 2, pp. 1590–1615, 2021.

[16] K. Sastry, D. Goldberg, and G. Kendall, *Genetic Algorithms*. Boston, MA: Springer US, 2005, pp. 97–125. [Online]. Available: https://doi.org/10.1007/0-387-28356-0_4

[17] T. Ye and S. Kalyanaraman, "A recursive random search algorithm for large-scale network parameter configuration," in *Proceedings of the 2003 ACM SIGMETRICS International conference on Measurement and modeling of computer systems*, 2003, pp. 196–205.

[18] A. Baharlouei and B. Jabbari, "Dynamic subchannel and power allocation using nash bargaining game for cognitive radio networks with imperfect pu activity sensing," in *8th International Conference on Cognitive Radio Oriented Wireless Networks*, 2013.

[19] F. Chen and R. Qiu, "Centralized and distributed spectrum sensing system models performance analysis based on three users," in *International Conference on Wireless Communications Networking and Mobile Computing (WiCOM)*, 2010.

[20] X. Xing, T. Jing, W. Cheng, Y. Huo, X. Cheng, and T. Znati, "Cooperative spectrum prediction in multi-pu multi-su cognitive radio networks," *Mobile Networks and Applications*, vol. 19, no. 4, pp. 502–511, 2014.

[21] L. B. Le and E. Hossain, "Resource allocation for spectrum underlay in cognitive radio networks," *IEEE Transactions on Wireless Communications*, pp. 5306–5315, 2008.

[22] W. Saad, Z. Han, M. Debbah, A. Hjorungnes, and T. Basar, "Coalitional games for distributed collaborative spectrum sensing in cognitive radio networks," in *IEEE INFOCOM 2009*, 2009.

[23] W. Saad, Z. Han, M. Debbah, A. Hjorungnes, and T. Basar, "Coalitional game theory for communication networks," *IEEE Signal Processing Magazine*, p. 77–97, 2009.

[24] T. Basar and G. Olsder, *Dynamic Noncooperative Game Theory: Second Edition.* Society for Industrial and Applied Mathematics, 1999.

[25] Yi-Bing, R. Yang, and F. Ye, "Non-cooperative spectrum allocation based on game theory in cognitive radio networks," in *2010 IEEE Fifth International Conference on Bio-Inspired Computing: Theories and Applications (BIC-TA)*, 2010, pp. 1134–1137.

[26] C. Jiang, H. Zhang, Y. Ren, and H. Chen, "Energy-efficient non-cooperative cognitive radio networks: micro, meso, and macro views," *IEEE Communications Magazine*, pp. 14–20, 2014.

[27] Z. Han, D. Niyato, W. Saad, T. Başar, and A. Hjørungnes, *Game Theory in Wireless and Communication Networks: Theory, Models, and Applications.* Cambridge University Press, 2012.

[28] Z. Han and K. Liu, *Resource Allocation for Wireless Networks: Basics, Techniques, and Applications.* Cambridge University Press, 2008.

[29] I. F. Akyildiz, B. F. Lo, and R. Balakrishnan, "Cooperative spectrum sensing in cognitive radio networks: A survey," *Physical Communication*, vol. 4, no. 1, pp. 40–62, 2011. [Online]. Available: https://www.sciencedirect.com/science/article/pii/S187449071000039X

[30] L. Bonati, P. Johari, M. Polese, S. D'Oro, S. Mohanti, M. Tehrani-Moayyed, D. Villa, S. Shrivastava, C. Tassie, K. Yoder, A. Bagga, P. Patel, V. Petkov, M. Seltser, F. Restuccia, A. Gosain, K. R. Chowdhury, S. Basagni, and T. Melodia, "Colosseum: Large-scale wireless experimentation through hardware-in-the-loop network emulation," in *2021 IEEE International Symposium on Dynamic Spectrum Access Networks (DySPAN)*. IEEE Press, 2021, p. 105–113. [Online]. Available: https://doi.org/10.1109/DySPAN53946.2021.9677430

[31] Tutorial: Colosseum, the world's largest wireless network emulator. [Online]. Available: https://ece.northeastern.edu/wineslab/papers/melodia2021colosseum_tutorial.pdf

[32] S. Mustafa, S. Seth, M. Yuksel, and M. Rahman, "Cellular service with settlement-free peering," in *2021 IEEE International Symposium on Dynamic Spectrum Access Networks (DySPAN)*, 2021, pp. 153–162.

[33] Y. Wang, Y. Niu, H. Wu, Z. Han, B. Ai, and Q. Wang, "Sub-channel allocation for device-to-device underlaying full-duplex mmwave small cells using coalition formation games," *IEEE Transactions on Vehicular Technology*, vol. 68, no. 12, pp. 11 915–11 927, 2019.

[34] Y. Niu, H. Shi, Y. Li, R. He, and Z. Zhong, "Coalition formation games based sub-channel allocation for device-to-device underlay mmwave small cells," in *2018 2nd URSI Atlantic Radio Science Meeting (AT-RASC)*, 2018, pp. 1–4.

[35] C. Gao, X. Sheng, J. Tang, W. Zhang, S. Zou, and M. Guizani, "Joint mode selection, channel allocation and power assignment for green device-to-device communications," in *2014 IEEE International Conference on Communications (ICC)*, 2014, pp. 178–183.

[36] Q. Chen, X. Peng, J. Yang, and F. Chin, "Spatial reuse strategy in mmwave wpans with directional antennas," in *2012 IEEE Global Communications Conference (GLOBECOM)*, 12 2012, pp. 5392–5397.

[37] Z. Wei, D. W. K. Ng, and J. Yuan, "Noma for hybrid mmwave communication systems with beamwidth control," *IEEE Journal of Selected Topics in Signal Processing*, vol. 13, no. 3, pp. 567–583, 2019.

[38] H. Jiang, Y. Niu, J. Zhang, B. Ai, and Z. Zhong, "Coalition game based full-duplex concurrent scheduling in millimeter wave wireless backhaul network," *China Communications*, vol. 16, no. 2, pp. 59–75, 2019.

[39] C. H. Doan, S. Emami, D. A. Sobel, A. M. Niknejad, and R. W. Brodersen, "Design considerations for 60 ghz cmos radios," *IEEE Communications Magazine*, vol. 42, no. 12, pp. 132–140, 2004.

[40] T. S. Rappaport, J. N. Murdock, and F. Gutierrez, "State of the art in 60-ghz integrated circuits and systems for wireless communications," *Proceedings of the IEEE*, vol. 99, no. 8, pp. 1390–1436, 2011.

[41] Z. Pi and F. Khan, "An introduction to millimeter-wave mobile broadband systems," *IEEE Communications Magazine*, vol. 49, no. 6, pp. 101–107, 2011.

[42] W. Roh, J. Seol, J. Park, B. Lee, J. Lee, Y. Kim, J. Cho, K. Cheun, and F. Aryanfar, "Millimeter-wave beamforming as an enabling technology for 5g cellular communications: theoretical feasibility and prototype results," *IEEE Communications Magazine*, vol. 52, no. 2, pp. 106–113, 2014.

[43] T. S. Rappaport, F. Gutierrez, E. Ben-Dor, J. N. Murdock, Y. Qiao, and J. I. Tamir, "Broadband millimeter-wave propagation measurements and models using adaptive-

beam antennas for outdoor urban cellular communications," *IEEE Transactions on Antennas and Propagation*, vol. 61, no. 4, pp. 1850–1859, 2013.

[44] H. Zhao, R. Mayzus, S. Sun, M. Samimi, J. K. Schulz, Y. Azar, K. Wang, G. N. Wong, F. Gutierrez, and T. S. Rappaport, "28 ghz millimeter wave cellular communication measurements for reflection and penetration loss in and around buildings in new york city," in *2013 IEEE International Conference on Communications (ICC)*, 2013, pp. 5163–5167.

[45] Y. Azar, G. N. Wong, K. Wang, R. Mayzus, J. K. Schulz, H. Zhao, F. Gutierrez, D. Hwang, and T. S. Rappaport, "28 ghz propagation measurements for outdoor cellular communications using steerable beam antennas in new york city," in *2013 IEEE International Conference on Communications (ICC)*, 2013, pp. 5143–5147.

[46] Y. Niu, Y. Li, D. Jin, L. Su, and A. V. Vasilakos, "A survey of millimeter wave communications (mmwave) for 5g: opportunities and challenges," *Wireless networks*, 2015.

[47] L. Li, H. Ren, Q. Cheng, K. Xue, W. Chen, M. Debbah, and Z. Han, "Millimeter-wave networking in the sky: A machine learning and mean field game approach for joint beamforming and beam-steering," *IEEE Tran. on Wireless Communications*, vol. 19, no. 10, pp. 6393–6408, 2020.

[48] M.-Y. Huang, Y.-W. Chen, P.-C. Peng, H. Wang, and G.-K. Chang, "A full field-of-view self-steering beamformer for 5G mm-wave fiber-wireless mobile fronthaul," *J. of Light. Tech.*, 2020.

[49] H. Yazdani, A. Vosoughi, and X. Gong, "Achievable rates of opportunistic cognitive radio systems using reconfigurable antennas with imperfect sensing and channel estimation," *IEEE Transactions on Cognitive Communications and Networking*, 2021.

[50] Z. Xiao, L. Zhu, Y. Liu, P. Yi, R. Zhang, X.-G. Xia, and R. Schober, "A survey on millimeter-wave beamforming enabled uav communications and networking," *IEEE Communications Surveys & Tutorials*, vol. 24, no. 1, pp. 557–610, 2022.

[51] M. Jean, E. Velazquez, X. Gong, and M. Yuksel, "A 30 ghz steerable patch array antenna for software-defined radio platforms," in *SoutheastCon 2023*, 2023, pp. 856–860.

[52] L. Li, Q. Cheng, K. Xue, C. Yang, and Z. Han, "Downlink transmit power control in ultra-dense uav network based on mean field game and deep reinforcement learning," *IEEE Transactions on Vehicular Technology*, vol. 69, no. 12, pp. 15 594–15 605, 2020.

[53] A. Elshafiy, K. Rose, and A. Sampath, "On optimal beam steering directions in millimeter wave systems," in *ICASSP 2019 - 2019 IEEE International Conference on Acoustics, Speech and Signal Processing (ICASSP)*, 2019, pp. 4709–4713.

[54] H. Yazdani, A. Vosoughi, and X. Gong, "Beam selection and discrete power allocation in opportunistic cognitive radio systems with limited feedback using espar antennas," *IEEE Transactions on Cognitive Communications and Networking*, 2020.

[55] H. Yazdani, S. Seth, A. Vosoughi, and M. Yuksel, "Throughput-optimal d2d mmwave communication: Joint coalition formation, power, and beam optimization," in *2022 IEEE Wireless Communications and Networking Conference (WCNC)*, 2022, pp. 1539–1544.

[56] S. Seth, H. Yazdani, M. Yuksel, and A. Vosoughi, "Rate-optimizing beamsteering for line-of-sight directional radios with random scheduling," in *2021 IEEE International Symposium on Dynamic Spectrum Access Networks (DySPAN)*, 2021, pp. 53–60.

[57] F. Fuschini, M. Zoli, E. M. Vitucci, M. Barbiroli, and V. Degli-Esposti, "A study on millimeter-wave multiuser directional beamforming based on measurements and ray tracing simulations," *IEEE Transactions on Antennas and Propagation*, vol. 67, no. 4, pp. 2633–2644, 2019.

[58] V. Raghavan, J. H. Ryu, O. H. Koymen, and J. Li, "Towards optimal cooperative beamforming in millimeter wave systems via directional transmissions." in *WCNC*, 2022, pp. 1581–1586.

[59] W. Alhakami, A. Mansour, and G. Safdar, "Spectrum sharing security and attacks in crns: a review," *International Journal of Advanced Computer Science and Applications*, vol. 5, 01 2014.

[60] D. Niyato and E. Hossain, "Competitive spectrum sharing in cognitive radio networks: a dynamic game approach," *IEEE Transactions on Wireless Communications*, pp. 2651–2660, 2008.

[61] V. Valenta, R. Maršálek, G. Baudoin, M. Villegas, M. Suarez, and F. Robert, "Survey on spectrum utilization in europe: Measurements, analyses and observations," in *2010 Proceedings of the Fifth International Conference on Cognitive Radio Oriented Wireless Networks and Communications*, 2010.

[62] D. Das and S. Das, "A survey on spectrum occupancy measurement for cognitive radio," *Wirel. Pers. Commun.*, pp. 2581–2598, 2015.

[63] D. Roy, T. Mukherjee, M. Chatterjee, and E. Pasiliao, "Defense against pue attacks in dsa networks using gan based learning," in *IEEE Global Communication Conference*, 2019.

[64] J. Yang, H. Zhou, R. Chen, J. Shi, and Z. Li, "Covert communication against a full-duplex adversary in cognitive radio networks," in *GLOBECOM 2022 - 2022 IEEE Global Communications Conference*, 2022, pp. 3144–3149.

[65] Z. Xu, Z. Zhang, S. Wang, A. Jolfaei, A. K. Bashir, Y. Yan, and S. Mumtaz, "Decentralized opportunistic channel access in crns using big-data driven learning algorithm," *IEEE Transactions on Emerging Topics in Computational Intelligence*, vol. 5, no. 1, pp. 57–69, 2021.

[66] H. A. B. Salameh, M. Krunz, and O. Younis, "Cooperative adaptive spectrum sharing in cognitive radio networks," *IEEE/ACM Transactions On Networking*, vol. 18, no. 4, pp. 1181–1194, 2010.

[67] FCC ET Docket No. 08-260, "Second Report and Order and Memorandum Opinion and Order – Unlicensed Operation in the TV Broadcast Bands / Additional Spectrum for Unlicensed Devices Below 900 MHz and in the 3GHz Band," US Federal Communications Commission, Washington DC, FCC 08-260, 2008.

[68] H. Xu, H. Gao, C. Zhou, R. Duan, and X. Zhou, "Resource allocation in cognitive radio wireless sensor networks with energy harvesting," *Sensors*, vol. 19, no. 23, p. 5115, 2019.

[69] J. Mitola and G. Q. Maguire, "Cognitive radio: making software radios more personal," *IEEE Personal Communications*, vol. 6, no. 4, pp. 13–18, 1999.

[70] G. Chalkiadakis, E. Elkind, and M. Wooldridge, "Cooperative game theory: Basic concepts and computational challenges," *IEEE Intelligent Systems*, 2012.

[71] A. Goldsmith, *Wireless Communications*. Cambridge University Press, 2005.

[72] What is the range of a typical wi-fi network? [Online]. Available: https://www.lifewire.com/range-of-typical-wifi-network-816564#:~:text=A%20general%20rule%20of%20thumb,one%2Dthird%20of%20these%20distances.

[73] Mark Rosker. Spectrum collaboration challenge (sc2) (archived). [Online]. Available: https://www.darpa.mil/program/spectrum-collaboration-challenge

[74] Platforms for advanced wireless research. [Online]. Available: https://advancedwireless.org/

[75] L. Bonati, P. Johari, M. Polese, S. D'Oro, S. Mohanti, M. Tehrani-Moayyed, D. Villa, S. Shrivastava, C. Tassie, K. Yoder, A. Bagga, P. Patel, V. Petkov, M. Seltser, F. Restuccia, A. Gosain, K. R. Chowdhury, S. Basagni, and T. Melodia, "Colosseum: Large-scale wireless experimentation through hardware-in-the-loop network emulation," in *2021 IEEE International Symposium on Dynamic Spectrum Access Networks (DySPAN)*, 2021, pp. 105–113.

[76] Colosseum architecture. [Online]. Available: https://colosseumneu.freshdesk.com/support/solutions/articles/61000253399-colosseum-architecture//

[77] Knowledge base. [Online]. Available: https://colosseumneu.freshdesk.com/support/home

[78] H. Ozpinar, S. Aksimsek, and N. T. Tokan, "A novel compact, broadband, high gain millimeter-wave antenna for 5g beam steering applications," *IEEE Transactions on Vehicular Technology*, vol. 69, no. 3, pp. 2389–2397, 2020.

[79] Z. Khan, J. Lehtomäki, Codreanu, and M. et al, "Throughput-efficient dynamic coalition formation in distributed cognitive radio networks," *J Wireless Com Network*, 2010.

[80] O. Namvar Gharehshiran, A. Attar, and V. Krishnamurthy, "Dynamic coalition formation for resource allocation in cognitive radio networks," in *2010 IEEE International Conference on Communications*, 2010, pp. 1–6.

[81] S. Seth, D. Roy, and M. Yuksel, "Spectrum sharing secondary users in presence of multiple adversaries," in *International Conference on NETwork Games COntrol and oPtimization 2020 (NetGCoop'20)*, Cargese Conference Center, France, Mar. 2020.

[82] S. Seth, M. Yuksel, and A. Vosoughi, "Forming coalition sets from directional radios," in *MILCOM 2022 - 2022 IEEE Military Communications Conference (MILCOM)*, 2022, pp. 507–514.

[83] ——, "Ad-hoc coalition set formation among directional radios," in *2023 IEEE 20th International Conference on Mobile Ad Hoc and Smart Systems (MASS)*, 2023, pp. 10–18.

[84] L. Militano, A. Orsino, G. Araniti, A. Molinaro, and A. Iera, "A constrained coalition formation game for multihop D2D content uploading," *IEEE Transactions on Wireless Communications*, vol. 15, no. 3, pp. 2012–2024, 2016.

[85] C. Hurley, R. Rogers, F. Thornton, D. Connelly, and B. Baker, "Chapter 2 - understanding antennas and antenna theory," in *WarDriving and Wireless Penetration Testing*. Syngress, 2007.

[86] H. Zhang, Y. Duan, K. Long, and V. C. M. Leung, "Energy efficient resource allocation in terahertz downlink noma systems," *IEEE Transactions on Communications*, vol. 69, no. 2, pp. 1375–1384, 2021.

[87] P. Nagaraj, "Impact of atmospheric impairments on mmWave-based outdoor communication," *arXiv preprint arXiv:1806.05176*, 2018.

[88] T. S. Rappaport, Y. Xing, O. Kanhere, S. Ju, A. Madanayake, S. Mandal, A. Alkhateeb, and G. C. Trichopoulos, "Wireless communications and applications above 100 GHz: Opportunities and challenges for 6G and beyond," *IEEE Access*, vol. 7, pp. 78 729–78 757, 2019.

[89] M. Erdelj, M. Król, and E. Natalizio, "Wireless sensor networks and multi-uav systems for natural disaster management," *Computer Networks*, vol. 124, pp. 72–86, 2017.

[90] S. Seth, H. Yazdani, M. Yuksel, and A. Vosoughi, "Rate-optimizing beamsteering for line-of-sight directional radios with random scheduling," in *2021 IEEE International Symposium on Dynamic Spectrum Access Networks (DySPAN)*, 2021, pp. 53–60.

[91] Z. Zhang, J. Ryu, S. Subramanian, and A. Sampath, "Coverage and channel characteristics of millimeter wave band using ray tracing," in *Proceedings of IEEE ICC*, 2015, pp. 1380–1385.

[92] R. Umar and W. Mesbah, "Distributed coalition formation and bandwidth allocation in ad hoc cognitive radio networks," in *IEEE 80th Vehicular Technology Conference (VTC2014-Fall)*, 2014, pp. 1–5.

[93] R. Branzei, D. Dimitrov, and S. Tijs, *Models in Cooperative Game Theory*. Springer, 2005.

[94] H. Pu, Z. Gu, Q.-S. Hua, and H. Jin, "Communication and block game in cognitive radio networks," in *Proceedings of the 18th ACM International Conference on Modeling, Analysis and Simulation of Wireless and Mobile Systems*, ser. MSWiM '15, 2015, pp. 211–218.

[95] M. J. Abdel-Rahman and M. Krunz, "Game-theoretic quorum-based frequency hopping for anti-jamming rendezvous in dsa networks," in *2014 IEEE International Symposium on Dynamic Spectrum Access Networks (DYSPAN)*, 2014, pp. 248–258.

[96] Z. Khan, S. Glisic, L. A. DaSilva, and J. Lehtomaki, "Modeling the dynamics of coalition formation games for cooperative spectrum sharing in an interference channel," *IEEE Transactions on Computational Intelligence and AI in Games*, vol. 3, no. 1, pp. 17–30, 2011.

[97] K. Liu and B. Wang, *Cognitive Radio Networking and Security: A Game-Theoretic View*. Cambridge University Press, 2010.

[98] Y. Liang, Y. Zeng, E. C. Y. Peh, and A. T. Hoang, "Sensing-throughput tradeoff for cognitive radio networks," *IEEE Transactions on Wireless Communications*, pp. 1326–1337, 2008.

[99] H. Li, Y. Dou, C. Lu, D. Zabransky, Y. Yang, and J. J. Park, "Preserving the incumbent users' location privacy in the 3.5 ghz band," in *2018 IEEE International Symposium on Dynamic Spectrum Access Networks (DySPAN)*, Oct 2018, pp. 1–10.

[100] Q. Cheng, L. Li, K. Xue, H. Ren, X. Li, W. Chen, and Z. Han, "Beam-steering optimization in multi-UAVs mmWave networks: A mean field game approach," in *Proc. of IEEE International Conference on Wireless Communications and Signal Processing (WCSP)*, 2019, pp. 1–5.

[101] D. Choudhury, "5g wireless and millimeter wave technology evolution: An overview," in *2015 IEEE MTT-S International Microwave Symposium*, 2015, pp. 1–4.

[102] A. I. Sulyman, A. Alwarafy, G. R. MacCartney, T. S. Rappaport, and A. Alsanie, "Directional radio propagation path loss models for millimeter-wave wireless networks

in the 28-, 60-, and 73-ghz bands," *IEEE Transactions on Wireless Communications*, vol. 15, no. 10, pp. 6939–6947, 2016.

[103] A. Sebak, "High gain millimeter wave antennas for 5g wireless and security imaging systems," in *2016 33rd National Radio Science Conference (NRSC)*, 2016, pp. 2–2.

[104] E. Erfani, S. Safavi-Naeini, and S. Tatu, "Design and analysis of a millimetre-wave high gain antenna," *IET Microwaves, Antennas Propagation*, vol. 13, no. 10, pp. 1586–1592, 2019.

[105] Z. Z. J. Peng and X. Z. K. L. F. Jiang, "Reverse auction based green offloading scheme for small cell heterogeneous networks," *Green Communication for Mobile and Wireless Networks*, 2016.

[106] B. Li, Z. Zhou, W. Zou, X. Sun, and G. Du, "On the efficient beam-forming training for 60ghz wireless personal area networks," *IEEE Transactions on Wireless Communications*, vol. 12, no. 2, pp. 504–515, 2013.

[107] W. Peng and F. Adachi, "Multi-user interference suppression by using frequency domain adaptive antenna array." [Online]. Available: https://www.intechopen.com/books/recent-trends-in-multi-user-mimo-communications/multi-user-interference-suppression-by-using-frequency-domain-adaptive-antenna-array

[108] L. Hui, L. Chun, and L. Hua, "Power control based on non-cooperative game in wireless sensor networks," in *2013 6th International Conference on Intelligent Networks and Intelligent Systems (ICINIS)*, 2013, pp. 135–138.

[109] J. Kelif and O. Simon, "Impact of directional receiving antennas on the performance and quality of service of wireless networks," in *2014 IEEE 80th Vehicular Technology Conference (VTC2014-Fall)*, 2014, pp. 1–6.

[110] R. Gonzalo, J. Teniente, and C. Del Río, "Improved radiation pattern performance of gaussian profiled horn antennas," *Antennas and Propagation, IEEE Transactions on*, vol. 50, pp. 1505 – 1513, 12 2002.

[111] P. Tracy. [Online]. Available: https://www.rcrwireless.com/20160815/fundamentals/mmwave-5g-tag31-tag99

[112] [Online]. Available: https://www.rcrwireless.com/20160815/fundamentals\/mmwave-5g-tag31-tag99

[113] T. S. Rappaport, Y. Qiao, J. I. Tamir, J. N. Murdock, and E. Ben-Dor, "Cellular broadband millimeter wave propagation and angle of arrival for adaptive beam steering systems," in *2012 IEEE Radio and Wireless Symposium*. IEEE, 2012, pp. 151–154.

[114] International Wireless Industry Consortium, "5G millimeter wave frequencies and mobile networks," 2019.

[115] W. Hassan. State of iot 2022: Number of connected iot devices growing 18% to 14.4 billion globally. [Online]. Available: https://iot-analytics.com/number-connected-iot-devices/